ZOË KUGLER

PERPENDICULAR ANISOTROPY IN MAGNETIC TUNNEL JUNCTIONS

UNIVERSITÄT BIELEFELD
FAKULTÄT FÜR PHYSIK

Perpendicular anisotropy in magnetic tunnel junctions

Thesis by Zoë Kugler

UNIVERSITÄT BIELEFELD
FAKULTÄT FÜR PHYSIK

Dissertation zur Erlangung des Doktorgrades

Diese Dissertation wurde von mir persönlich verfasst. Einige Textpassagen sind in veränderter Form aus Publikationen, deren Autor ich war, übernommen. Ich versichere weiterhin, dass ich, abgesehen von den ausdrücklich bezeichneten Hilfsmitteln, die Dissertation selbständig und ohne unerlaubte Hilfe angefertigt habe.

Gutachter:
Prof. Dr. Günter Reiss
Prof. Dr. Walter Pfeiffer

Mai 2012

Contents

Introduction

The introduction gives a motivation and an overview about the present thesis. The structure of the introduction is designed analog to the text. The chapters of this thesis are summarized and the main findings are figured out. A section about magnetic tunnel junctions in combination with perpendicular magnetic anisotropy at the beginning of the introduction integrates the work in the scientific context.

The cited articles and references are denoted directly at the margin of the text. Additionally, a list of the citations in alphabetical order is given in the chapter "References". The methods, such as sample preparation and measurement techniques, that have been used in the framework of this thesis are described in the appendix. Furthermore, a list of my publications can also be found in the appendix.

Magnetic tunnel junctions and perpendicular anisotropy

Using the spin of an electron in addition to its charge provides an additional degree of freedom for the realization of electronic devices. The field of research, that functionalizes the electron's spin, is called *spinelectronic*, or short *spintronic*. It is a relatively new field, that is still in progress.[1]

An important device for spintronics with many possible applications is the *magnetic tunnel junction* (MTJ). In principle, an MTJ consists of two magnetic electrodes, separated by an insulating layer, the so-called barrier of the MTJ. An electron is able to pass the barrier due to the quantum mechanical tunneling process if the barrier is sufficiently thin.[2] A current results if a voltage is applied between the two electrodes. This is illustrated in figure 1. The resistance of the MTJ shows a strong dependence on the rela-

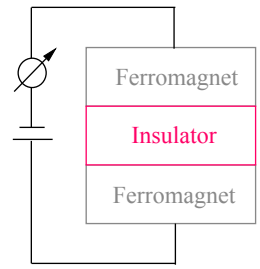

Figure 1: The MTJ: An electron is able to pass the insulating barrier due to the quantum mechanical tunneling process if the barrier is sufficiently thin. A current results if a voltage is applied between the two magnetic electrodes.

[1] A nice review concerning the topic spintronic can be found in:

S. Bader et al., Annu. Rev. Condens. Matter Phys. **1**, 71 (2010)

[2] Sufficiently thin means in the range of some nanometers.

tive orientation of the magnetization of the electrodes. Normally, the resistance is minimized for a parallel alignment of the magnetization and maximized for the configuration with antiparallel alignment. This effect is called *tunneling magneto resistance* (TMR) and can be quantified by the *TMR-ratio*, defined by the difference of the resistance with antiparallel (R_{ap}) and with parallel (R_p) orientation of the magnetization and normalized to the resistance with parallel orientation.[3]

$$TMR := \frac{R_{ap} - R_p}{R_p}$$

[3]

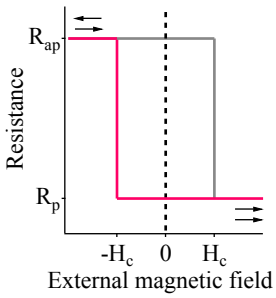

Figure 2: The resistance of a magnetic tunnel junction in dependence of the external magnetic field. The resistance for decreasing external field (from positive to negative) is marked in pink, the resistance for increasing magnetic field (from negative to positive) in grey. The arrows denote the corresponding magnetization states.

The realization of the antiparallel alignment of the magnetization is a precondition for the investigation of the TMR-effect. One method to tailor this antiparallel alignment is to use electrodes with different coercive fields. The electrode with the larger coercive field is called *hard magnetic* and the one with the smaller coercive field accordant *soft magnetic*. If a sufficient external magnetic field is applied to the MTJ, the electrodes can be saturated with parallel orientation of the magnetization. If the external field is now reduced, inversed and finally reaches the coercive field value of the soft magnetic electrode, the magnetization of the this electrode switches. The orientation of the magnetization in the electrodes is now antiparallel. This configuration is preserved until the external magnetic field is further reduced and finally reaches the coercive field of the hard magnetic electrode and leads to a switching of this electrode, as well. The resulting resistance curve in dependence of the external magnetic field is called *major loop*. If the external magnetic field is not further reduced, but increased after the antiparallel alignment has been obtained, the antiparallel orientation remains until the (opposite) coercive field of the soft magnetic layer is reached. The resulting resistance curve in dependence of the external magnetic field is called *minor loop*. Figure 2 shows the minor loop of a magnetic tunnel junction, as well as the corresponding magnetization states in the electrodes. The resistance for decreasing external field (from positive to negative) is marked in pink, the resistance for increasing magnetic field (from negative to positive) in grey. Two possible states of the resistance, R_p and R_{ap}, are adjustable at zero magnetic field.

The TMR-effect was first observed in 1975 by Jullière et al.[4] But its evidence at room-temperature was not reported before 1995 by Moodera et al.[5] and by Miyazaki et al.[6] Jullière introduced

[4] M. Julliere, Phys. Lett. A **54**, 225 (1975)

[5] J. S. Moodera et al., Phys. Rev. Lett. **74**, 3273 (1995)

[6] T. Miyazaki et al., J. Magn. Magn. Mater. **139**, L231 (1995)

a model that linked the TMR-effect to the spin polarization P of the magnetic electrodes. The spin polarization quantifies the excess of charge carriers $n_\uparrow$ with one spin-state ($up \uparrow$) compared to the charge carriers $n_\downarrow$ with the other spin-state ($down \downarrow$).[7] A high TMR-effect is important for the use of MTJs as spintronic devices. Thus, a high spin polarization of the magnetic electrodes is desirable as it goes along with the high TMR.

Beside the kind of electrode, the barrier material has a large influence on the TMR-effect. Basically, two kinds of materials have been investigated intensively so far. While the first studies reported about MTJs based on amorphous alumina barriers with a maximum TMR-effect of about 80 % at room-temperature,[8] a large TMR-effect of more than 1000 % was predicted in 2001 for fully epitaxial Fe/MgO/Fe junctions. This prediction was made by two different groups independently.[9] The reason for the large TMR-effect is the so-called *symmetry filtering*. The crystallinity of the system causes a slower decay of the wave-functions of some electronic bands compared to others. This symmetry filtering results in a *spin filtering* for Fe, Co and CoFe electrodes, as the different bands of this materials are filled with electrons of different spin states. Thus, the spin polarization is effectively increased by using a fully epitaxial junction with an MgO barrier. This leads to a high TMR-effect.

And indeed, it has been shown experimentally in 2004 that the TMR-effect is increased by using crystalline MgO instead of amorphous alumina as a barrier material in magnetic tunnel junctions.[10] From that time on, a lot of research was done in order to optimize the epitaxy of MgO based magnetic tunnel junctions and thus, increase the TMR-ratio.[11] Up to now, a maximum TMR-effect of about 600 % at room-temperature and of more than 1100 % at low temperature has been attained.[12] A detailed chronology of the maximum TMR-effect for alumina and MgO based magnetic tunnel junctions is shown by Schebaum.[13]

Spinelectronic, and the TMR-effect in magnetic tunnel junctions in particular, are of large interest for many possible applications. For example, high-density read heads[14] and non-volatile memory devices,[15] especially the *magnetic random access memory*

[7] $$P := \frac{n_\uparrow - n_\downarrow}{n_\uparrow + n_\downarrow}$$

$$TMR = \frac{2P_1P_2}{1 - P_1P_2}$$

[8] H. X. Wei et al., J. Appl. Phys. **101**, 09B501 (2007); and D. Wang et al., IEEE Trans. Magn. **40**, 2269 (2004)

[9] W. H. Butler et al., Phys. Rev. B **63**, 054416 (2001); and J. Mathon et al., Phys. Rev. B **63**, 220403 (2001)

[10] S. Yuasa et al., Nat. Mater. **3**, 868 (2004); and S. S. P. Parkin et al., Nat. Mater. **3**, 862 (2004)

[11] D. D. Djayaprawira et al., Appl. Phys. Lett. **86**, 092502 (2005); S. Yuasa et al., Appl. Phys. Lett. **87**, 222508 (2005); S. Yuasa et al., Appl. Phys. Lett. **89**, 042505 (2006); and Y. M. Lee et al., Appl. Phys. Lett. **90**, 212507 (2007)

[12] S. Ikeda et al., Appl. Phys. Lett. **93**, 082508 (2008)

[13] O. Schebaum, PhD thesis, Universität Bielefeld, 2011

[14] K. Kobayashi et al., FUJITSU Sci. Tech. J. **42**, 139 (2006)

[15] G. A. Prinz, Science **282**, 1660 (1998)

(MRAM), can be realized by using MTJs. Basically, such an MRAM consists of a large number of memory cells, that are arranged as a matrix. Every memory cell in this matrix is a magnetic tunnel junction. The parallel and antiparallel orientation of the magnetization in the electrodes of a single magnetic tunnel junctions is related to the logical "0" and to the logical "1", respectively. The writing process is induced by a magnetization reversal in the soft electrode. The magnetization direction of the hard magnetic electrode is not changed. The reading process corresponds to the detection of the resistance of the MTJ. The magnetization reversal in the soft magnetic electrode can be induced by a magnetic field or alternatively by a spin polarized current. This method, the *current induced switching* (CIS), was first predicted theoretically in 1996 by Slonczewsky et al.[16] and Berger et al.[17] If a spin-polarized current is directed into a magnetic layer, angular momentum can be transferred to the magnetic layer and change the orientation of the magnetization. This can be used to excite oscillations or, as it is the case for the CIS, even flip the orientation of the magnetization. A critical current density must be reached for the CIS. Thus, a low resistivity barrier is required as otherwise a dielectrical breakdown of the barrier is caused.

The main advantages of such an MRAM compared to the common memory devices are a lower power consumption, an infinite number of possible writing and reading processes, a high velocity for switching and reading, and the non-volatility, combined in one device.[18] However, remaining challenges for a future commercialization are a low memory density and thermal stability, a poor scalability due to the geometrically induced vortex magnetization at submicron dimensions, and the high operation current density.

Theoretical calculations predict that MTJs based on electrodes with *perpendicular magnetic anisotropy* (pMA), so-called *perpendicular magnetic tunnel junctions* (pMTJs), have the potential to cope with these challenges. Figure 3 shows such a pMTJ with (a) parallel and (b) antiparallel relative orientation of the magnetization.

The switching current density for pMTJs is predicted to be lower than for devices with the same magnetic anisotropy field, but in-plane magnetic anisotropy.[19] The reason for the reduced switching current density is the absence of an easy-plane anisot-

[16] J. Slonczewski, J. Magn. Magn. Mater. **159**, L1 (1996)

[17] L. Berger, Phys. Rev. B **54**, 9353 (1996)

[18] J. Wecker et al., *Nichtflüchtige Datenspeicherund mit magnetischen Tunnelelementen: Das Magnetic Random Access Memory (MRAM)* (Forschungszentrum Jülich GmbH: Vorlesungsmanuskripte des 30. IFF-Ferienkurses, 1999)

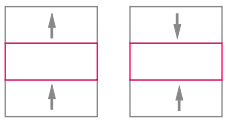

Figure 3: A magnetic tunnel junction based on electrodes with perpendicular magnetic anisotropy. (a) Parallel and (b) antiparallel orientation of the magnetization.

[19] S. Mangin et al., Nat. Mater. **5**, 210 (2006); and H. Meng et al., Appl. Phys. Lett. **88**, 172506 (2006)

ropy term caused by the demagnetization field, which increases the switching current density without contributing to the activation energy.[20] For devices with in-plane anisotropy, the current must overcome an additional additive factor $2\pi M_s$ where M_s is the saturation magnetization.

The thermal stability factor Δ[21] of the soft magnetic layer in an MRAM cell has to be larger than 40-60 for data retention of 10 years.[22] Devices with in-plane anisotropy and dimensions of less than 40 nm show difficulties in maintaining the required Δ for non-volatility. In contrast, MTJs adopting perpendicular magnetic anisotropy electrodes, are predicted to have a larger magnetic anisotropy constant K compared to devices with electrodes based on materials with in-plane anisotropy.[23] As the thermal stability factor Δ is proportional to both, the anisotropy K, and the volume V of the memory cell, a further miniaturization of the MRAM devices, and thus an increase of the memory density is possible by using electrodes with pMA.

Not only the size limitations, but also the shape limitations of MTJ elements are eliminated by using materials with pMA.[24] Up to now, the scalability of the devices with in-plane anisotropy is limited. If these materials are patterned into submicron elements, magnetization curling occurs at the edge of the film, resulting in vortex magnetization. Additionally, a fluctuation of the switching fields can be caused by the shape of the tunnel junctions. The conventional in-plane MTJ must have an aspect ratio (length/width) of 2 or more to ensure information storing. Such an MTJ with a high aspect ratio decreases the density of an MRAM.[25] Furthermore, partial demagnetization and incoherent switching is possible in an MRAM based on in-plane MTJs, if the MTJ cell is selected by only one current line. These prevent the uniform alignment of magnetic moments and selection failure resulting in the fail bit, which cannot be determined as a clear signal.[26]

However, pMTJs in general have no limit on the cell aspect ratio of patterned elements.[27] A relatively low saturation magnetization and the shape independence of materials with pMA causes a coherent magnetization reversal in the magnetized thin film and little fluctuation of the switching field during the writing process.[28]

[20] Z. R. Tadisina et al., J. Appl. Phys. **107**, 09C703 (2010)

[21]
$$\Delta = \frac{KV}{k_B T}$$
with K: magnetic anisotropy constant, V: Volume of the soft layer, KV: energy barrier separating the two magnetization directions, k_B: Boltzmann constant, T: Temperature

[22] S. Ikeda et al., IEEE Trans. Electr. Dev. **54**, 991 (2007)

[23] S. Mangin et al., Nat. Mater. **5**, 210 (2006)

[24] I. Yoo et al., J. Appl. Phys. **97**, 10C919 (2005); and N. Nishimura et al., J. Appl. Phys. **91**, 5246 (2002)

[25] S. Lim et al., J. Magn. Magn. Mater. **223**, 192 (2001)

[26] W. Park et al., J. Appl. Phys. **96**, 1748 (2004)

[27] I. Yoo et al., J. Appl. Phys. **97**, 10C919 (2005); and N. Nishimura et al., J. Appl. Phys. **91**, 5246 (2002)

[28] N. Nishimura et al., J. Appl. Phys. **91**, 5246 (2002)

Up to now, different materials have been integrated as perpendicularly magnetized electrodes into magnetic tunnel junctions. The pMA in these materials originates from different mechanisms. Here, an overview about the main research concerning materials with pMA for the use in MTJs, is given.

The first class of materials, that has been used for realizing current induced switching of pMTJs, are amorphous rare earth (RE) transition metal (TM) alloys, such as Tb-Co-Fe or Gd-Co-Fe. These are ferrimagnets with the RE and the TM having antiparallel magnetic moments. The moments are aligned perpendicular to the sample surface and a perpendicular magnetic anisotropy results.[29] The reason for the occurrence of this perpendicular anisotropy is a short-range order on the nearest neighbor atomic scale.[30] TMR-ratios of about 50 % at room-temperature have been reported for junctions with electrodes based on RE-TM alloys and an alumina barrier.[31] This value is comparable to the recent results for alumina based magnetic tunnel junctions with in-plane anisotropy.[32]

Ohmori et al.[33] succeeded in overcoming the difficulties of using RE-TM alloys in combination with an MgO (100) tunneling barrier and showed a TMR-effect of 64 % at room-temperature. The first report of current induced switching for a pMTJ has been realized with tunnel junctions with Tb-Co-Fe electrodes.[34] The free layer of the junction was switched by a 100 ns pulse current with a current density of $4.7\,\mathrm{MA/cm^2}$.

However, since a high temperature treatment may cause a degradation of the pMA of RE-TM films,[35] these pMTJs are not easy to fabricate because of the requirement of the high temperature process[36] to attain MgO (100) textured films.

A straightforward method to fabricate perpendicular magnetized electrodes for magnetic tunnel junctions is using multilayers of alternating nonmagnetic and magnetic materials. The pMA in these structures is a result of the broken symmetry at the interfaces between the magnetic and the nonmagnetic layers. In particular, Co-based multilayers, such as Co/Pd and Co/Pt have gained considerable attention. The magnetic properties of these materials, such as the saturation magnetization and the coercivity, can be manipulated easily, as a lot of parameters are accessible. For

[29] Y. Mimura et al., J. Appl. Phys. **49**, 1208 (1978); M. Mansuripur et al., J. Appl. Phys. **69**, 4844 (1991); A. Lyberatos et al., Phys. Rev. B **53**, 5493 (1996); and F. Hellman et al., J. Appl. Phys. **86**, 1047 (1999)

[30] R. B. van Dover et al., J. Appl. Phys. **57**, 3897 (1985)

[31] N. Nishimura et al., J. Appl. Phys. **91**, 5246 (2002)

[32] H. X. Wei et al., J. Appl. Phys. **101**, 09B501 (2007); and D. Wang et al., IEEE Trans. Magn. **40**, 2269 (2004)

[33] H. Ohmori et al., J. Appl. Phys. **103**, 07A911 (2008)

[34] M. Nakayama et al., J. Appl. Phys. **103**, 07A710 (2008)

[35] T. Katayama et al., J. Appl. Phys. **49**, 1759 (1978)

[36] D. D. Djayaprawira et al., Appl. Phys. Lett. **86**, 092502 (2005)

example, the number and the thickness of the multilayers can be changed. In addition, multilayer films show high magnetic thermal stability.[37] Recently, a lot of research has been done to successfully integrate these materials into MTJs.[38] However, only low TMR-effects of about 15 % at room-temperature could be realized so far.

$L1_0$ ordered FePt with (001) orientation is another promising material for the use as perpendicularly magnetized electrode in pMTJs. The large perpendicular magnetic anisotropy with (001) easy axis results from a tetragonal lattice distortion by inducing a strong external strain/stress to the system. The (001) orientation of the FePt together with a lattice mismatch with the MgO (001) plane of less than 10 % are important conditions for the fabrication of fully epitaxial MTJs with a (001) orientated crystalline MgO barrier and therefore high TMR-ratios. The main research on $L1_0$ FePt is focused on the fabrication and optimization of single layers. Only a few studies report about the use of this layers as electrodes in pMTJs.[39] A maximum TMR-ratio of more than 100 % at room-temperature has been observed.

Another material that has been recently reported as perpendicular magnetized electrode in a MTJ, is a thin layer of Co-Fe-B.[40] The pMA in this system is attributed entirely to the Ta/Co-Fe-B/MgO interfacial anisotropy. These structures show a high TMR-ratio of about 120 %, high thermal stability at dimension as low as 40 nm diameter, and a low switching current of 49 μA.

[37] T. Onoue et al., J. Magn. Magn. Mater. **235**, 82 (2001)

[38] Z. R. Tadisina et al., J. Appl. Phys. **107**, 09C703 (2010); L.-X. Ye et al., IEEE Trans. Magn. **44**, 3601 (2008); J.-H. Park et al., J. Appl. Phys. **103**, 07A917 (2008); R. Law et al., Appl. Phys. Lett. **91**, 242504 (2007); G. Kim et al., Appl. Phys. Lett. **92**, 172502 (2008); Y. Wang et al., J. Appl. Phys. **107**, 09C711 (2010); K. Mizunuma et al., Appl. Phys. Express **4**, 023002 (2011); M. T. Rahman et al., J. Appl. Phys. **109**, 07C709 (2011); and B. Carvello et al., Appl. Phys. Lett. **92**, 102508 (2008)

[39] G. Kim et al., Appl. Phys. Lett. **92**, 172502 (2008); and M. Yoshikawa et al., IEEE Trans. Magn. **44**, 2573 (2008)

[40] S. Ikeda et al., Nat. Mater. **9**, 721 (2010)

This thesis

Although the research has focused on integrating different materials with perpendicular magnetic anisotropy into magnetic tunnel junctions in the recent years, the reported TMR-effects are still small compared to the values of conventional magnetic tunnel junctions with in-plane anisotropy. As both, a high TMR-effect and perpendicular magnetic anisotropy are important conditions for a future commercialization of the MTJs as MRAM-devices, a further investigation and optimization of pMTJs is still essential.

In this thesis, magnetic tunnel junctions based on electrodes with pMA are investigated. Each chapters of the thesis deals with

a certain electrode material. The pMA of the investigated materials originates from different mechanisms, such as a broken symmetry at interfaces for multilayer systems, mechanical stress due to a lattice distortion, and ferrimagnetic coupling of rare-earth transition metal alloys. Each chapter starts with a short introduction about the properties of the used material. Subsequently, the magnetic electrodes are investigated. The last section of each chapter deals with the integration of the electrodes into MTJs.

The first chapter deals with the investigation of Co/Pd multilayers. For tailoring different switching fields of the electrodes in a MTJ it is essential to know the magnetic properties of the electrode material. The magnetic behavior of a Co/Pd multilayer system is characterized in dependence of the Co thickness in the multilayers as the pMA in this systems is due to a broken symmetry at the interface between the magnetic and the nonmagnetic layers. For every Co layer thickness a careful investigation of the annealing temperature dependence is carried out. The Co thickness and annealing temperature dependence of the saturation magnetization M_s and the remanent magnetization M_r, as well as their absolute values are very similar. Thus, the squareness (M_r/M_s) is nearly one for all of the investigated samples. This shows the very strong pMA and good quality of the Co-based superlattices. The surface and volume anisotropy densities as well as the critical Co thickness where the in-plane anisotropy turns into perpendicular magnetic anisotropy are calculated from the experimental data. The anisotropies increase exponentially with the annealing temperature, and the critical Co thickness stays roughly constant. The average is about 0.76 nm. This value matches the experimental data quite well.

The multilayers are successfully integrated into MTJs. To obtain a maximum TMR-ratio, a lot of parameters, such as the Co thickness in the electrodes, the material at the barrier interface, the number of multilayers, and the annealing temperature are investigated. The in-plane components of the magnetization, the stray field coupling of the individual electrodes and the diffusion of the Pd to the MgO barrier can be influenced, or rather suppressed. The optimized sample shows a maximum TMR-ratio of

about 11 % at room-temperature with two well-defined switching fields. The rectangular minor loop has two separated magnetic states at zero field. The temperature dependence of the TMR-effect and the bias-voltage dependence of the TMR-effect show similar behavior compared to a reference sample with Co-Fe-B electrodes and in-plane anisotropy. The TMR-ratio changes by a factor of 1.7 to 18.5 % at 13 K. This is the highest value reported for pMTJs with Co/Pd multilayers as perpendicular magnetized electrodes.

In the second chapter, the Pd of the multilayers is replaced by Pt, as the Pd turned out to be diffusing to the barrier at high annealing temperatures. Similar investigations, as shown in the previous chapter for Co/Pd based superlattices, are made for Co/Pt multilayers. A detailed comparison between the use of Pd and Pt as nonmagnetic layer in pMTJs based on multilayers with pMA is given.

The saturation magnetization is in the same range for Co/Pd and for Co/Pt because the magnetic material in the multilayers is the same for both systems. The coercivity of the Co/Pt is about a factor of 10 smaller compared to the Co/Pd. This is due to the fact that the Pt layers have a rougher surface than the Pd layers and, thus, the domain-wall pinning effect is not so serious in Co/Pt films. The annealing temperature behavior of the anisotropies is similar for Pt and Pd as nonmagnetic material, but the absolute values are smaller for Co/Pt since they are a result from the saturation magnetization and from the coercvity. The Co thickness-range with a squareness larger or equal to 0.9, and therefore perpendicular magnetic anisotropy, is shifted to larger values for the Co/Pt compared to the Co/Pd multilayers. This shift is also explained by the rougher surface of the Pt. If the deposited layer is rough, the effective thickness is reduced. Thus, more material has to be deposited for reaching the same effect compared to a system with the flatter surface.

The Co/Pt multilayer system is also integrated into a MTJ and the annealing temperature dependence of the TMR-effect is investigated. It is shown that, in contrast to the Pd, no diffusion takes place for the Pt based multilayer electrodes. TMR-ratios of

about 19 % at room temperature and two well-defined switching fields are observed. The TMR-effect changes by a factor of 1.9 if cooled to 13 K. It is supposed, that the magnetic coupling behavior of both Co/Pt multilayer electrodes has a stronger influence on the annealing- and measurement-temperature dependence of the TMR-effect, than reported for Co/Pd based samples.

The third chapter shows and discusses the results concerning FePt. The properties of the material are successfully optimized in order to induce a tetragonal lattice distortion. The resulting $L1_0$ structure is strongly correlated with the perpendicular magnetic anisotropy. The lattice structure and the magnetic behavior of the FePt samples are investigated in dependence of various parameters, such as the substrate temperature, the argon pressure during the sputtering process, and the Fe content in the FePt layer. A tetragonal lattice structure and a strong perpendicular magnetic anisotropy is obtained by imposing a strong internal strain/stress to the thin films via a high argon pressure and temperatures between 500 °C and 600 °C during sputtering.

The argon pressure dependence of the coherence length and of the strain tensor's averaged [001] component emphasizes the improvement of the structure with increasing pressure. The calculated coherence length matches the sputtered film thickness quite well and an increasing amount of epitaxy with increasing argon pressure is concluded from the analysis of the strain tensor. The possibility of controlling the coercivity is of large importance for practical applications of the material. In this work, the coercivity of the FePt could be manipulated by a slight variation of the Fe content compared to the equiatomic composition.

The FePt layer is integrated as the lower electrode into a pMTJ. The upper electrode is a Co/Pt multilayer system as the FePt cannot grow in the $L1_0$ structure if used as upper electrode. The room-temperature TMR-effect of this system is about 9 %.

In the last chapter of this thesis, the rare earth transition metal alloy Co-Fe-Tb is investigated. A perpendicular magnetic anisotropy with a rectangular hysteresis loop is successfully generated by carefully varying the Tb content in the Co-Fe-Tb layer.

Furthermore, the magnetic behavior of the samples is investigated in dependence of the Co-Fe-Tb thickness. The optimum conditions for a pMA are a Tb content between 13 at. % and 21 at. % and a layer thickness larger than 10 nm. The Co-Fe-Tb layers are integrated as electrodes into magnetic tunnel junctions with an MgO tunneling barrier. The Tb content in the electrodes is kept constant. The difference in the coercive fields is controlled by the thickness of the Co-Fe-Tb layers. The electrodes cannot be saturated at room-temperature with the available magnetic field of 10 kOe as the coercivity of the Co-Fe-Tb layers is large. Thus, the sample is carefully heated in small steps to align the magnetization. A temperature of 360 K is sufficient for saturating both electrodes. A TMR-effect of 16 % at 360 K and of 30 % at 13 K is attained. The transport properties of the Co-Fe-Tb based samples show no significant change compared to a reference sample with Co-Fe-B electrodes and in-plane anisotropy. It is concluded, that the available measurement temperature range between 13 K and 360 K is not close to the compensation point temperature of the Co-Fe-Tb electrodes.

Acknowledgments

First, I would like to thank my supervisors Prof. Günter Reiss as well as PD Andy Thomas for giving me the opportunity to work in their research groups and for supporting me with the work on the presented topic.

I am grateful to Andreas Hütten and Jan Schmalhorst for a lot of support and helpful discussions, to Karsten Rott for his help with the machinery, and to Aggi Windmann for the support concerning bureaucratic matter.

To all the colleagues who worked with me in the last years I am appreciative. Daniel Ebke, Volker Drewello, Savio Fabretti, Jan-Philipp Grote, Patryk Krzysteczko, Markus Meinert, Markus Schäfers, and Oliver Schebaum, should be mentioned here in particular.

Finally, I thank Volker. For everything.

Bielefeld
May 2012

Co/Pd multilayers

The first chapter deals with the investigation of Co/Pd multilayers. The discussion is based on the experimental results. The magnetic behavior of a Co/Pd multilayer system is characterized in order to tailor different switching fields for possible electrodes in a pMTJ. The surface and volume anisotropy densities as well as the critical Co thickness for the perpendicular anisotropy are calculated from fits of the experimental data. The multilayers are integrated into MTJs. A lot of parameters, such as the Co thickness in the electrodes, the material at the barrier interface, the number of multilayers, and the annealing temperature are investigated to obtain a maximum TMR-ratio. The temperature dependence of the TMR-effect and of the bias-voltage dependence of the TMR-effect are compared to a reference sample with Co-Fe-B electrodes and in-plane anisotropy.

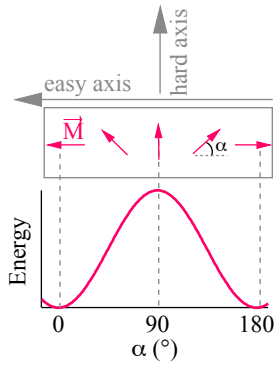

Figure 4: The magnetization of a ferromagnet has energetically preferred directions: The easy axes. The directions with maximum energy are the hard axes.

Perpendicular anisotropy in multilayers

Magnetic anisotropy (MA) is defined as the property of the magnetization in a magnetic material of being directionally dependent. In a ferromagnetic material, the direction of the magnetization has energetically preferred directions: The so-called *easy axes*.[41] The directions with maximum energy are the *hard axes*. A schematic picture is shown in figure 4.

It is possible to tailor the MA by changing the parameters of the magnetic material, such as the layer thickness, the lattice parameters and the texture or the interface layers.[42] A change of the magnetization direction from the usual direction in the film plane to the direction perpendicular to the film plane is possible.[43] This

[41] K. Kopitzki et al., *Einführung in die Festkörperphysik* (G. B. Teubner Verlag, 2004)

[42] H. Draaisma et al., J. Magn. Magn. Mater. **66**, 351 (1987); U. F. Kocks et al., *Texture and anisotropy* (Camebridge university press, 1998); and S. Ikeda et al., Nat. Mater. **9**, 721 (2010)

[43] F. J. A. den Broeder et al., Phys. Rev. Lett. **60**, 2769 (1988)

is the *perpendicular magnetic anisotropy* (pMA). Promising materials with pMA are multilayers, consisting of alternating magnetic and nonmagnetic materials.[44] The first report about a pMA in a multilayer based system has been published in 1985 by Carcia et al.[45] The pMA has been demonstrated experimentally in a multilayer system consisting of alternating layers of Cobalt and Palladium. From that time on, a lot of Co-based multilayers with pMA, such as Co/Au,[46] Co/Ru,[47] and Co/Ir[48] have been designed in order to improve the pMA.

This extensive experimental research has stimulated theoretical descriptions, particularly with regard to the microscopic origin. Despite the numerous experimental and theoretical studies, a complete, material-specific understanding of the pMA in multilayers has not yet been achieved.[49] In general, the pMA in thin films and multilayers is a result of a broken symmetry at the interface between the magnetic and the nonmagnetic material, which differs from the symmetry in the bulk. The role of interfaces or surfaces may dominate compared to the bulk contribution to the magnetic anisotropy in a system with thin magnetic layers.[50]

In a microscopic picture, the MA results from two main sources. These are the magnetic dipolar interaction and the spin-orbit interaction.[51] The dipolar interaction generally depends on the shape of the material because dipolar interactions have long range character.[52] Therefore, the contribution to the MA generated by the dipolar interaction is largely responsible for the usually observed in-plane magnetization. In the microscopic picture, the spins are coupled via the spin-orbit interaction to the orbits. The orbits are influenced by the crystal lattice. The orbital momentum and, therefore, the total magnetic moment couples to the crystal axes. Thus, the total energy depends on the orientation of the magnetization relative to the crystal axes. This so-called *magnetocrystalline* contribution to the anisotropy is strongly modified at an interface due to a lowered symmetry compared to the bulk. This interface anisotropy was first predicted by Néel in 1954.[53] The spin-orbit interaction is also responsible for the magneto-elastic or magnetostrictive anisotropy induced in a strained system. This is often the case in a multilayer-based system due to the lattice mismatch between the alternating layers. It has been shown that the in-plane

[44] A nice and detailed overview regarding the anisotropy in magnetic multilayers can be found in:
M. T. Johnson et al., Rep. Prog. Phys. **59**, 1409 (1996)

[45] P. F. Carcia et al., Appl. Phys. Lett. **47**, 178 (1985)

[46] F. J. A. den Broeder et al., Phys. Rev. Lett. **60**, 2769 (1988)

[47] M. Sakurai et al., J. Magn. Soc. Japan **15**, 411 (1991)

[48] F. J. A. den Broeder et al., J. Magn. Magn. Mater. **93**, 562 (1991)

[49] N. Nakajima et al., Phys. Rev. Lett. **81**, 5229 (1998)

[50] P. Bruno et al., Appl. Phys. A: Mater. Sci. Process. **49**, 499 (1989)

[51] P. Bruno, Phys. Rev. B **39**, 865 (1989)

[52] M. E. Fisher et al., Phys. Rev. Lett. **30**, 559 (1973)

[53] L. Néel, J. Phys. Radium **15**, 225 (1954)

volume contribution and the perpendicular interface contribution to the magnetic anisotropy can be separated into terms related to mechanical stress, crystallographic structure, roughness, and the planar shape of the films.[54]

[54] M. T. Johnson et al., Rep. Prog. Phys. **59**, 1409 (1996); and B. N. Engel et al., Phys. Rev. Lett. **67**, 1910 (1991)

MULTILAYER BASED ELECTRODES in magnetic tunnel junctions are promising materials for realizing pMTJs, as the magnetic properties of these materials, such as the saturation magnetization, and the coercivity can be easily manipulated. A lot of parameters, such as the number and the thickness of the multilayers, are accessible. In addition, multilayer films show a high magnetic thermal stability.[55] This is an important condition for realizing high TMR-effects.[56] Recently, a lot of research has been done to successfully integrate these materials into MTJs.[57] However, only low TMR-effects of about 15 % at room-temperature could be realized so far. As these values are still small compared to the maximum TMR-effects in MTJs with in-plane anisotropy,[58] a further investigation and optimization of these systems is necessary.

[55] T. Onoue et al., J. Magn. Magn. Mater. **235**, 82 (2001)

[56] D. D. Djayaprawira et al., Appl. Phys. Lett. **86**, 092502 (2005)

[57] Z. R. Tadisina et al., J. Appl. Phys. **107**, 09C703 (2010); L.-X. Ye et al., IEEE Trans. Magn. **44**, 3601 (2008); J.-H. Park et al., J. Appl. Phys. **103**, 07A917 (2008); R. Law et al., Appl. Phys. Lett. **91**, 242504 (2007); G. Kim et al., Appl. Phys. Lett. **92**, 172502 (2008); Y. Wang et al., J. Appl. Phys. **107**, 09C711 (2010); K. Mizunuma et al., Appl. Phys. Express **4**, 023002 (2011); M. T. Rahman et al., J. Appl. Phys. **109**, 07C709 (2011); and B. Carvello et al., Appl. Phys. Lett. **92**, 102508 (2008)

[58] S. Ikeda et al., Appl. Phys. Lett. **93**, 082508 (2008)

Co/Pd multilayers: The electrodes

For tailoring different switching fields of the electrodes and for reaching a maximal TMR-effect, it is essential to understand the magnetic properties of the electrode material. Therefore, the magnetic behavior of a Co/Pd multilayer system is investigated. The samples were prepared in a magnetron sputter system with a base pressure of 1×10^{-7} mbar. The layer stacks were sputtered on top of a thermally oxidized (500 nm) silicon (001) wafer. The sample structure is Si wafer/SiO/Ta 5/(Co t_{Co}/Pd 1.8)$_9$/MgO2.1 (all numbers in nm) as shown in figure 5. The samples have been annealed after sputtering at different temperatures for 60 minutes in a magnetic field of 6500 Oe perpendicular to the film plane. The annealing was done to enhance the perpendicular magnetic anisotropy of the Co/Pd multilayers. The Co layer thickness t_{Co} in the multilayer system was changed from 0.3 nm to 0.55 nm in steps of 0.05 nm. For magnetron sputtering, the deposition time is controlled to deposit a certain amount of material. As the growth of a layer is a statistical process, the thickness can only be seen as

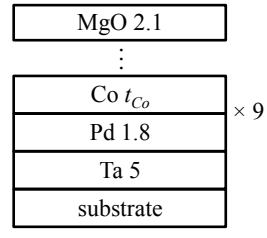

Figure 5: Stack of the electrodes. A Co/Pd multilayer system.

an effective value. Nevertheless, more effective thickness is equal to more material deposited and indeed differences are visible in the magnetization measurements for these small steps, even if the morphology of the layer is not accessible.

For every sample with a certain t_{Co} the annealing temperature T_a has been varied from room temperature (as-prepared state) to 450 °C. The magnetization measurements have been done with an alternating gradient magnetometer (Micro Mag 2900, Princeton Measurements Corporation). A special sample holder has been used to place the sample surface perpendicular to the applied external magnetic field.

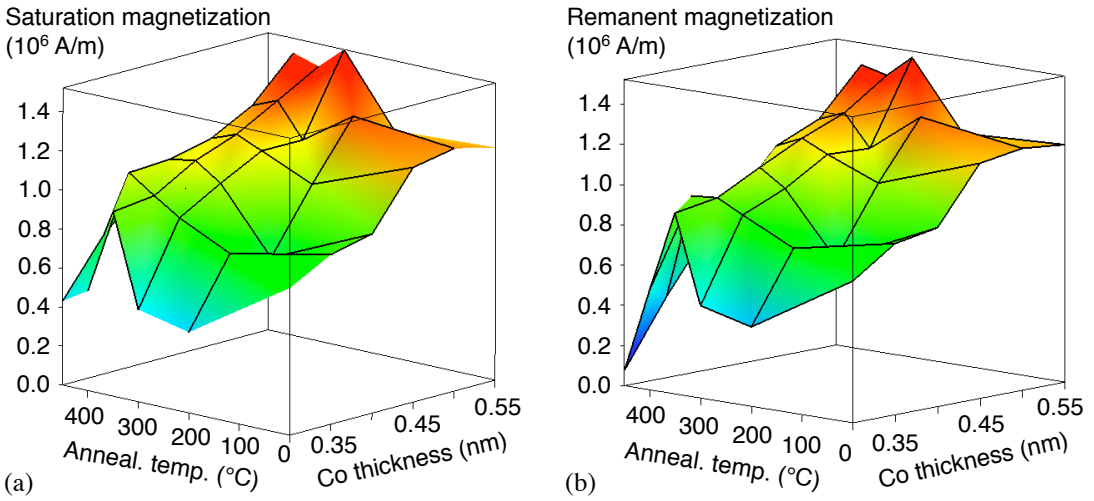

Figure 6: (a) Saturation and (b) remanent magnetization of the Co/Pd multilayer system in dependence of the Co layer thickness t_{Co} and the annealing temperature T_a.

Figure 6 (a) and (b) show the saturation magnetization (M_s) and the remanent magnetization (M_r), respectively. M_s increases with increasing Co layer thickness. The annealing temperature dependence of M_s shows that M_s first increases with increasing T_a. The maximum M_s is reached for annealing temperatures between 200 °C and 350 °C, dependent on the Co layer thickness. After reaching this maximum M_s decreases. The lowest value of M_s is about 0.413 MA/m for 0.3 nm Co, annealed at 200 °C, whereas the highest value of M_s is 1.522 MA/m at 0.55 nm Co and 300 °C.

The t_{Co} and T_a dependence of M_s and M_r, as well as their absolute values are very similar, as one can see by comparing figure

6 (a) and 6 (b). Thus, the squareness (M_r/M_s) is nearly one for all of the investigated samples. This shows the very strong pMA and good quality of the Co-based superlattices. The samples could not be saturated in the in-plane direction with an maximum magnetic field of 1.4 T available at the AGM due to the strong perpendicular magnetic anisotropy. Exemplarily, the in-plane (grey line) and perpendicular (pink line) hysteresis loops of the sample with t_{Co}=0.45 nm, annealed at 300 °C are shown in figure 7.

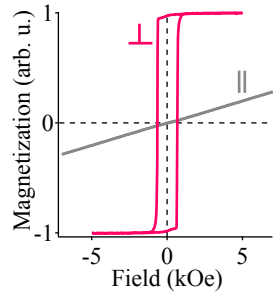

Figure 7: In-plane (grey line) and perpendicular (pink line) hysteresis loops of the Co/Pd multilayer system with 0.45 nm Co thickness, annealed at 300 °C.

Figure 8 shows the coercivity H_c of the samples in dependence of t_{Co} and in dependence of T_a. The coercivity increases with the annealing temperature for all investigated Co thicknesses. After

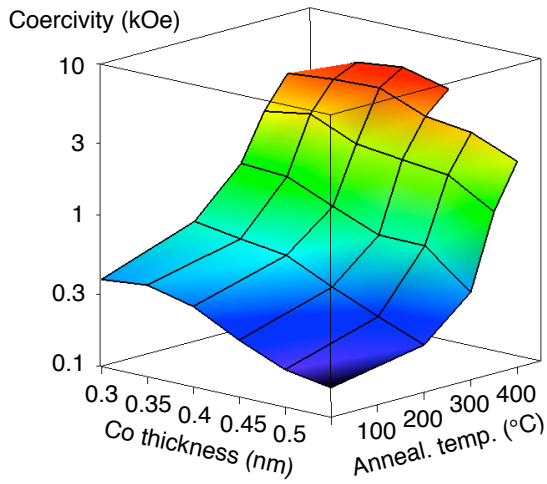

Figure 8: Coercivity of the Co/Pd multilayer system in dependence of the Co layer thickness and the annealing temperature. Please not the log-scale of the coercivity axis.

being roughly constant for Co thicknesses between 0.3 nm and 0.4 nm, dependent on the annealing temperature, the coercivity decreases with increasing t_{Co}. The lowest value is about 157 Oe for 0.55 nm Co in the as-prepared state, whereas the highest value of H_c is 5520 Oe at 0.4 nm Co and 450 °C. These values are in a typical range for Co/Pd multilayers.[59] It is reasonable that the coercivity of the Co/Pd multilayers decreases with increasing Co thickness as bulk Co has in-plane anisotropy. In the Stoner-Wohlfarth model[60] a system with in-plane anisotropy has no coercivity if magnetized with an external magnetic field perpendicular to the film plane.[61]

[59] S. Hashimoto et al., J. Magn. Magn. Mater. **88**, 211 (1990)

[60] E. C. Stoner et al., Phil. Trans. R. Soc. A **240**, 599 (1948)

[61] H. Zabel et al., *Magnetic Heterostructures* (Springer, 2008)

[62] B. N. Engel et al., Phys. Rev. Lett. **67**, 1910 (1991)

[63] L. Néel, J. Phys. Radium **15**, 225 (1954)

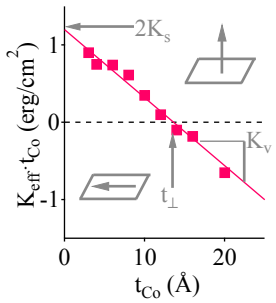

Figure 9: $K_{eff} \cdot t_{Co}$ is linear in t_{Co} with a slope of K_v and an intercept of $2K_s$. For positive values the anisotropy is perpendicular and for negative values in the film plane. The critical thickness where the in-plane anisotropy turns into perpendicular magnetic anisotropy is $t_\perp$.

The critical Co thickness $t_\perp$ at which the perpendicular magnetic anisotropy turns into in-plane anisotropy in a multilayer system can be determined from the magnetization measurements. The assumed model was established by Engel et al.[62] and is based on the inclusion of an interface and a volume term as first introduced by Néel in 1954[63] for a multilayer system. Not only $t_\perp$, but also the surface and the volume anisotropy density K_s and K_v of the Co/Pd multilayers can be determined with this model. Here, the effective anisotropy energy density K_{eff} for a multilayer system is modeled phenomenologically by the inclusion of an interface contribution, proportional to $1/t_{Co}$, and a volume term, independent of t_{Co}:

$$K_{eff} = K_v + \frac{2K_s}{t_{Co}}.$$

Thus, the product of K_{eff} and of the Co layer thickness t_{Co} can be written as

$$K_{eff} \cdot t_{Co} = K_v \cdot t_{Co} + 2K_s.$$

The product $K_{eff} \cdot t_{Co}$ should be linear in t_{Co} with a slope of K_v and an intercept of $2K_s$. A schematic picture of $K_{eff} \cdot t_{Co}$ in dependence of t_{Co} is shown in figure 9. The system has perpendicular magnetic anisotropy if the values of $K_{eff} \cdot t_{Co}$ are positive, whereas the system has in-plane anisotropy for negative values. Thus, the critical Co layer thickness $t_\perp$ where the in-plane anisotropy turns into perpendicular magnetic anisotropy can be concluded from $K_{eff} \cdot t_{Co}(t_\perp) = 0$. For every Co layer thickness, K_{eff} can be determined from the two magnetization measurements with the applied field in in-plane direction and perpendicular to the film plane. The annealing temperature dependent K_s and K_v are the fit parameters from the linear fit of $K_{eff} \cdot t_{Co}$ for every fixed T_a.

Figure 10 (a) and (b) show the volume and interface anisotropy K_v and K_s in dependence of the annealing temperature. The anisotropy K_v, as well as K_s increases exponentially with the annealing temperature. The lowest value of K_v is 0.809 Merg/cm^3 in the as prepared state, whereas the highest value is 16.911 Merg/cm^3. K_s increases from 0.033 erg/cm^2 to 0.654 erg/cm^2.

Figure 11 shows the critical Co layer thickness $t_\perp$ where the in-plane anisotropy turns into perpendicular anisotropy in dependence of the annealing temperature. Within the errors of the fits

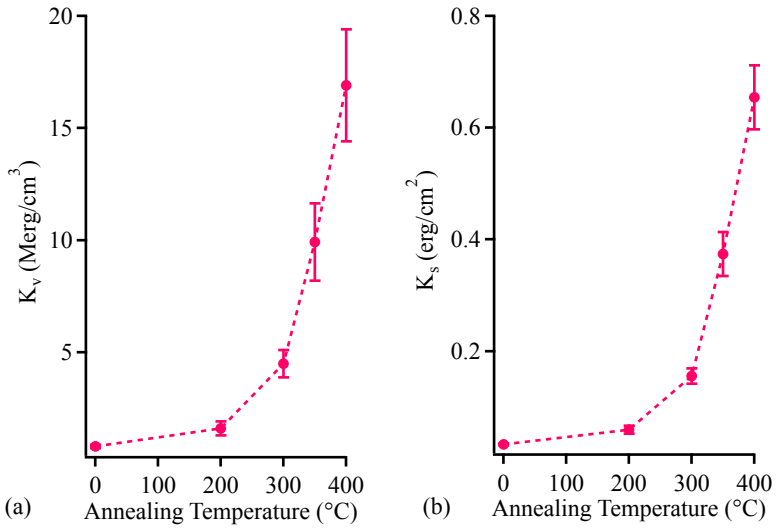

Figure 10: (a) Volume and (b) interface anisotropy K_v and K_s of the Co/Pd multilayer system in dependence of the annealing temperature.

$t_\perp$ stays constant with the annealing temperature. The average is about 0.76 nm. This value matches the experimental data quite well and is close to the literature values.[64]

The volume as well as the surface anisotropy can be slightly increased by changing the number of Co/Pd multilayers. The same magnetic investigations were made for 19 alternating layers of Co/Pd instead of 9 multilayers as already discussed. The

[64] J. V. Harzer et al., J. Appl. Phys. **69**, 2448 (1991)

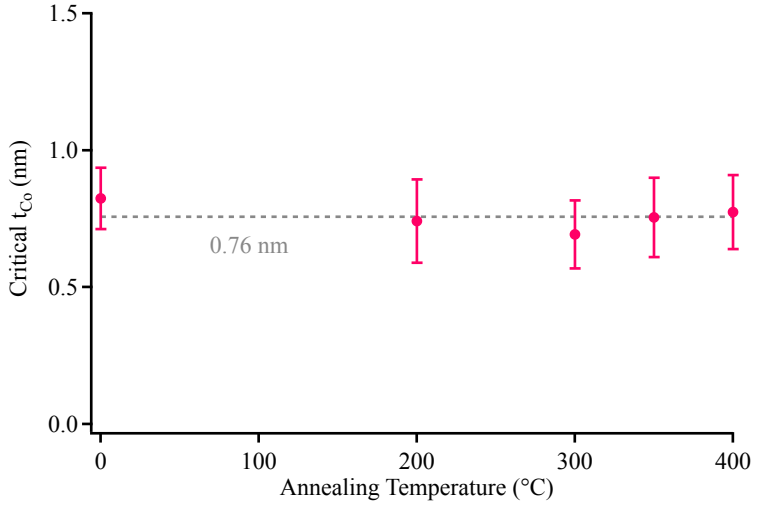

Figure 11: Critical Co layer thickness $t_\perp$ where in-plane turns into out of plane anisotropy in dependence of the annealing temperature.

anisotropies K_v, as well as K_s are increased by a factor of about 2 and 1.5, respectively. This factor is the same for all annealing temperatures. The critical Co thickness is 0.72 nm for the system with 18 multilayers. Nevertheless, all further samples were prepared with 9 Co/Pd multilayers. The increase of the anisotropy by using more multilayers is not as large that it justifies the preparation effort for such a large number of multilayers. Please note here, that two electrodes with Co/Pd multilayers are necessary for magnetic tunnel junctions. For technical reasons it is much more efficient to prepare layer stacks with a maximal number of 20 layers. Thus, further samples were prepared with 9 alternating Co/Pd layers.

Co/Pd multilayer integrated into MTJs

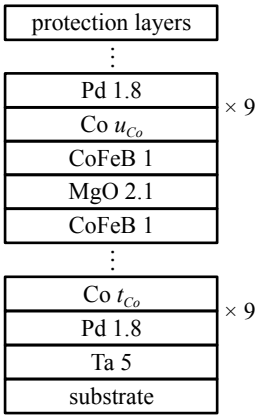

Figure 12: Stack of the pMTJs. The Co/Pd multilayer system with different Co thickness t_{Co} and u_{Co} integrated as electrodes in a magnetic tunnel junction.

The magnetization measurements demonstrate that it is possible to tune the switching field of the multilayers by changing the Co layer thickness in the Co/Pd multilayers. This is an important factor for the use of such multilayers as electrodes in pMTJs to achieve two well-defined switching fields and to stabilize the antiparallel state of the magnetization in the electrodes. Consequently, the multilayers have been integrated as electrodes in magnetic tunnel junctions. The sample stack is SiO_2/Ta 5/(Pd 1.8/Co t_{Co})$_9$/ CoFeB 1/MgO 2.1/CoFeB 1/(Co u_{Co}/Pd 1.8)$_9$/protection layers as shown in figure 12.

The Co layer thickness t_{Co} of the lower electrode has been changed from 0.25 nm to 0.5 nm to improve the switching behavior of the pMTJs and thus, the TMR-effect. For every sample with one fixed t_{Co}, the Co layer thickness u_{Co} of the upper electrode has been varied. The lower electrode was always used as the hard magnetic electrode and the upper electrode as the soft one. This means, that u_{Co} is always larger than t_{Co}. The 1 nm layer of Co-Fe-B has been used as an interface layer to improve the growth of the MgO barrier on top of the Pd/Co electrode.[65] The samples were annealed after sputtering at 150 °C for 60 minutes in a magnetic field of 6500 Oe perpendicular to the film plane to enhance the perpendicular magnetic anisotropy of the Co/Pd multilayers and to crystallize the MgO barrier. The stack was patterned by

[65] K. Mizunuma et al., Appl. Phys. Lett. **95**, 232516 (2009); and K. Yakushiji et al., Appl. Phys. Express **3**, 053003 (2010)

laser lithography and ion beam etching. The resulting patterns are squares of $7.5 \times 7.5\,\mu m^2$ and $12.5 \times 12.5\,\mu m^2$. These structures were capped with gold contact pads. The transport measurements have been done by a conventional two-probe technique with a 10 mV bias voltage in a perpendicular magnetic field.

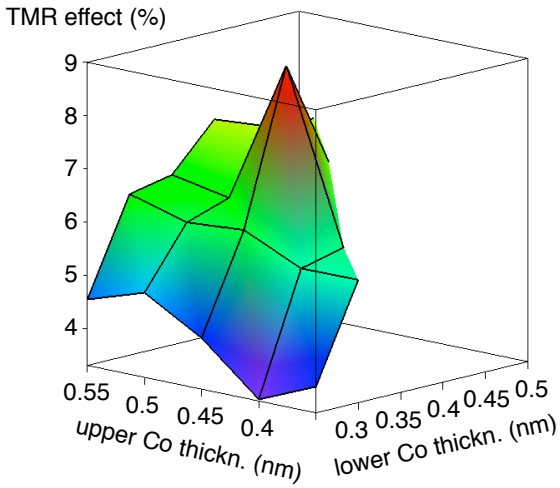

Figure 13: Room temperature TMR of samples SiO_2/Ta/(Pd 1.8/Co t_{Co})$_9$/CoFeB 1/MgO 2.1/CoFeB 1/(Co u_{Co}/Pd 1.8)$_9$/protection layers as a function of the Co layer thickness t_{Co} in the lower electrode and u_{Co} in the upper electrode.

Figure 13 shows the TMR effect as a function of the Co layer thickness in the lower electrode (t_{Co}), as well as in the upper electrode (u_{Co}). A maximum TMR effect of about 9 % is observed for t_{Co}=0.35 nm and u_{Co}=0.45 nm. This maximum is in the middle of the investigated Co thicknesses: for smaller and larger t_{Co} and u_{Co}, the TMR ratio decreases to about 3.3 %. The area-resistance products of the samples are in the range of 2 to 6 $M\Omega\mu m^2$.

The annealing temperature T_a has been optimized as it is known to have a large influence on the TMR-effect of MgO based MTJs.[66] For this investigation the best sample from figure 13 with t_{Co}=0.35 nm and u_{Co}=0.45 nm was chosen. The sample stack is shown in figure 14. The samples were annealed for one hour at different temperatures in a perpendicular magnetic field of 6500 Oe. Figure 15 (a) shows the T_a dependence of the TMR-effect.

The TMR increases from about 7 % in the as-prepared state to about 9 % at an annealing temperature of 150 °C. For T_a larger than 150 °C, the TMR decreases to 0.6 % at 300 °C. In figure 15 (b)

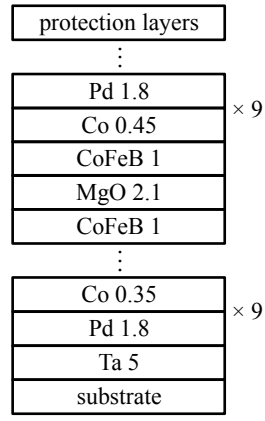

Figure 14: Stack of the pMTJ. The Co/Pd multilayer system integrated as electrodes in a magnetic tunnel junction.

[66] D. D. Djayaprawira et al., Appl. Phys. Lett. **86**, 092502 (2005)

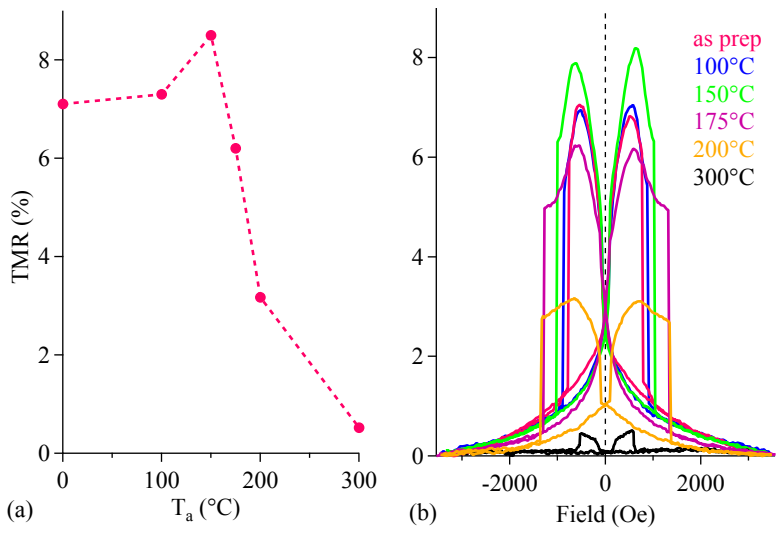

Figure 15: (a) TMR as a function of annealing temperature T_a for the sample stack .../(Pd 1.8/Co 0.35)$_9$/ Co-Fe-B 1/MgO 2.1/Co-Fe-B 1/(Co 0.45/Pd 1.8)$_9$/... (all numbers in nm). (b) Major loops of the sample annealed at different temperatures.

the major loops of the pMTJ are shown for the different T_a. The switching field of the hard electrode increases from about 770 Oe in the as prepared state to about 1360 Oe at 200 °C with increasing annealing temperature. This behavior is consistent with the results of the Co thickness dependent magnetization measurements of the Co/Pd multilayer electrodes as described in the previous section. For annealing temperatures higher than 200 °C not only the TMR-effect decreases, but also the switching field drops down to about 580 Oe.

The composition depth profiles of Pd, Co, O and Mg have been measured to clarify the origin of the strong decrease of the TMR-effect. For the determination of the depth profiles the samples were etched in many short etching steps. The intensity of each element was measured by auger electron spectroscopy after every etching step. In figure 16 (a) and 16 (b), the composition depth profiles are shown for the sample in the as-prepared state and after annealing at 300 °C for one hour, respectively.

The Pd intensity in the region of the MgO is higher in the measurement of the annealed sample, whereas a comparison of the Co intensities in the MgO region shows less Co after annealing. This indicates a diffusion of the Pd to the MgO interface, where the Pd replaces the Co at high T_a. Thus, it can be supposed here, that the

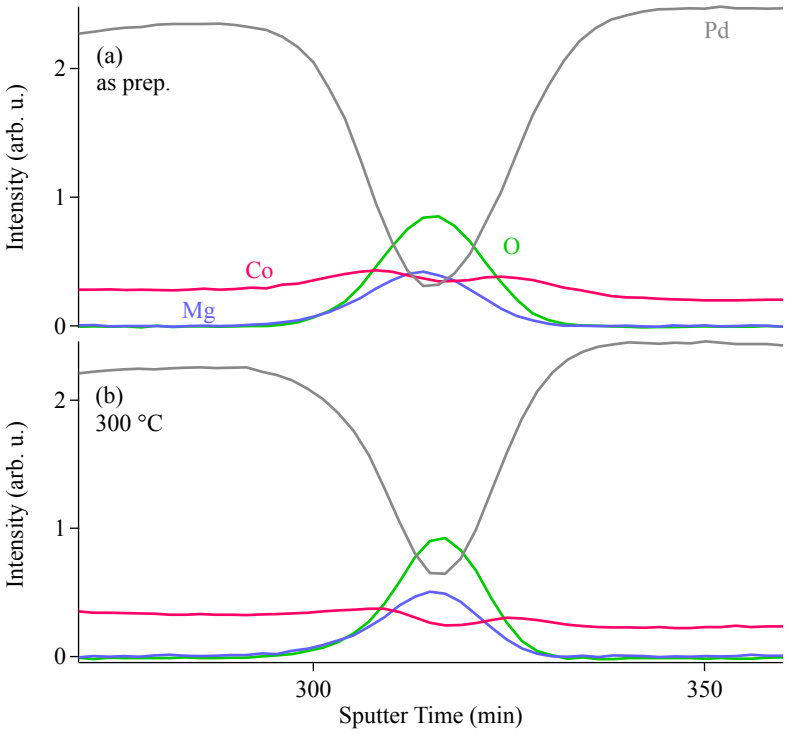

Figure 16: Composition depth profiles of Pd, Co, O, and Mg in the sample (a) before and (b) after annealing at 300 °C for 1 hour.

annealing temperature limits the TMR-effect due to the diffusion of the Pd. All further Co/Pd based samples were prepared with an annealing temperature of 150 °C.

The TMR increases before reaching zero field for all annealing temperatures, as seen in figure 15. The electrodes cannot be completely saturated in perpendicular direction with the available magnetic field of about 3200 Oe. The increase before zero field is due to a slow relative change of the magnetization directions in the electrodes. An energy term that turns the magnetization of samples with pMA before zero field is probably caused by an additional in-plane component of the anisotropy. This in-plane component is most likely caused by the Co-Fe-B layers. In figure 17 the TMR measurement of the sample annealed at 150 °C is shown with the magnetic field applied in the film plane. The relative orientation of the magnetization turns slowly with the applied field in the in-plane direction and thus causes the measured resistance change.

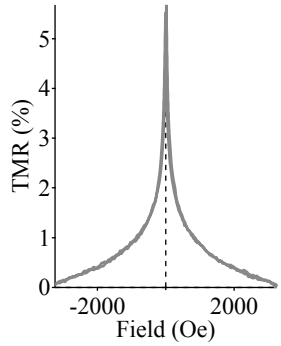

Figure 17: TMR measurement with applied magnetic field in the film plane of the sample annealed at 150 °C.

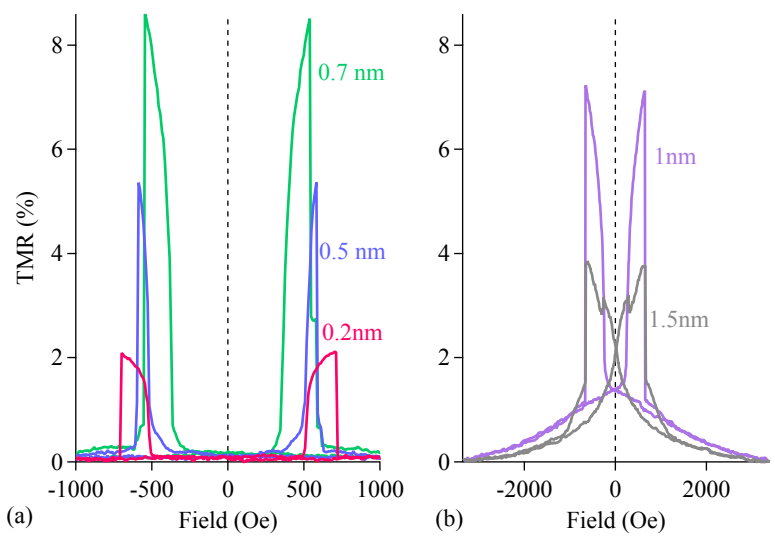

Figure 18: (a) TMR loops of samples with 0.2 nm, 0.5 nm and 0.7 nm and (b) with 1 nm and 1.5 nm Co thicknesses v at the MgO interface.

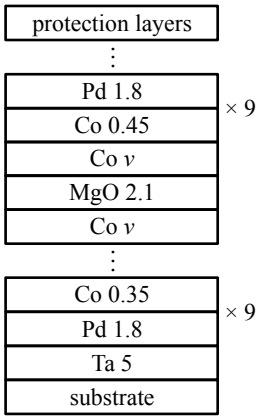

Figure 19: Stack of the pMTJ with Co as interface layer.

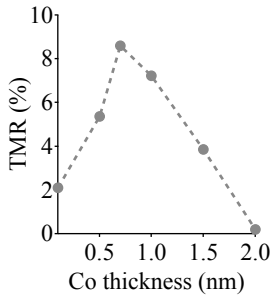

Figure 20: TMR of the pMTJ in dependence of the Co interface layer thickness v.

PMTJs WITHOUT Co-Fe-B INTERFACE LAYERS were fabricated to prove the assumption that the additional in-plane component is caused by the Co-Fe-B layers. The Co-Fe-B layers were replaced by a Co interface layer with different thicknesses v. This means, that the effective thickness of the last Co layer of the lower multilayer electrode and the effective thickness of the first Co layer of the upper multilayer electrode have been changed. Figure 19 shows the layer stack of the pMTJ with different Co thicknesses v as interface layer. In figure 18 (a) and (b) the TMR loops of samples with 0.2 nm, 0.5 nm, 0.7 nm and with 1 nm and 1.5 nm Co thicknesses v at the MgO interface are shown, respectively. The corresponding TMR-values in dependence of v are summarized in figure 20. The TMR first increases with v. After reaching a maximum at v=0.7 nm the TMR decreases again.

The highest TMR of about 9 % is similar to the TMR-ratio of the sample with 1 nm of Co-Fe-B at the MgO interface. For the samples with v smaller than 1 nm, shown in figure 18 (a), no in-plane component can be concluded from the TMR measurement. The hard electrode has a sharp switching field. This switching field decreases from about 700 Oe for 0.2 nm Co to about 550 Oe for 0.7 nm Co. In figure 18 (b) the major loops of the samples

with a Co thickness v>0.7 nm are shown. As the TMR increases before reaching zero field, an in-plane component is concluded for those samples as also described for the samples with Co-Fe-B interface layer. The samples could not be saturated with a maximum magnetic field of 3200 Oe in perpendicular direction due to this in-plane component.

In contrast to the sharp switching of the hard electrode for all investigated v in figure 18 (a) and (b), the magnetization of the soft electrode turns slowly. This broad switching is likely due to the strong magneto-static interaction between the soft and hard magnetic layers in the patterned pMTJs. The stray field of one of the perpendicular electrodes on the other electrode always assists the parallel alignment of the magnetization of the other electrode.

The number X of bilayers in a multilayer system is an important factor to influence the magnetic anisotropy of the superlattice as shown in the section "*Co/Pd multilayers: The electrodes*". In a magnetic tunnel junction consisting of two multilayer based electrodes, the magneto-static interaction of the electrodes can possibly be controlled by X. Here, the number X of Co/Pd bilayers in the lower electrode is varied from 9 to 3 to control the magneto-static interaction and to ensure the antiparallel alignment of the magnetization in the electrodes over a certain field range. The number of bilayers in the upper electrode is kept constant at 2 with a thickness of 0.7 nm. The Co thickness in the lower multilayer is 0.6 nm. A thin Mg layer was inserted under the MgO to enable better growth of the barrier.[67] The resulting sample stack is SiO_2/Ta 5/(Co 0.6/Pd 1.8)$_X$/Co 0.7/Mg 0.5/MgO 2.1/Co 0.7/(Co 0.7/Pd 1.8)$_2$/protection layers as shown in figure 21. A similar electrode configuration was used by Park et al.[68] for pMTJs based on an alumina barrier. Figure 22 shows the major loops for the different numbers X of multilayers. The samples show a room temperature TMR-effect between 8 % for X=9 and 12 % for X=3. The area resistance product is about 8.5 M$\Omega\mu$m^2. The switching field of the hard electrode increases from 300 Oe for X=9 to about 640 Oe for X=3. While the magnetization of the soft electrode turns slowly and has no sharp switching field for X=9, a hard switching is reached for X<5. The magneto-static interaction of

[67] K. Tsunekawa et al., Appl. Phys. Let. **87**, 072503 (2005)

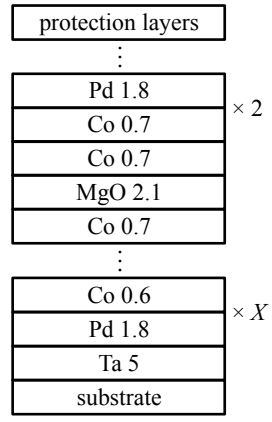

Figure 21: Stack of the pMTJ. The Co/Pd multilayer number X is varied.

[68] J.-H. Park et al., J. Appl. Phys. **103**, 07A917 (2008)

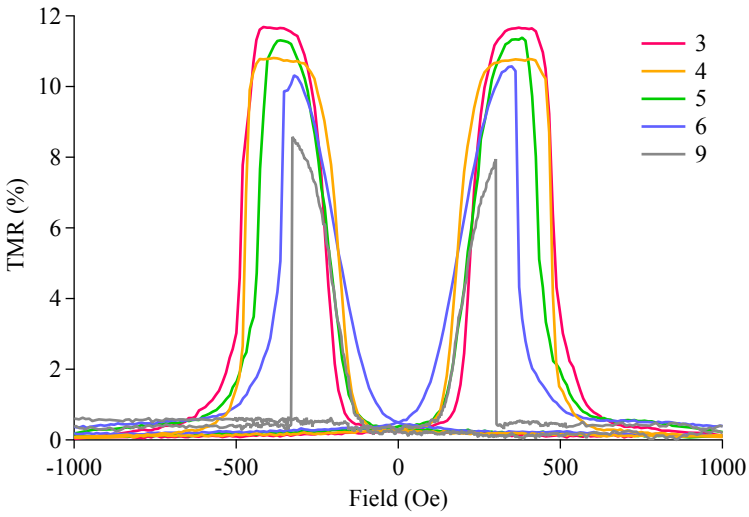

Figure 22: TMR loops of samples .../(Co 0.6/Pd 1.8)$_X$/ Co 0.7/Mg 0.5/MgO 2.1/ Co 0.7/(Co 0.7/Pd 1.8)$_2$/... with different numbers X of Co/Pd bilayers in the lower electrode.

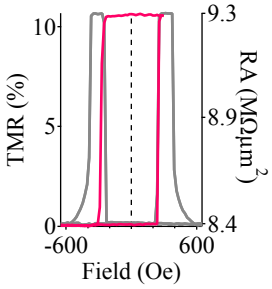

Figure 23: Major (grey line) and minor loop (pink line) of the optimized sample with X=4.

the two electrodes can successfully be controlled by reducing X, and the antiparallel alignment of the magnetization over a certain field range is finally ensured for these samples. The sample with X=4 shows optimum behavior: Two well-defined switching fields of the electrodes and a rectangular minor loop with two separated magnetic states at zero field. The major and minor loop of this optimized sample are shown in figure 23.

For magnetic tunnel junctions with perpendicularly magnetized electrodes it is known, that the stray field from the hard layer assists the switching to the parallel state due to the magnetic interaction of the electrodes. Consequently, the switching of the soft layer from the antiparallel state to the parallel state occurs at a lower field than the switching from the parallel to the antiparallel state in a minor loop.[69] Within the accuracy of the measurement procedure no shift is visible in the minor loop of the optimized sample shown in figure 23. Thus, the magneto-static interaction is small for the optimized sample and both electrodes can be supposed to be independent from each other.

[69] J.-H. Park et al., J. Appl. Phys. **103**, 07A917 (2008)

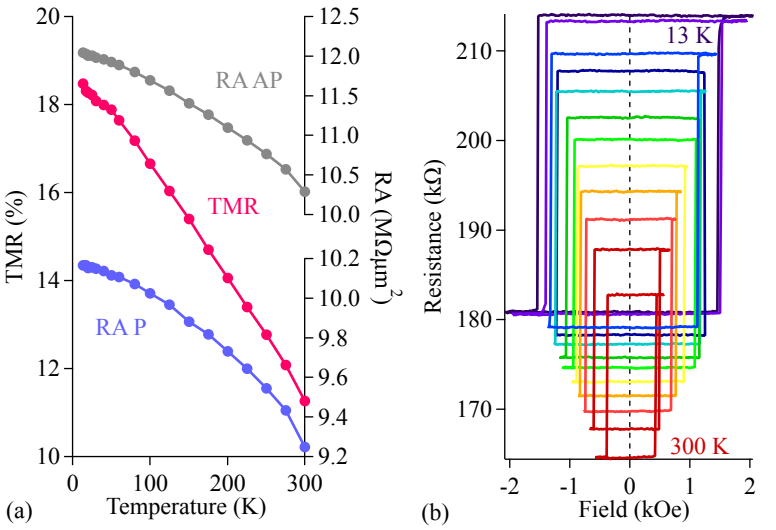

Figure 24: (a) Temperature dependent transport measurement of the sample .../(Co 0.6/Pd 1.8)$_4$/Co 0.7/Mg 0.5/MgO 2.1/Co 0.7 /(Co 0.7/Pd 1.8)$_2$/... (all numbers in nm). (b) Corresponding majorloops for the different temperatures.

Transport measurements of the optimized sample annealed at 150 °C were performed at different temperatures. The temperature dependent measurements have been carried out in a closed-cycle helium cryostat [70] with a temperature range of 13 K to 360 K.

Figure 24 (a) shows the temperature dependence of the TMR and of the area resistance products in the parallel state P and in the antiparallel state AP. The area resistance product in the P state changes from 9.2 to 10.2 MΩμm^2, this is a change of 9.8 % with the temperature which is in the typical range for the P state of MTJs.[71] The area resistance product in the AP state changes by 14.5 %, which changes the TMR-ratio by a factor of 1.7 to 18.5 % at 13 K. This is the highest value that has been reported for pMTJs with Co/Pd multilayers as perpendicular magnetized electrodes.[72] Figure 24 (b) shows some of the corresponding temperature dependent minor loops. The switching of the soft electrodes stays very sharp with the temperature. The switching field changes from about 400 Oe at room temperature to about 1540 Oe at low temperature.

The results of the temperature dependent measurement are compared to measurements of a reference sample with Co-Fe-B electrodes and in-plane anisotropy. The MgO barrier of the pMTJs is not considered to be textured, as the TMR-effects are not close

[70] Oxford Cryodrive 1.5

[71] V. Drewello et al., Phys. Rev. B **77**, 014440 (2008); and J. Schmalhorst et al., Phys. Rev. B **75**, 014403 (2007)

[72] K. Mizunuma et al., Appl. Phys. Lett. **95**, 232516 (2009); and D. Lim et al., J. Appl. Phys. **97**, 10C902 (2005)

[73] D. D. Djayaprawira et al., Appl. Phys. Lett. **86**, 092502 (2005); and S. Ikeda et al., Appl. Phys. Lett. **93**, 082508 (2008)

[74] J. O. Hauch et al., Appl. Phys. Lett. **93**, 083512 (2008)

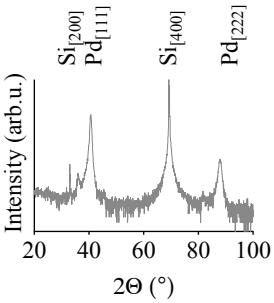

Figure 25: The x-ray diffraction measurement shows that the electrode Ta 5/(Co 0.6/Pd 1.8)$_4$/Co 0.7/MgO 2.1 has fcc (111) orientation

protection layers
NiFe 3
CoFeB 4
Al 1.2 + Ox
CoFeB 4
MnIr 12
Cu 5
Ta 5
Cu 30
Ta 5
substrate

Figure 26: Stack of the reference sample. An Alumina based system with in-plane anisotropy.

Figure 27: (a) Normalized TMR as a function of the temperature for the pMTJ and for a reference sample .../Mn-Ir 12/Co-Fe-B 4/Al 1.2+Oxidation/Co-Fe-B 4/Ni-Fe 3/... with in-plane anisotropy. (b) Normalized TMR as a function of the bias voltage for the pMTJ and for the reference sample measured at 13 K.

to that in the coherence tunneling scheme in epitaxially MgO-bcc systems.[73] Furthermore, x-ray diffraction measurements show that the Co/Pd electrodes have fcc (111) orientation as shown in figure 25. Even for MgO barriers with (111) texture coherent tunneling can not be expected.[74] Thus, an MTJ with an amorphous alumina-based barrier has been chosen as the reference sample. The sample structure of the reference sample is Si wafer/SiO/Ta 5/Cu 30/Ta 5/Cu 5/Mn-Ir 12/Co-Fe-B 4/Al 1.2+Oxidation/Co-Fe-B 4/Ni-Fe 3/Ta 5/Cu 20/Au 20 as shown in figure 26. The reference sample has been annealed at 275°C and shows a TMR-ratio of 110 % at 10 mV and 13 K.

In figure 27 (a) the temperature dependence of the TMR-effect and in (b) the bias voltage dependence of the TMR-effect are shown for the pMTJ and the reference sample. The TMR of the pMTJ changes by a factor of 1.7 if cooled to 13 K, whereas the reference sample changes by a factor of 1.6. This is no fundamental change in the temperature dependence of the samples. Also the bias voltage dependence of the TMR for the pMTJ with Co/Pd electrodes shows no significant change compared to the in-plane reference sample. A peak-like maximum is observed for zero bias, and the TMR decreases to the half-value for bias voltages of about 400 mV.

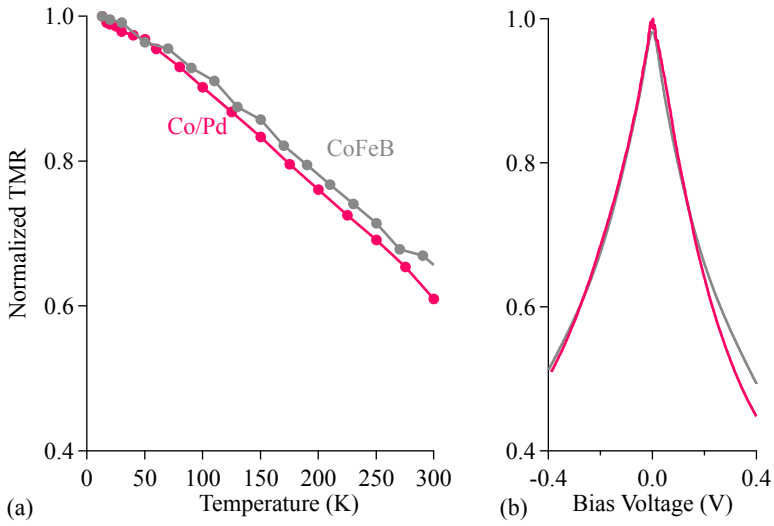

In summary, magnetic measurements of the Co/Pd multilayers were performed. The Co layer thickness in the multilayers has carefully been varied as the perpendicular magnetic anisotropy is a result of a broken symmetry between the nonmagnetic and the magnetic layers. For every Co layer thickness, a detailed investigation of the annealing temperature dependence has been carried out. This is of large importance as the interface anisotropy, the surface anisotropy, the critical Co thickness, as well as the interface magnetization have been calculated from the results. The Co thickness- and annealing temperature-dependence of the saturation magnetization and the remanent magnetization, as well as their absolute values are very similar for all of the investigated samples with Pd as nonmagnetic layer. Thus, the squareness is nearly one for all of the investigated samples. This shows the very strong perpendicular magnetic anisotropy and good quality of the Co/Pd based superlattices. The anisotropies increase exponentially with the annealing temperature, and the critical Co thickness stays roughly constant.

The Co/Pd multilayers have successfully been integrated as electrodes into MTJs. A detailed analysis of the influence of the preparation parameters on the TMR-effect has been given. The effects of the Co layer thickness in the multilayer electrodes, the annealing temperature, the Co thickness at the MgO barrier interface, and the number of Co/Pd bilayers on the TMR-effect were investigated. The in-plane components of the magnetization, the stray field coupling of the individual electrodes and a diffusion of the Pd to the MgO barrier have been successfully controlled. Finally, a TMR-effect of about 11 % at room temperature with two well-defined switching fields has been observed with the optimized conditions. A rectangular minor loop with two separated magnetic states at zero field has been observed. The TMR-ratio changes by a factor of 1.7 to 18.5 % at 13 K. This is the highest value reported for magnetic tunnel junctions with Co/Pd multilayers as perpendicular magnetized electrodes.

Most of the results of this chapter have been published in Journal of Magnetism and magnetic Materials in 2011.[75]

[75] Z. Kugler et al., J. Magn. Magn. Mater. **323**, 198 (2011)

Co/Pt multiayers

In this chapter, pMTJs with Co/Pt multilayer based electrodes are investigated. The results are compared to the measurements of the Pd based samples and a detailed comparison of the use of Pd and Pt as the nonmagnetic material in multilayers is given. The obtained differences are related to a rougher surface of the Pt layers compared to the Pd layers. For the MTJs it will be shown in this chapter that no diffusion at high annealing temperatures takes place for the Pt based multilayer electrodes. The magnetic coupling behavior of the two Co/Pt electrodes has a stronger influence on the annealing- and measurement-temperature dependence of the TMR-effect than reported for Co/Pd based samples.

Another material has to be used as nonmagnetic layer in the multilayer system, so that the Pd layers are substituted by this material. The annealing temperature for Co/Pd based pMTJs is limited to 150 °C as shown in the last chapter. A diffusion of the Pd to the MgO barrier causes a reduction of the TMR-effect at higher annealing temperatures. It is possible to use Pt instead of Pd as the nonmagnetic layer in Co-based superlattices for reaching a high pMA. The advantage of using Co/Pt compared to Co/Pd multilayers as perpendicular magnetized electrodes in tunnel junctions is not only a smaller diffusion probability of the Pt,[76] but also a smaller coercivity of the Co/Pt based electrodes.[77] A small coercivity but still large pMA is an essential condition for the applicability of pMTJs in memory devices.

In this chapter, similar investigations are made for Co/Pt multilayers and pMTJs as shown in the last chapter for Co/Pd based samples. Thus, a detailed comparison between the use of Pd and Pt as the nonmagnetic layer in multilayers and pMTJs is possible.

[76] M. T. Johnson et al., Rep. Prog. Phys. **59**, 1409 (1996)

[77] S. Hashimoto et al., J. Appl. Phys. **66**, 4909 (1989); and Y. Ochiai et al., IEEE Trans. Magn. **25**, 3755 (1989)

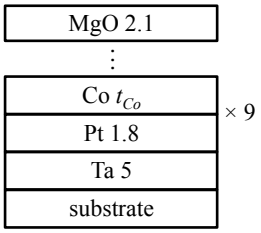

Figure 28: Stack of the Co/Pt multilayer sample. A possible electrode for pMTJs.

The electrodes: A Co/Pt multilayer system

First, the magnetic behavior of the Co/Pt multilayer system is investigated. The sample layer structure used here is Si wafer/SiO/Ta 5/(Co t_{Co}/Pt 1.8)$_9$/MgO 2.1, even thought the electrodes of the optimized Co/Pd pMTJ have another multilayer structure. The layer stack is sketched in figure 28. This sample structure has been used for a better comparison between the Co/Pd and the Co/Pt system, because this kind of multilayer system was used for the Co/Pd multilayers before optimizing the system. The Co layer thickness t_{Co} and the annealing temperature T_a have been varied. Figure 29 (a)-(d) show the saturation magnetization (M_s), remanent magnetization (M_r), squareness (S=M_r/M_s), and coercivity (H_c) in dependence of t_{Co} and of T_a. Here, t_{Co} is varied in the range of 0.35 nm to 0.95 nm in steps of 0.05 nm. The annealing

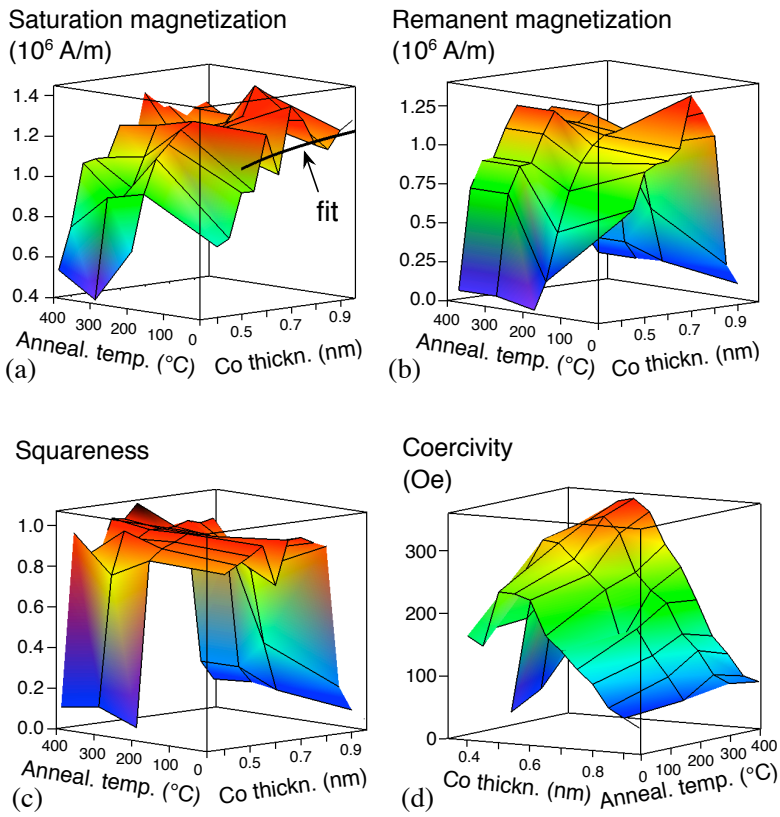

Figure 29: Magnetic properties of Co/Pt multilayers in dependence of the Co layer thickness t_{Co} and annealing temperature T_a. The black curve in (a) shows the fit of the saturation magnetization with the interface magnetization as fit parameter for the as prepared state.

temperature is changed for every fixed t_{Co} from room temperature (as-prepared state) to 400 °C in steps of 100 °C.

The saturation magnetization M_s increases with increasing Co layer thickness, as shown in figure 29 (a). M_s increases faster for small t_{Co}, and adapts the Cobalt bulk magnetization of about 1334 ± 194 kA/m for larger t_{Co}. The error results from the inaccuracy of the magnetic volume determination and the measurement procedure. The bulk magnetization was measured on the sample Si wafer/SiO/Ta 5/Pt 1.8/Co 30/Pt 1.8/MgO 2.1. This sample stack is shown in figure 30.

MgO 2.1
Pt 1.8
Co 30
Pt 1.8
Ta 5
substrate

Figure 30: Stack of the Co-bulk sample. The determined magnetization is 1365 kA/m.

M_s stays roughly constant with the annealing temperature for all investigated t_{Co}. The lowest value is about 412 kA/m for 0.35 nm Co and 300 °C annealing temperature, whereas the highest value is about 1365 kA/m for 0.90 nm Co and 200 °C.

Figure 29 (b) shows the remanent magnetization in dependence of the annealing temperature and of the Co thickness. M_r increases for small t_{Co}. After reaching a maximum at $t_{Co} = 0.7$ nm M_r decreases rapidly. The annealing temperature dependence of M_r shows that it is roughly constant as also shown for M_s. The lowest value is about 0.3 kA/m for 0.35 nm Co and 200 °C annealing temperature. The highest value is about 1387 kA/m for 0.7 nm Co in the as prepared state.

The behavior of M_s and M_r, as well as the absolute values are similar for $0.4\,\text{nm} \leq t_{Co} \leq 0.8\,\text{nm}$, as one can see by comparing figure 29 (a) and 29 (b). The squareness $S = M_r/M_s$, shown in figure 29 (c), is about one for the samples with t_{Co} between 0.4 nm and 0.8 nm. Thus, not only for Pd, but also for Pt based superlattices, a strong pMA and good quality of the samples in this t_{Co}-range is obtained. For t_{Co} smaller than 0.4 nm or larger than 0.8 nm S decreases. Also S stays roughly constant with T_a since M_r and M_s are independent of T_a.

The coercivity, shown in figure 29 (d), increases with the annealing temperature. The coercivity first increases with increasing t_{Co}. For $t_{Co} > 0.55$ nm H_c decreases. The lowest value is about 27 Oe for 0.35 nm Co and 200 °C, whereas the highest value of H_c is 351 Oe at 0.55 nm Co and 400 °C.

Figure 31 shows the magnetization measurement with perpendicular (pink line) and in-plane (grey line) magnetic field of the

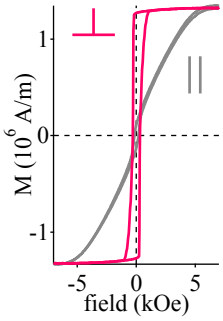

Figure 31: Perpendicular (pink line) and in-plane (grey line) hysteresis of the Co/Pt multilayer sample with 0.55 nm Co thickness, annealed at 300 °C.

sample with 0.55 nm Co, annealed at 300 °C. In contrast to the Co/Pd multilayer system, the Co/Pt based one can be saturated in the in-plane direction with an external field of about 7000 Oe.

The critical Co thickness $t_\perp$ where the perpendicular magnetic anisotropy turns into in-plane anisotropy as well as the effective interface and volumeanisotropy density constants K_s and K_v are determined from the magnetization measurements. This has also be done for the Co/Pd multilayer system. The assumed model and the calculation process are described in the chapter "*Co/Pd multilayers: The electrodes*".

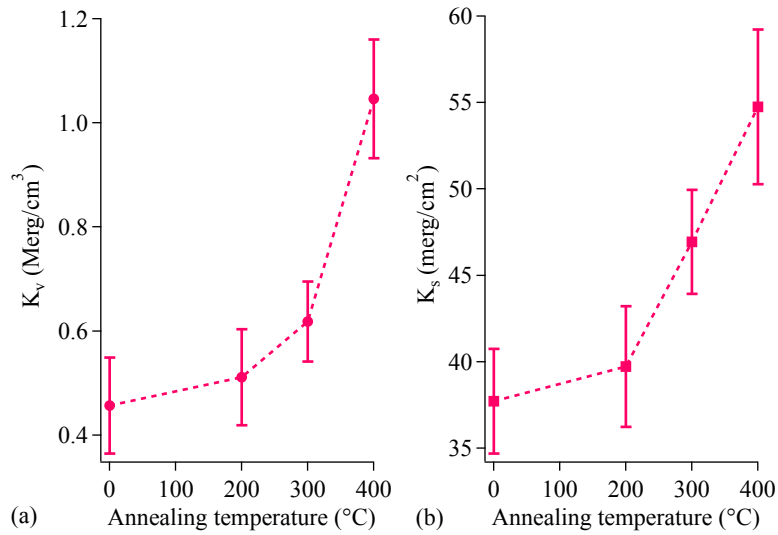

Figure 32: (a) Volume and (b) interface anisotropy of the Co/Pt multilayer system.

Figure 32 (a) and (b) show the volume and interface anisotropy constants K_v and K_s in dependence of the annealing temperature. K_v and K_s increase with the annealing temperature. The lowest value of K_v is 0.46 Merg/cm^3 in the as prepared state, whereas the highest value is 1.06 Merg/cm^3. K_s increases from 38 merg/cm^2 to 55 merg/cm^2.

Figure 33 shows the critical Co layer thickness $t_\perp$ where the in-plane anisotropy turns into perpendicular anisotropy in dependence of T_a. Within the errors of the fits $t_\perp$ stays constant. The average is about 1.1 nm. This value matches the experimental data quite well and is close to the literature values.[78]

[78] M. T. Johnson et al., Rep. Prog. Phys. **59**, 1409 (1996)

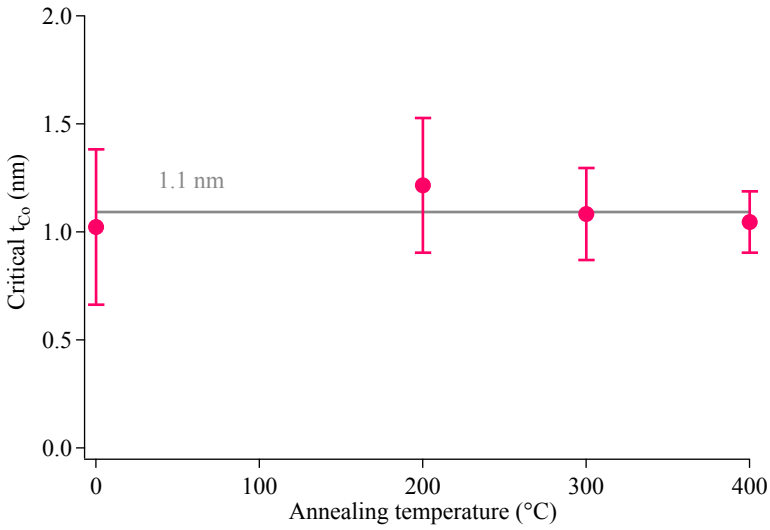

Figure 33: Critical Co layer thickness $t_\perp$ where in-plane turns into out of plane anisotropy in dependence of the annealing temperature.

The pMA of the Co/Pt multilayers is a phenomenon that occurs due to the broken symmetry at the interface of the alternating magnetic and nonmagnetic layers.[79] Thus, the interface magnetization M_{inter} at the interface to the Pt layer is an important factor for the realization of the perpendicular magnetic anisotropy. In the following paragraph, the Cobalt magnetization at the interface to the Pt layer is determined from the saturation magnetization measurements of the multilayers for all investigated annealing temperatures. A sketch of the assumed model is shown in figure 34. Here, the first Co monolayer at the Pt interface has a thickness t_{ML} and a magnetization M_{inter}. The magnetization of the rest of the Co layer with thickness t_{Co}–2·t_{ML} is called M_{bulk}. For t_{Co}>2·t_{ML} the total magnetization M_{tot} can be described by an interface term and a bulk term as

$$M_{tot} = \frac{2 \cdot t_{ML}}{t_{Co}} \cdot M_{inter} + \frac{t_{Co} - 2 \cdot t_{ML}}{t_{Co}} \cdot M_{bulk} \,.$$

M_{bulk} was measured on the sample Si wafer/SiO/Ta 5/Pt 1.8/Co 30/Pt 1.8/MgO 2.1 to be 1335 kA/m (already shown in figure 30) and t_{ML} is assumed to be 2.6 Å.[80] The T_a-dependent interface magnetization M_{inter} was determined by fitting the saturation magnetization M_s from figure 29 (a) with the equation for M_{tot} for

[79] L. Néel, J. Phys. Radium **15**, 225 (1954)

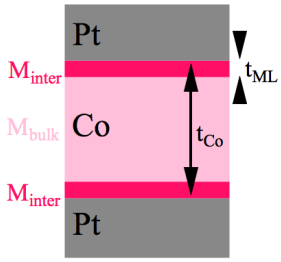

Figure 34: Sketch of Co layer with thickness t_{Co} between two Pt layers. The first monolayer of Co at the Pt interface has a thickness of t_{ML} and a magnetization of M_{inter}. The Cobalt bulk magnetization is M_{bulk}.

[80] T. Devolder et al., Z. Phys. B **22**, 193 (1975)

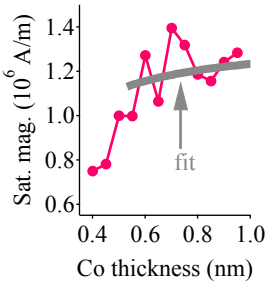

Figure 35: Fit (grey line) of the saturation magnetization (pink line) in dependence of the Co layer thickness in the as prepared state for the determination of M_{inter}.

$t_{Co}>2 \cdot t_{ML}$. The fit was done for every fixed T_a. Exemplarily, M_s and the fit for the as prepared state are shown in figure 35.

The results of the fits are summarized in figure 36. The dashed grey line marks the measured bulk value of Co. M_{inter} stays constant with the annealing temperature within the errors of the fit and measurement parameters. The average is about 1141.1 kA/m. This is about 85.5 % of the bulk value.

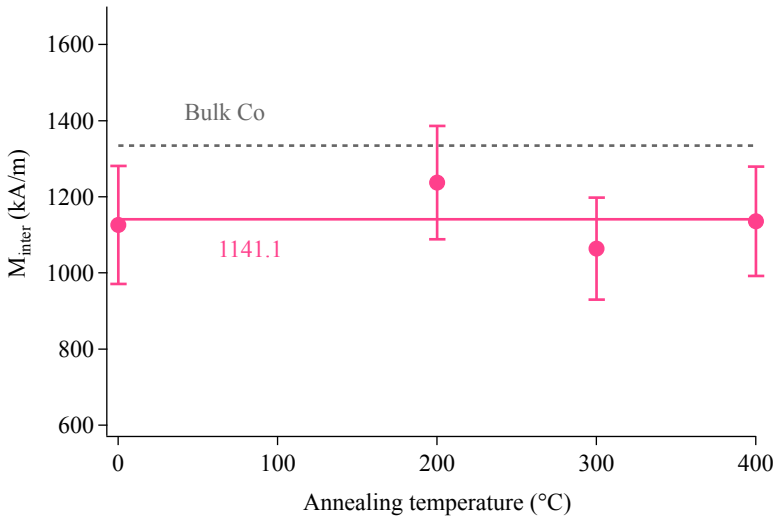

Figure 36: Calculated interface magnetization M_{inter} in dependence of the annealing temperature. The dashed grey line marks the measured bulk value of Co.

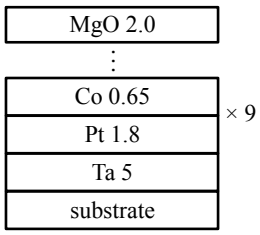

Figure 37: Stack of a Co/Pt multilayer sample for MFM measurements.

MAGNETIC FORCE MICROSCOPY (MFM) measurements were carried out on a Co/Pt multilayer sample to map the perpendicular magnetized domaines. A measurement setup from DIGITAL INSTRUMENTS has been used in combination with a standard (ML3) Co-alloy hard magnetic coated tip. A magnetic field perpendicular to the sample surface was applied during the measurement. The sample stack that has been used for the MFM measurement is MgO substrate/Ta 5/(Pt 1.8/Co 0.65)$_9$/Pt 1.8 MgO 2.0, as shown in figure 37.

Figure 38 (a) shows the MFM image of a 10 μm^2 x 20 μm^2 large area of the sample. This area has been scanned in single lines, starting at the bottom of the image. The image scale is the same for both directions. The external magnetic field has been changed during the measurement. The applied magnetic field values are

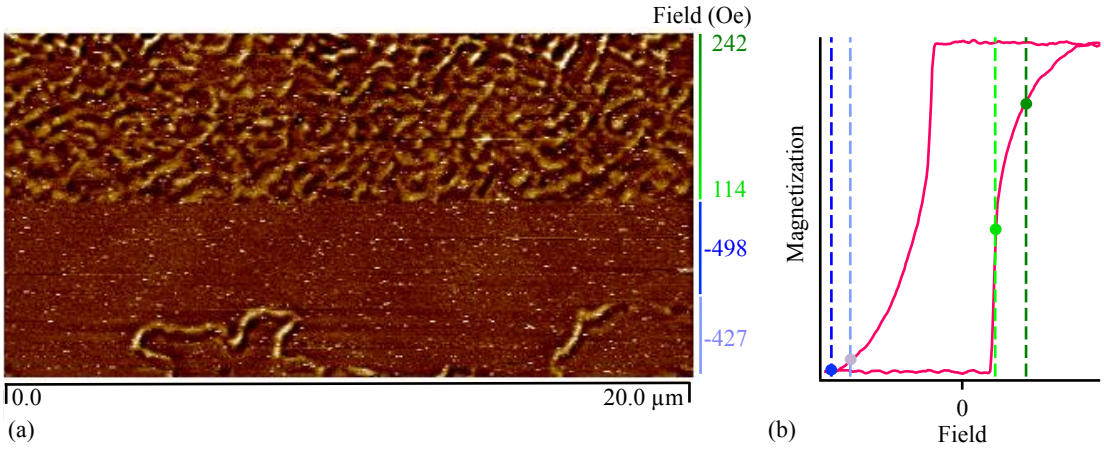

Figure 38: (a) MFM image of an $10\mu m^2 x 20\mu m^2$ large area of the sample MgO substrate/Ta 5/(Pt 1.8/ Co 0.65)$_9$/Pt 1.8 MgO 2.0. The external magnetic field has been changed during the measurement as sketched at the right margin. (b) A sketch of a hysteresis for a sample with pMA.

labeled in different colors at the corresponding areas of the sample at the right margin of the image.

A sketched hysteresis curve of a material with pMA is shown in figure 38 (b) to explain the occurrence of the different states of the magnetization in the MFM image. The field values, that have been applied during the MFM measurement are marked in the same colors as in the MFM image. The sketch should not be understood as a real magnetization measurement of the sample that has been used for the MFM investigation. The field values in a magnetization measurement differ from the values obtained with the MFM by a factor of 2. The origin for this difference could not be finally clarified, but is most likely related to the fact that different measurement setups have been used for the MFM and for the magnetization measurement. An influence of the magnetic tip or of the sample holder in the MFM setup is supposable.

The mapping of the MFM image starts at the bottom of figure 38 (a) with a perpendicular applied field of -427 Oe. The corresponding field value in figure 38 (b) is marked in violet. The light stripes in the MFM image with applied field of -427 Oe correspond to the areas of the sample with oppositely magnetized domains compared to the rest of the sample. The sample is not completely saturated in this field range as these oppositely magnetized domains occur. The corresponding magnetization state in the hysteresis is, thus, the one with decreasing magnetic field. This point is marked in violet.

The next area in the MFM image has been measured with an external magnetic field of about -489 Oe. This field value is indicated by the blue line in the hysteresis curve. All domains are forced into the same magnetization direction, and the stripes vanish: The sample is saturated. The corresponding magnetization state is indicated by the blue point in the hysteresis curve. The saturated state of the magnetization persists if the external magnetic field is now reversed.

The domain wall nucleation field is reached at 114 Oe. This field has been applied at the beginning of the last area in the MFM scan. The field has been increased from 114 Oe to 242 Oe during the scan. The minimum and the maximum field value is marked in light green and in dark green in the hysteresis curve, respectively. The accordant states in the hysteresis are indicated with points in the same colors. The light and dark stripes in the MFM image correspond to the domains with opposite magnetization direction perpendicular to the film plane. Only a small or even no net magnetization can be concluded from the state with an applied field of 114 Oe, as the domains are oppositely magnetized. This is in accordance to the corresponding state in the magnetization sketch (light green point). The domains have a diameter of about 2μm and get quenched with the increasing magnetic field to about 242 Oe. This is the dark green point in the hysteresis curve.

A COMPARISON of the measurement results and physical properties for the Co/Pd and Co/Pt multilayers is given in table 1.

The saturation magnetization is in the same range for Co/Pd and for Co/Pt because the magnetic material in the multilayers is the same for both systems. The coercivity of the Co/Pt is about a factor of 10 smaller compared to the Co/Pd. It is proposed here, that the Pt layers have a rougher surface than the Pd layers. Therefore, it is possible that the domain-wall pinning effect is not so serious in Co/Pt films and causes the reduced coercivity of Co/Pt compared to Co/Pd. Oh et al. showed similar behavior for Co/Pt and Co/Pd multilayers.[81] The surface and volume anisotropies are smaller for Co/Pt than for Co/Pd since they are a result from M_s and from H_c. The t_{Co}-range with $S \geq 0.9$ (and therefore perpendicular magnetic anisotropy) is shifted to larger t_{Co} for

[81] H.-S. Oh et al., IEEE Trans. Magn. **32**, 4061 (1996)

	M_s^{min}-M_s^{max} (kA/m)	H_c^{min}-H_c^{max} (Oe)	t_{Co} with S>0.9 (nm)
Co/Pd	413-1522	157-5520	0.3-0.55
Co/Pt	412-1365	27-351	0.4-0.8
	K_v^{asprep}-K_v^{400} (Merg/cm^3)	K_s^{asprep}-K_s^{400} (erg/cm^2)	$t_\perp$ (nm)
Co/Pd	0.809-16.911	0.033-0.654	0.76
Co/Pt	0.457-1.047	0.0377-0.0547	1.1

Table 1: A comparison of the Co/Pd and the Co/Pt system. The measurement results are listed in the first table. The second table shows the results from the fit.

the Co/Pt compared to the Co/Pd multilayers. This means, that the perpendicular magnetic anisotropy occurs at larger Co thicknesses for the Co/Pt. Therefore, it is reasonable that also $t_\perp$ is larger for the Co/Pt multilayer. The shift in the Co thickness can also be explained by a rougher surface of the Pt compared to the Pd layer. As already discussed in the first chapter, the deposition time is controlled to deposit a certain amount of material and the resulting thickness can only be seen as an effective value as the growth of the layer is a statistical process. Nevertheless, more effective thickness is equal to more deposited material. If the deposited layer is rough, the effective thickness is reduced. Thus, more material has to be deposited for reaching the same effect compared to a system with a flatter surface as it is the case for the Co/Pd multilayers.

The assumption $t_{Co}>2\cdot t_{ML}$ could not be fulfilled for the Co/Pd multilayers, as the Co thickness range for the Co/Pd multilayers with perpendicular anisotropy occurs at smaller t_{Co} than for Co/Pt multilayers and the investigated Co/Pd samples have t_{Co} between 0.2 nm and 0.55 nm. This means, that the assumed model for calculating the interface magnetization does not describe the Co/Pd based multilayer system. Thus, the fit of the interface magnetization and therefore a comparison between the interface magnetization of Co/Pt and Co/Pd is not possible.

Co/Pt multilayers integrated into MTJs

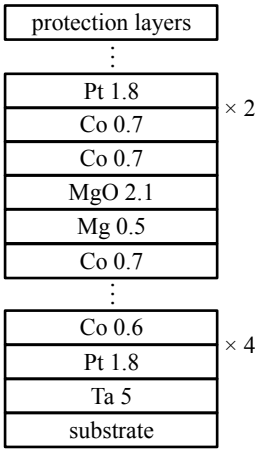

Figure 39: Stack of the Co/Pt pMTJ. A multilayer based system.

Figure 40: (a) TMR loops of sample .../(Co 0.6/Pt 1.8)$_4$/Co 0.7/Mg 0.5/MgO 2.1/(Co 0.7/Pt 1.8)$_2$/... and (b) corresponding TMR values for the different annealing temperatures.

The annealing temperature of the Co/Pt based pMTJs has been investigated to clarify if annealing at higher temperatures than for the Co/Pd based system is possible. The optimized sample stack with Co/Pd electrodes from the first chapter was used, but Pt was inserted as nonmagnetic material in the multilayers instead of Pd. The resulting sample stack is SiO_2/Ta/(Pt 1.8/Co 0.7)$_4$/Mg 0.5/MgO 2.1/Co 0.7/(Co 0.6/Pt 1.8)$_2$/protection layers as shown in figure 39.

Figure 40 (a) shows the TMR loops in the positive field range for the different T_a. In figure 40 (b) the corresponding TMR-values in dependence of the annealing temperature are shown. The TMR increases from about 16 % in the as-prepared state to about 18.6 % at an annealing temperature of 250 °C. For T_a larger than 250 °C, the TMR-ratio decreases to 0.7 %. The area-resistance product in

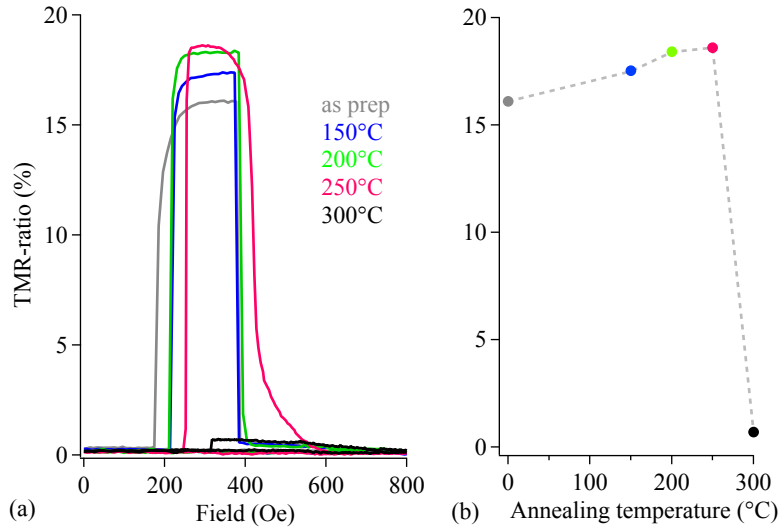

the parallel state of the samples is about 60 MΩμm^2. The optimum T_a of 250 °C is higher than the one for the Co/Pd electrodes, which was 150 °C. The maximum TMR of the pMTJ with Co/Pt is about a factor of 1.7 larger compared to the one of the Co/Pd based system. The switching field of the soft Co/Pt electrode in-

creases with increasing T_a, whereas the switching field of the hard electrode is very sharp and first remains unchanged as shown in figure 40 (a). This means, that the field range of the antiparallel alignment of the magnetization becomes smaller. For $T_a \geq 250\,^{\circ}C$ the behavior of the hard electrode changes and the magnetization turns slowly. The annealing temperature changes the magnetic behavior of Co/Pt multilayers integrated into magnetic tunnel junctions. It is proposed here, that the abrupt breakdown of the TMR for higher annealing temperatures is due to a change of the magnetic behavior of the perpendicularly magnetized electrodes. The system shows a very different behavior compared to the slow decrease of the TMR-ratio due to a diffusion as shown in the previous chapter "*Co/Pd multilayers*".

Measurements of the composition depth profiles on the Co/Pt pMTJ in the as prepared state and after annealing at 300 °C for one hour were carried out to exclude the possibility that Pt diffuses

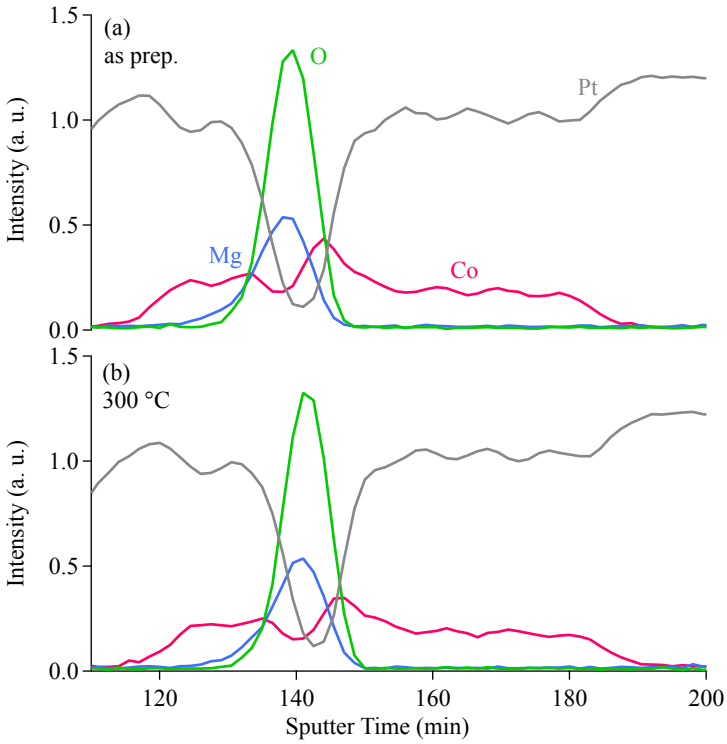

Figure 41: Composition depth profiles of Pt, Co, O, and Mg in the sample .../(Co 0.6/Pt 1.8)$_4$/Co 0.7/Mg 0.5/MgO 2.1/(Co 0.7/Pt 1.8)$_2$/... (a) before and (b) after annealing at 300 °C for 1 hour.

at high annealing temperatures. In Figure 41 (a) and 41 (b), the composition depth profiles of Pt, Co, O, and Mg are shown for the sample in the as-prepared state and after annealing at 300 °C. The Pt intensity in the region of the MgO is almost the same in the measurement of the as prepared and of the annealed sample. A comparison of the Co intensities in the MgO region shows also almost the same intensity after annealing. This indicates that, in contrast to the Pd samples, no diffusion of the Pt to the MgO interface takes place.

It is possible that the decrease of the TMR of the Co/Pt based pMTJs is due to the fact that the antiparallel alignment of the electrodes over a certain field range vanishes for $T_a > 250\,^{\circ}\mathrm{C}$ and the electrodes switch simultaneously. Supposably, the healing of defects leads to a higher energy barrier for the nucleation of domains, which explains the increase of the switching field of the soft electrode with increasing T_a. This leads up to the point where the difference in the switching fields is small enough to be overcome by the coupling of the electrodes. To clarify the situation, the magnetization switching of a structured MTJ element must be investigated. As this magnetization is a very small quantity, a special experimental method is needed. Especially, the investigation is not possible on the standard TMR structures, that have been used here.

THE TEMPERATURE DEPENDENCE of the TMR of the Co/Pt pMTJ was investigated and compared to the temperature dependence of the Co/Pd pMTJ. As the Co/Pd system showed a very sharp switching of both electrodes, and rectangular minor-loops at all measurement temperatures (see figure 24), a complete antiparallel alignment of the electrodes is assumed for the Co/Pd sample. Figure 42 shows the temperature dependence of the TMR-effects for the samples. The TMR of the Co/Pt based MTJ changes by a factor of 1.9 if cooled to 13 K, whereas the TMR of the Co/Pd based sample changes by a factor of 1.7. It can be suspected that the temperature dependent magnetic switching behavior of the Co/Pt pMTJ gives an additional component to the overall temperature dependence of the TMR-ratio. This behavior is known for tunnel junctions based on materials with perpendicularly magne-

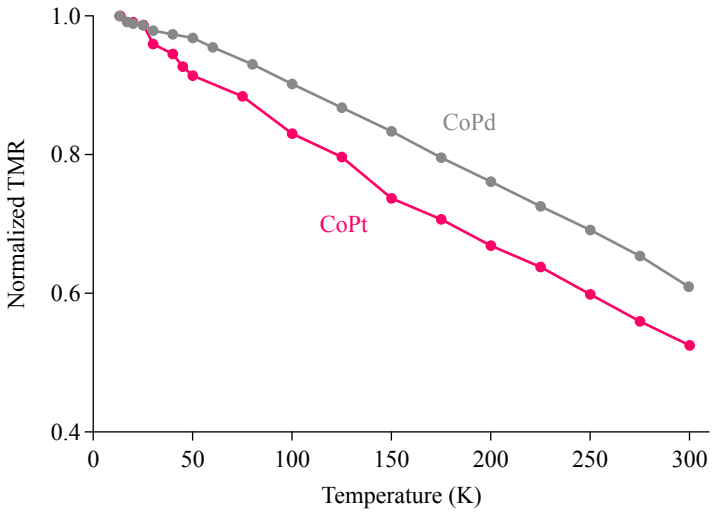

Figure 42: Temperature dependence of the TMR for the pMTJ .../(Co 0.6/Pt 1.8)$_4$/Co 0.7/Mg 0.5/MgO 2.1/(Co 0.7/Pt 1.8)$_2$/... and of the Co/Pd pMTJ with Pd layers instead of Pt.

tized electrodes and can have a large influence on the TMR-ratio.[82] This additional effect is hard to model, as it depends on the specific junction. Therefore, a straightforward fit of the temperature dependence is not possible here.

The bias voltage dependence of the TMR effect is shown and compared to the Co/Pd sample in figure 43. The bias voltage dependence of the TMR for the pMTJ with Co/Pt electrodes shows no fundamental change compared to the Co/Pd based sample. A peak-like maximum is observed for zero bias, and the TMR decreases to the half-value for bias voltages of about 350 mV.

A COMPARISON between the results of the transport measurements for the Co/Pd and Co/Pt multilayer based MTJs is shown in table 2. The maximum TMR-effect as well as the optimum annealing temperature are increased by using Pt instead of Pd as nonmagnetic material in the multilayer electrodes. Nevertheless, annealing at high temperatures is not possible for both materials as the TMR vanishes. The decrease of the TMR with the annealing temperature seems to originate from different effects for the two materials. In the case of the Co/Pd based electrodes, the intensity of the Pd at the MgO barrier is about a factor of 2.75 higher for the annealed sample compared to the as prepared one, whereas the Pt intensity stays roughly the same (last column in table 2). Thus,

[82] G. Feng et al., Appl. Phys. Lett. **99**, 042502 (2011)

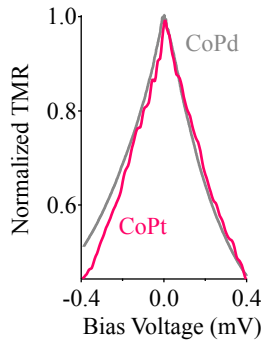

Figure 43: Normalized TMR as a function of the bias voltage for the Co/Pt and the Co/Pd pMTJ measured at 13 K.

	TMR_{rt}^{max} (%)	TMR_{lt}/TMR_{rt}	$V_{1/2}$ (mV)	opt. T_a (°C)	$Int_{300°C}/Int_{asprep}$
Co/Pd	11.0	1.7	150	390	2.75
Co/Pt	18.6	1.9	250	350	~ 1

Table 2: A comparison of the Co/Pd and the Co/Pt system. Properties of the transport measurements of the multilayers based pMTJs.

on the one hand the TMR-ratio is most likely limited due to a Pd diffusion at high annealing temperatures. On the other hand, no diffusion takes place for the Pt based multilayer electrodes, but the TMR-ratio is limited due to a change of the magnetic coupling behavior of the electrodes with increasing annealing temperature.

SUMMARIZING this chapter, Co/Pt multilayers have successfully been investigated and integrated into magnetic tunnel junctions and a detailed comparison between Pd and Pt as nonmagnetic material in Co-based multilayers is given.

Similar investigations as shown in the previous chapter for the Pd based multilayers have been carried out to characterize the electrodes of the pMTJs. The obtained differences in the coercivity, in the squareness, in the anisotropy, and in the critical Co thickness are due to a rougher surface of the Pt layers compared to the Pd layers. The coercivity of the Co/Pt is about a factor of 10 smaller compared to the Co/Pd as the domain-wall pinning effect is not so serious in the rough Co/Pt films. The annealing temperature behavior of the anisotropies is similar for Pt and Pd as nonmagnetic material, but the absolute values are smaller for Co/Pt. The Co thickness-range with a squareness larger or equal to 0.9, and therefore perpendicular magnetic anisotropy, is shifted to larger values for the Co/Pt compared to the Co/Pd multilayers. If the deposited layer is rough, the effective thickness is reduced. Thus, more material has to be deposited for reaching the same effect compared to a system with the flatter surface.

The Pd from the previous chapter has also been replaced by Pt in the pMTJs of this chapter, as the Pd turned out to be diffusing to the barrier of the tunnel junction at high annealing temperatures. The annealing temperature dependence of the TMR-effect has been investigated for the Pt based sample. It has been shown that, in contrast to the Pd, no diffusion takes place for the Pt based multilayer electrodes. TMR-ratios of about 19 % at room temper-

ature and two well-defined switching fields were observed. The TMR-effect changes by a factor of 1.9 if cooled to 13 K. The magnetic coupling behavior of both Co/Pt multilayer electrodes has a stronger influence on the annealing- and measurement-temperature dependence of TMR-effect, than reported for Co/Pd based samples.

Some of the results regarding Co/Pt samples have been published in a special conference issue of the Journal of Applied Physics in 2012.[83]

[83] Z. Kugler et al., J. Appl. Phys. **111**, 07C703 (2012)

Tetragonal FePt

This chapter deals with the characterization of thin films of FePt. The properties are optimized with the aim to induce a tetragonal $L1_0$ structure. This structure is strongly correlated with a perpendicular magnetic anisotropy. The lattice structure and the magnetic behavior of the samples are investigated in dependence of the substrate temperature, in dependence of the argon pressure during the sputtering process, and in dependence of the Fe content in the FePt layer. The coherence length and the averaged [001] component of the strain tensor are determined in dependence of the pressure. An increasing amount of epitaxy, tetragonality and perpendicular anisotropy can be concluded as the results of the optimization process. The FePt layer is integrated as the lower electrode into a pMTJ. The upper electrode is a Co/Pt multilayer system. The room-temperature TMR-effect of this system is about 9 %.

Some properties of FePt

The $L1_0$ phase of FePt thin films has gained considerable attention as a material for high-density recording[84] due to its exceptional properties, such as high magnetocrystalline anisotropy of $K_u \sim 7 \cdot 10^7\,\mathrm{erg/cm^3}$ along the c axis,[85] a Curie temperature of about 450 °C,[86] and chemical stability.

The room-temperature prepared state of FePt thin films and nanoparticles is the chemical disordered, face-centered cubic (fcc) $A1$ structure with a lattice constant of 3.8160 Å[87] and soft magnetic properties.[88] The cubic state of the FePt is shown in figure 44 (a). This state transforms to the chemical ordered, face-centered tetragonal (fct) $L1_0$ phase with hard magnetic proper-

[84] K. Coffey et al., IEEE Trans. Magn. **31**, 2737 (1995)

[85] D. Weller et al., IEEE Trans. Magn. **36**, 10 (2000)

[86] S. N. Hsiao et al., Appl. Phys. Lett. **94**, 232505 (2009)

[87] Joint Committee on Powder Diffraction Standards, *JCPDS-ICDD Powder Diffraction Database (2000)*, card No. 29-718

[88] R. A. Ristau et al., J. Appl. Phys. **86**, 4527 (1999)

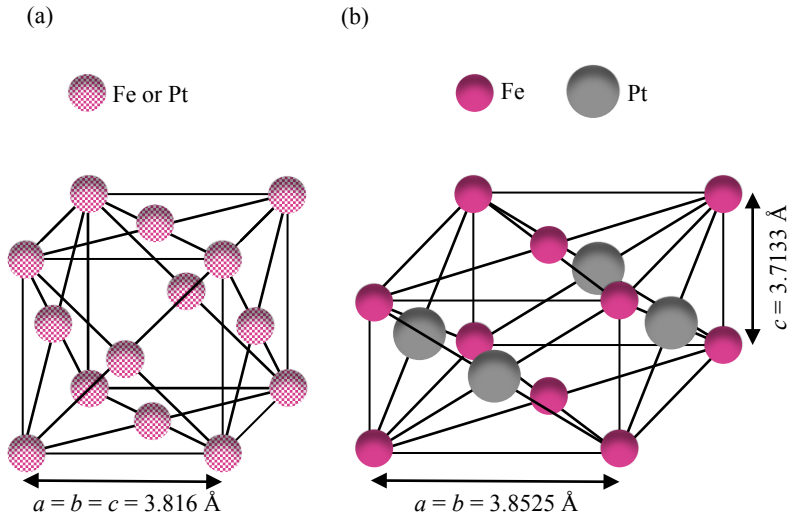

Figure 44: (a) Chemical disordered, face-centered cubic (fcc) $A1$ structure of FePt. (b) Chemical ordered, face-centered tetragonal (fct) $L1_0$ structure of FePt with equiatomic composition.

ties if the sample is prepared or post annealed at high temperatures. The ordering temperature is usually above 500 °C.[89] Theoretically, the composition of FePt has to be equiatomic for the formation of the $L1_0$ structure. It was shown experimentally that the ordering of FePt thin films can be increased by preparing slightly off-stoichiometric layers.[90] This results in a reduced ordering temperature. Figure 44 (b) shows the lattice structure of the $L1_0$ phase of the FePt at the equiatomic composition. This phase is formed of alternating monoatomic planes of Fe and Pt along the unit-cell c axis. The lattice constants are c=3.7133 Å, and a=b=3.8525 Å.[91] This structure manifests a large uniaxial magnetocrystalline anisotropy along the c axis and, thus, results in perpendicular magnetic anisotropy when grown with the monoatomic layers parallel to the film plane. This is the case for the (001) orientation with the c axis in the film normal direction.[92] The magnetic anisotropy of the $L1_0$ phase originates from a large spin-orbit coupling of the Pt atom and a strong hybridization of the Pt d-bands with highly polarized Fe d-bands. The magnetocrystalline magnetic anisotropy has the trend to increase with increasing axial ratio c/a. This is associated with the property of the magnetocrystalline magnetic anisotropy to decrease with increasing band filling as shown by Sakuma.[93] A lot of research was

[89] T. Suzuki et al., J. Appl. Phys. **85**, 4301 (1999)

[90] T. Seki et al., Appl. Phys. Lett. **82**, 2461 (2003); K. Barmak et al., J. Appl. Phys. **98**, 033904 (2005); and K. Barmak et al., J. Appl. Phys. **95**, 7501 (2004)

[91] Joint Committee on Powder Diffraction Standards, *JCPDS-ICDD Powder Diffraction Database (2000)*, card No. 43-1359

[92] T. B. Massalski, *Binary Alloy Phase Diagrams* (ASM International, 2nd ed., 1990)

[93] A. Sakuma, J. Phys. Soc. Jpn. **63**, 3053 (1994)

done to reduce the ordering temperature, because high temperatures are a challenge for practical applications of the FePt. It has been shown that the ordering of FePt thin films can be increased and the ordering temperature is reduced by several parameters, such as the buffer layer[94] and substrate,[95] the addition of third elements,[96] ion irradiation,[97] alternate monoatomic layer deposition,[98] film thickness,[99] and sputtering with high argon gas pressure.[100] The basic mechanism in all these processes is the raise of internal strain/stress, that causes a lattice distortion. Unlike bulk material, strong internal strain/stress can be imposed on thin films due to high traction interface between film and surrounding layers or substrate. This intrinsic strain/stress is equivalent to an external pressure and can be manipulated by varying the conditions of the thin film deposition process, such as the argon pressure.[101]

$L1_0$ ordered FePt with (001) orientation and therefore perpendicular magnetic anisotropy is a promising material for the use as perpendicularly magnetized electrode in pMTJs. The large perpendicular magnetic anisotropy with (001) easy axis and a lattice mismatch with the MgO (001) plane of less than 10 % are important conditions for the fabrication of full epitaxial MTJs with a (001) orientated crystalline MgO barrier and therefore high TMR-ratios. The main research on $L1_0$ FePt is focused on the fabrication and optimization of single layers. Only a few studies report on the use of this layers as electrodes in pMTJs[102] withTMR-ratios of more than 100 % at room temperature.

[94] Y.-N. Hsu et al., J. Appl. Phys. **89**, 7068 (2001); J. S. Chen et al., J. Appl. Phys. **93**, 1661 (2003); and T. Seki et al., J. Appl. Phys. **96**, 1127 (2004)

[95] M. Weisheit et al., J. Appl. Phys. **95**, 7489 (2004)

[96] T. Maeda et al., Appl. Phys. Lett. **80**, 2147 (2002); and Y. Takahashi et al., J. Magn. Magn. Mater. **246**, 259 (2002)

[97] D. Ravelosona et al., Appl. Phys. Lett. **76**, 236 (2000)

[98] T. Shima et al., Appl. Phys. Lett. **80**, 288 (2002); and Y. Endo et al., J. Appl. Phys. **89**, 7065 (2001)

[99] M. F. Toney et al., J. Appl. Phys. **93**, 9902 (2003)

[100] S. N. Hsiao et al., Appl. Phys. Lett. **94**, 232505 (2009)

[101] R. M. Hazeni et al., Am. Mineral. **81**, 1021 (1996)

[102] G. Kim et al., Appl. Phys. Lett. **92**, 172502 (2008); and M. Yoshikawa et al., IEEE Trans. Magn. **44**, 2573 (2008)

The FePt electrode

In this section, the structural and magnetic properties of FePt layers are optimized with regard to a high ordered $L1_0$ structure with (001) orientation and perpendicular magnetic anisotropy. Afterwards, the aim is to integrate the optimized FePt layers as electrodes into pMTJs.

For the first investigations, a 20 nm thick FePt layer has been sputtered on top of MgO substrate/MgO 5. The 5 nm MgO layer was sputtered to obtain a clean surface. Figure 45 shows the re-

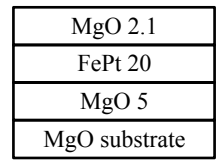

Figure 45: Stack of a FePt sample. A system without buffer layer.

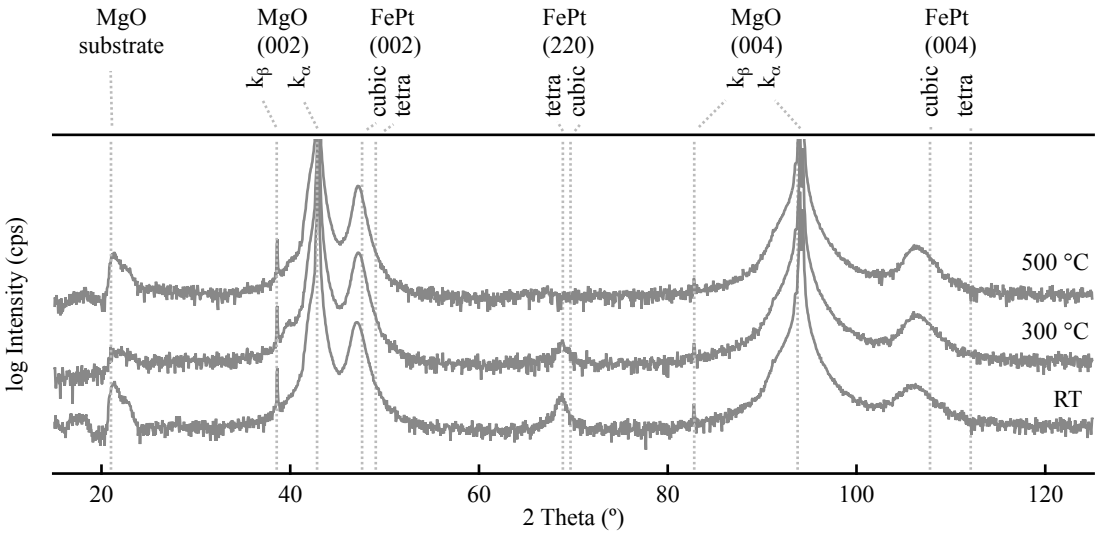

Figure 46: XRD measurements of the samples MgO substrate/MgO 5/$Fe_{50}Pt_{50}$ 20/MgO 2.1 for different substrate temperatures T_s during the sputtering of the FePt layer. The thickness of the layer, the pressure during the sputtering process, and the Fe content in the FePt layer remained unchanged at X=20 nm and p=2·10^{-3} mbar, and c=50 at. %, respectively.

sulting layer stack of MgO substrate/MgO 5/FePt 20/MgO 2.1. The samples were prepared in a magnetron sputter system with a base pressure of 5·10^{-10} mbar. The FePt was prepared by sputtering Fe and Pt from two independent sputtering guns simultaneously. Elemental targets of Fe and Pt of 99.95% purity were used. The sputter power ratios to obtain a desired amount of Fe and Pt in the layer were determined by using a combined x-ray reflectivity and x-ray fluorescence technique. The substrate has to be heated to induce the phase transition from the chemical disordered face-centered cubic A_1 structure to the ordered tetragonal $L1_0$ structure with perpendicular magnetic anisotropy.[103] Therefore, the first series of FePt samples has been prepared with varying substrate temperature T_s during the sputtering of the FePt. T_s was changed in the range between room temperature and 500 °C. The thickness of the FePt layer, the pressure during the sputtering process, and the Fe content in the FePt layer remained unchanged at X=20 nm, p=2·10^{-3} mbar and c=50 at. %, respectively. Figure 46 shows the x-ray diffraction (XRD) measurements of the samples with different T_s. The dashed lines mark the literature values of the peak positions[104] and the upper labels describe the corresponding peaks. The strong peaks at 2Θ=42.9 ° and 2Θ=94 ° are the k_α and the smaller peaks at 2Θ=38.6 ° and 2Θ=82.8 ° are the

[103] T. Suzuki et al., J. Appl. Phys. **85**, 4301 (1999)

[104] Joint Committee on Powder Diffraction Standards, *JCPDS-ICDD Powder Diffraction Database (2000)*, cards No. 29-718 and No. 43-1359

k_β peaks of the MgO substrate. The peak at 2Θ=21.3 ° is also due to the MgO substrate. The reflections at 2Θ=47 ° and 2Θ=106 ° are attributed to the FePt (002) and (004) peaks of the cubic structure. Compared to the literature values, the measured peak positions are shifted to smaller angles. Thus, the lattice constant c=3.86 Å in (00n) direction is larger than the literature value of 3.82 Å.[105] The lattice constant c of the FePt was determined from the XRD measurements by using Bragg's law.[106] The literature values for the peak positions and for c are measured on a powder sample. A microprobe analysis of this powder sample showed $Pt_{0.51}Fe_{0.44}Cu_{0.03}Ir_{0.02}$.[105] Regarding these differences between the literature sample and the one used in this work, the deviating peak positions as well as the differences in c are comprehensible. The peak at 2Θ=68.8 ° in the measurement with T_s=RT is associated with the FePt (220) reflection. The occurrence of both, (00n) and (nn0) peaks in the same measurement indicates the formation of FePt clusters with different orientations. The amount of FePt clusters with (nn0) orientation is less than the one with (00n) direction, as the intensity of the (220) peak is much smaller compared to the intensity of the (002) peak. The (220) peak, and thus the areas of FePt with (nn0) direction, vanish with increasing substrate temperature. Beside the (220) peak no changing with the substrate temperature is visible in the x-ray diffraction measurements. Especially the positions of the (002) and of the (004) peak remain unchanged. This means, that no phase transition from the cubic to the tetragonal structure with perpendicular magnetic anisotropy is observed.

[105] Joint Committee on Powder Diffraction Standards, *JCPDS-ICDD Powder Diffraction Database (2000)*, card No. 43-1359

[106]

$$n \cdot \lambda = 2d \cdot sin\Theta$$

Bragg's law

n: integer, λ: wavelength of incident wave, d: spacing between planes in atomic lattice, Θ: angle between incident ray and scattering planes.

W. L. Bragg, Proc. Cambridge Philos. Soc. **17**, 43 (1913)

The buffer layer as well as the substrate are important for the growth of a certain material, in this case the FePt layer. The texture is induced by the lattice constant and by the orientation of the substrate and of the buffer layer.[107] The lattice mismatch between the MgO and the tetragonal FePt is 8.6 %. Thus, the formation of the tetragonal structure of FePt directly on MgO is disabled even if high substrate temperatures are provided. Several groups used buffer layers based on Cr to induce the $L1_0$ ordered FePt phase.[108] The aim in this work is to use the FePt as electrode in a pMTJ. Thus, this kind of buffer is not desired as a Cr diffusion during

[107] S. Seal, *Functional Nanostructures: Processing, Characterization, and Application* (Springer US, 2007)

[108] Y. Xu et al., Appl. Phys. Lett. **80**, 3325 (2002); A.-C. Sun et al., J. Appl. Phys. **98**, 076109 (2005); and Y. Ding et al., J. Magn. Magn. Mater. **303**, e238 (2006)

the annealing of a MTJ causes a reduction of the TMR-effect.[109] In this work, a Fe 1/Pt 20 buffer layer is inserted in between the MgO and the FePt. The resulting sample stack is MgO substrate/ MgO 5/Fe 1/Pt 20 /FePt 20/MgO 2.1. Figure 47 shows the sample stack. The lattice mismatch between MgO and Fe is 4.2 % if the Fe lattice grows shifted by 45 ° with respect to the MgO lattice. The lattice mismatch between Fe and Pt is 3.06 % if the Pt lattice grows shifted by 45 ° with respect to the Fe lattice. The Pt lattice and the FePt "in-plane lattice" of the tetragonal phase have a mismatch of 1.8 %. Thus, the formation of the tetragonal phase is possible with this kind of buffer.

[109] N. Tezuka et al., Appl. Phys. Lett. **89**, 112514 (2006)

MgO 2.1
FePt 20
Pt 20
Fe 1
MgO 5
MgO substrate

Figure 47: Stack of a FePt sample. A system with Fe/Pt buffer layer.

THE SUBSTRATE TEMPERATURE T_s during the sputtering process of the FePt layer has been varied between room temperature and 700 °C to induce the $L1_0$ structure with (001) orientation and pMA of the samples with the Fe/Pt buffer layer. The thickness of the FePt layer, the pressure during the sputtering process, and the stoichiometry have been kept constant at X=20 nm, p=2·10^{-3} mbar and c=50 at. %, respectively. Figure 48(a) shows the XRD measurements of the samples for the different substrate temperatures. The dashed lines mark the literature values of the peak positions[110] and the upper labels describe the corresponding peaks. The peaks due to the MgO substrate are the same as already described in figure 46 for the system without buffer layer. At 2Θ=46.1 ° and 2Θ=103 ° the Pt (002) and Pt (004) peaks of the 20 nm Pt buffer layer appear. If the measurement with T_s=700 °C is not accounted for, the FePt (002) and (004) peaks are shifted from 2Θ=47.2 ° and 2Θ=106.4 ° to 2Θ=48.88 ° and 2Θ=111.97 ° with increasing T_s. This indicates the transition from the chemical disordered fcc A_1 FePt phase at room temperature to the tetragonal $L1_0$ ordered structure for T_s between 500 °C and 600 °C. Since only (00n) diffraction peaks of the FePt are observed for T_s>400 °C, the films are strongly textured to the (001) planes, indicating that the film was grown epitaxially on the MgO substrate. In addition to the fundamental FePt (002) and (004) peaks, the superlattice FePt (001) and (003) peaks occur at about 2Θ=25 ° and 2Θ=77 ° or $T_s \geq$500°C. This superlattice reflections are strongly associated with the formation of the $L1_0$ ordered structure.[111] The temperature range

[110] Joint Committee on Powder Diffraction Standards, *JCPDS-ICDD Powder Diffraction Database (2000)*, cards No. 29-718 and No. 43-1359

[111] Please note here, that no information about the chemical ordering of the samples was accessible. A lowered symmetry compared to the highly ordered $L1_0$ structure is possible.

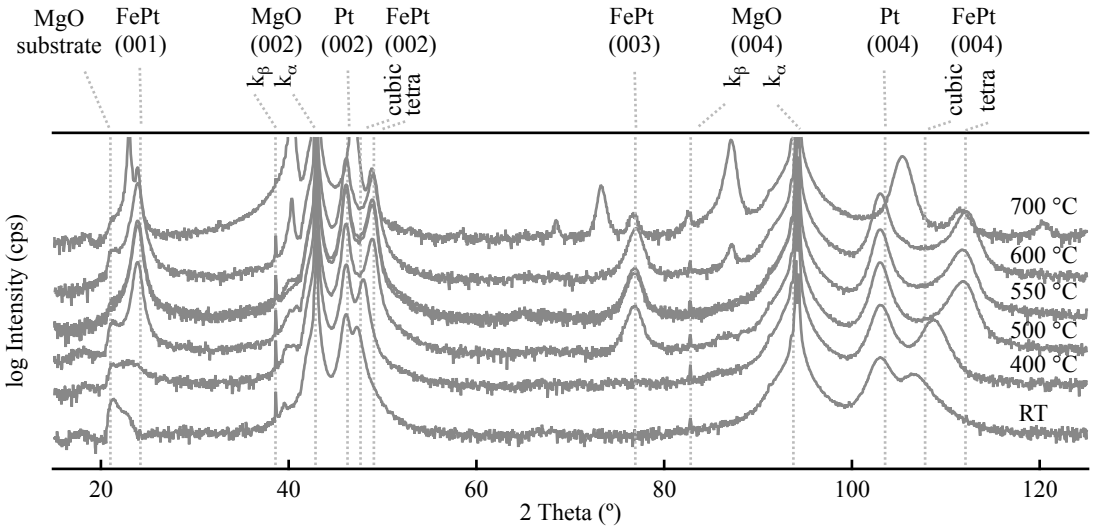

Figure 48: XRD measurements of the samples MgO substrate/MgO 5/Fe 1/Pt 20 /FePt 20/MgO 2.1 for different substrate temperatures T_s during the sputtering of the FePt layer. The thickness of the FePt layer, the pressure during the sputtering process, and the stoichiometry remained unchanged at X=20 nm, p=2·10^{-3} mbar and c=50 at. %.

between 500 °C and 600 °C for the formation of the tetragonal structure is consistent with the findings in other works.[112] Additional peaks at 2Θ=40.33 ° and 2Θ=87.18 ° occur in the XRD spectrum of the sample with T_s=600 °C. These peaks could not be clearly identified. They are probably caused by a mixed phase due to a diffusion of the materials. In the spectrum of the sample with T_s=700 °C a lot of additional peaks are observed, the intensity of the tetragonal (00n) FePt peaks decreases, and the Pt peaks are shifted to higher angles. In summary, the tetragonal structure of FePt is formed in the temperature range between 500 °C and 600 °C, wheras temperatures of 600 °C and larger are to high for the formation of the chemical ordered $L1_0$ structure, as they probably cause an interdiffusion of the materials.

[112] T. Suzuki et al., J. Magn. Magn. Mater. **193**, 85 (1999); and C. M. Kuo et al., J. Appl. Phys. **85**, 4886 (1999)

The lattice constant c of the FePt in (00n) direction is determined from the XRD measurements by using Bragg's law.[113] Figure 49 (a) shows c in dependence of T_s. The dashed lines denote the literature values of the bulk lattice constants for the cubic A_1 and for the tetragonal $L1_0$ structure.[114] The lattice constant of 3.84 Å at T_s=RT is near the literature value of 3.82 Å of the cubic bulk FePt phase. The lattice constant c decreases with increasing T_s and reaches the minimum of 3.71 Å at 600 °C. The values be-

[113] W. L. Bragg, Proc. Cambridge Philos. Soc. **17**, 43 (1913)

[114] Joint Committee on Powder Diffraction Standards, *JCPDS-ICDD Powder Diffraction Database (2000)*, cards No. 29-718 and No. 43-1359

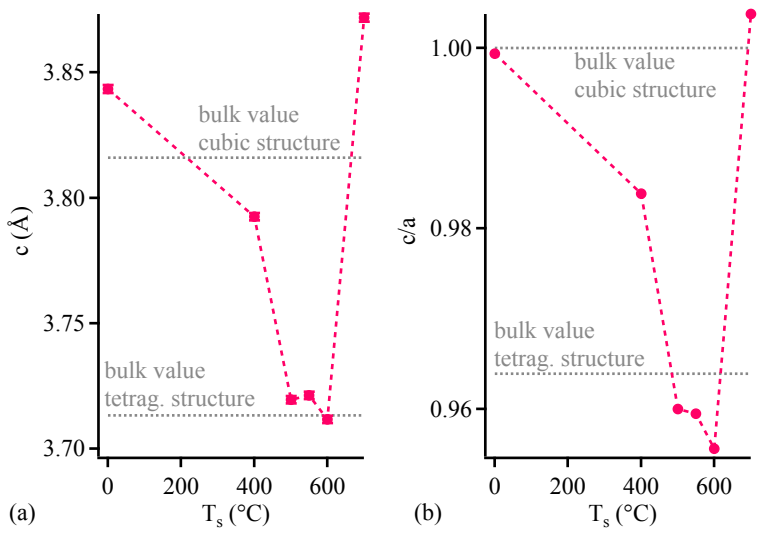

Figure 49: (a) Lattice constant c of the samples MgO substrate/MgO 5/Fe 1/Pt 20 /FePt 20/MgO 2.1 for different substrate temperatures T_s. The values were determined from the XRD measurements. The light grey lines mark the bulk lattice constants for the cubic A_1 and for the tetragonal $L1_0$ structure. (b) The ratio of the out-of-plane and in-plane lattice constants c and a represents the degree of tetragonality.

tween 500 °C and 600 °C are close to the literature value for the bulk lattice constant of the tetragonal $L1_0$ structure. For T_s higher than 600 °C, c increases again to 3.87 Å, indicating that the tetragonal phase is destroyed for T_s> 600 °C.

The sample can be tilted in the x-ray beam by using an Eulerian cradle in the XRD measurement setup. Thus, the (202), (201), and (222) peaks are accessible and the in-plane lattice constants a and b with a=b can be determined. The ratio c/a of the out of plane and in-plane lattice constants represents the degree of tetragonality. In figure 49 (b) the ratio c/a in dependence of T_s is shown. The dashed grey lines are the literature values of the cubic and of the tetragonal $L1_0$ structure. The ratio c/a is 1 for T_s=RT. With increasing T_s, the ratio c/a decreases and reaches a minimum of about 0.956 at 600 °C. The ratio c/a increases again for T_s>600 °C. The behavior of c/a shows a high amount of tetragonality for 500 °C$\leq$ T_s $\leq$600 °C. The structure is cubic for T_s=RT and for T_s > 600 °C.

THE MAGNETIZATION of the samples with the different T_s has been measured by using an alternating gradient magnetometer. The applied external magnetic field was perpendicular to the film

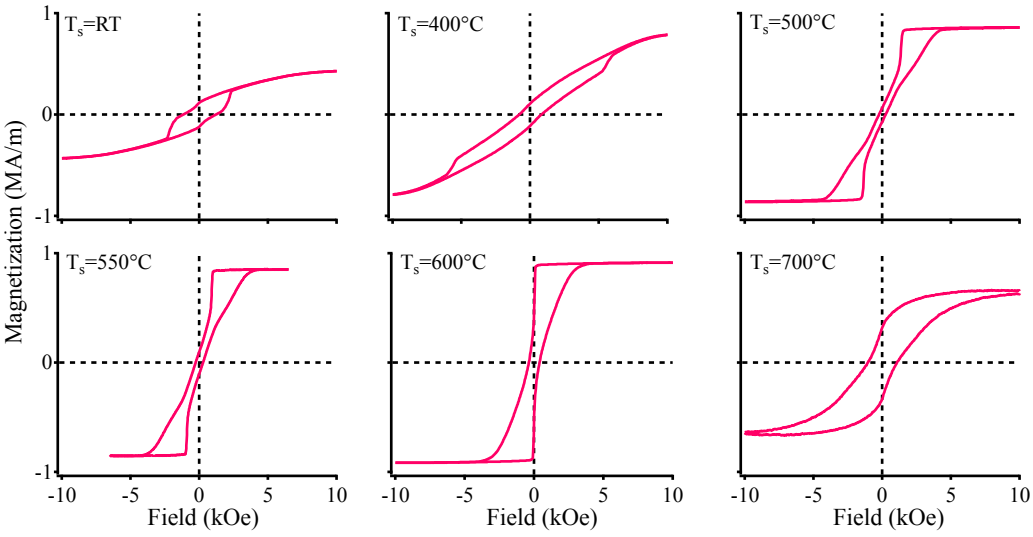

Figure 50: AGM measurements of the samples MgO substrate/MgO 5/Fe 1/Pt 20 /FePt 20/MgO 2.1 for different substrate temperatures T_s during the sputtering of the FePt layer. The thickness of the FePt layer, the pressure during the sputtering process, and the Fe content remained unchanged at X=20 nm and p=2·10^{-3} mbar, and c=50 at. %, respectively.

plane. The magnetization measurements are shown in figure 50. For temperatures lower than 500 °C and higher than 600 °C the magnetization turns slowly and no sharp switching is observed. In the temperature range between 500 °C and 600 °C a sharp magnetic switching is observed, indicating a nucleation barrier for the formation of the oppositely magnetized domains. The nucleation of the oppositely magnetized domains occurs before the external field is reduced to zero, because of the demagnetization field of the samples in the perpendicular direction.

Summarizing, the structural and magnetic investigations showed that a temperature range of 500 °C - 600 °C is optimal to generate the tetragonal phase with perpendicular magnetic anisotropy. The phase transition from the chemical disordered cubic A_1 structure to the tetragonal structure is visible in the structural analysis as well as in the magnetic measurements as a sharp magnetic switching occurs. The sample with T_s=600 °C shows best perpendicular magnetic properties but the XRD measurement of this sample shows an additional peak, indicating a diffusion of the materials. Thus, all further samples are prepared with a substrate temperature of T_s=550 °C during the sputtering process of the FePt layer.

As all investigated samples show a squareness smaller than 0.9, a further enhancement of the pMA of the FePt is desired.

THE INFLUENCE OF THE ARGON PRESSURE p during the sputtering process of the FePt layer on the structural and magnetic properties of the sample is now investigated. The pressure has been varied from $2{\cdot}10^{-3}$ mbar to $10{\cdot}10^{-3}$ mbar to enhance the $L1_0$ ordering and the pMA. An improvement is expected by imposing a strong internal strain/stress to thin films via the high argon pressure.

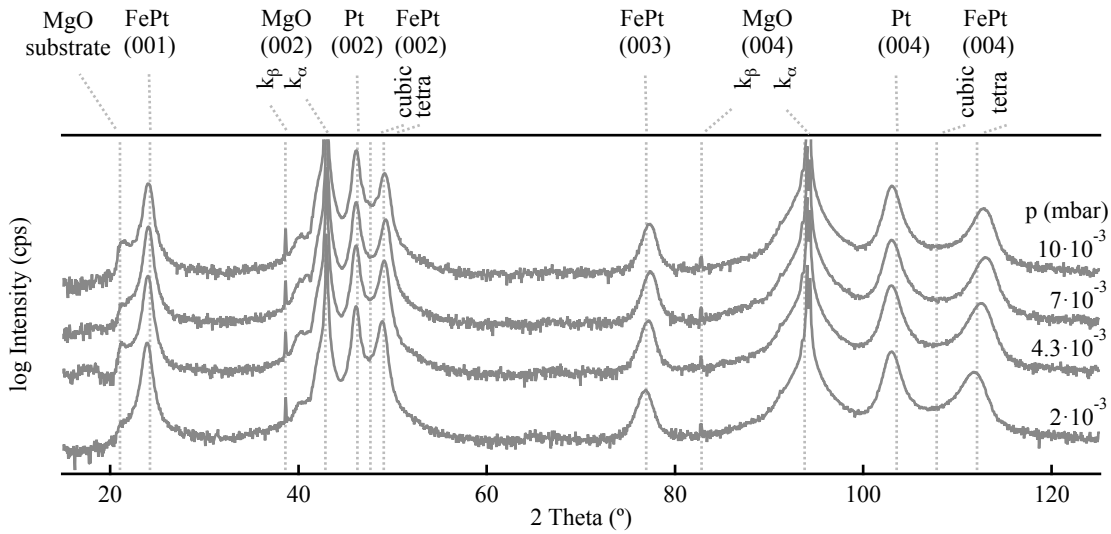

Figure 51: (a) XRD measurements of the samples MgO substrate/MgO 5/Fe 1/Pt 20 /FePt 20/MgO 2.1 for different argon pressures at the sputtering of the FePt layer. The thickness of the FePt layer, the substrate temperature, and the Fe content remained unchanged at X=20 nm and T_s=550 °C, and c=50 at. %, respectively.

The pressure has been regulated by the position of a throttle at the vacuum pump. The layer stack remained unchanged compared to the system used for the substrate temperature dependence. All layers, except the FePt, have been sputtered with the usual argon pressure of $2{\cdot}10^{-3}$ mbar. The substrate temperature during the sputtering process of the FePt, the FePt thickness, and the Fe content has been kept constant at T_s=550 °C, 20 nm, and 50 at. %, respectively. Figure 51 shows the XRD measurements of the samples with different p. The dashed lines denote the literature values of the peak positions and the peaks are labeled at the top margin of the figure. In general, the same peaks,

as already described for the T_s dependence (see figure 48) with 500 °C$\leq T_s \leq$600 °C, occur. The FePt (001), (002), (003) and (004) peaks are shifted from 2Θ=23.88 °, 2Θ=48.88 °, 2Θ=76.88 ° and 2Θ=111.97 ° to 2Θ=24.03 °, 2Θ=49.18 °, 2Θ=77.33 ° and 2Θ=112.68,° with increasing p. Actually, the observed peak positions for a pressure $p \geq 4.3 \cdot 10^{-3}$ mbar are larger than the literature values for the tetragonal $L1_0$ structure. Thus, the lattice constant c in (001) direction is smaller than the literature value of c. Figure 52 (a) shows c in dependence of p. The literature value is marked in grey. All observed lattice constants are near the literature value of 3.7133 Å for tetragonal bulk FePt. The largest difference between the literature value and the measurement value is 0.72 %. The minimum of 3.6965 appears at $7 \cdot 10^{-3}$ mbar.

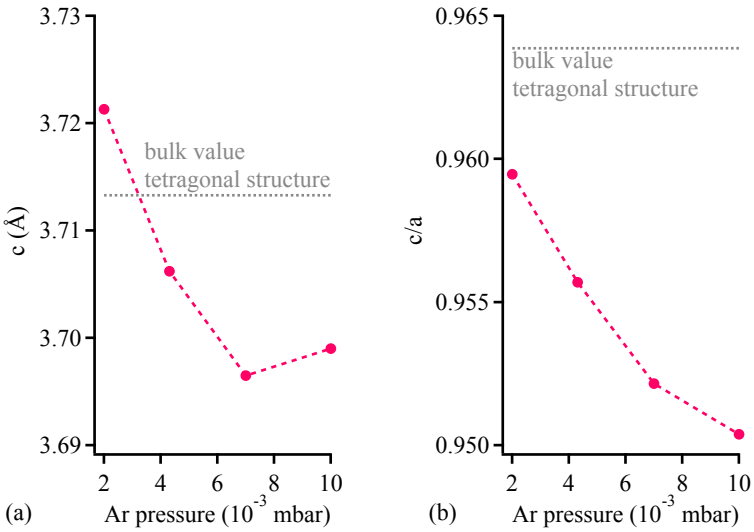

Figure 52: (a) Lattice constant c of the samples MgO substrate/MgO 5/Fe 1/Pt 20 / FePt 20/MgO 2.1 for different argon pressures p determined from the XRD measurements. (b) Ratio c/a of the samples for different Ar pressures p. The grey line denote the bulk values for the tetragonal $L1_0$ structure.

Figure 52 (b) shows the ratio c/a in dependence of p. The ratio c/a decreases from 0.9595 to 0.9504 with increasing p. Thus, the amount of tetragonality increases and the maximum of 4.96 % is reached at the highest pressure of $10 \cdot 10^{-3}$ mbar. The observed ratios are even smaller than the literature value for bulk FePt. In this work, thin films of FePt are investigated and an MgO (001) substrate is used. As the MgO has a larger in-plane lattice constant than the FePt, an enhancement of a and a reduction of c, compared

to the bulk value, are comprehensible. This behavior is desirable as the amount of tetragonality increases.

THE STRAIN TENSOR'S averaged [001] component $\epsilon_{[001]}$ and the coherence length (grain size) D of the FePt film can be determined by a Williamson-Hall analysis[115] of the integral peak widths of the (001), (002), (003) and (004) reflections. Descriptive, $\epsilon_{[001]}$ quantifies the variation in the distance between the lattice planes within the (001) direction. A Gaussian instrumental peak broadening and a Lorentzian convolution of the grain size and the strain effects are assumed. The peak widths are described by

[115] G. Williamson et al., Acta Metall. **1**, 22 (1953)

$$B_{obs}^2 = B_{inst}^2 + B_{ss}^2$$

and

$$B_{ss} \cdot \cos\Theta = \frac{k\lambda}{D} + 4\epsilon_{[001]} \sin\Theta$$

with B_{obs} being the observed width, B_{inst} the instrumental width, B_{ss} the size-strain width, and the shape factor $k = 1$.

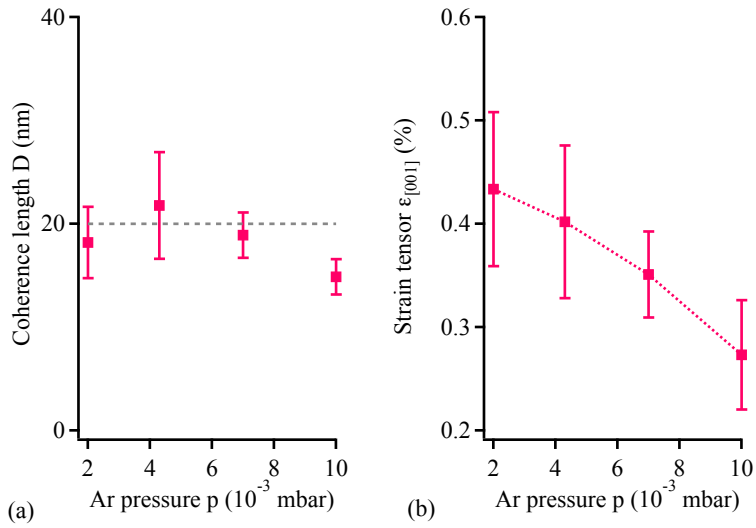

Figure 53: (a) Coherence length D and (b) microstrain $\epsilon_{[001]}$ in dependence of the argon pressure p during the sputter process of the FePt layer. The dashed grey line in (a) denotes the film thickness.

The strain tensor $\epsilon_{[001]}$ and the coherence length (grain size) D are calculated in dependence of the Ar pressure by analyzing the peak width in the XRD-spectrum of the samples prepared with different p. Figure 53 (a) and (b) show D and $\epsilon_{[001]}$ in dependence

of p as the results of the analysis. The dashed grey line in figure 53 (a) denotes the sputtered film thickness. The estimated coherence length matches the film thicknesses quite well within the accuracy of the measuring and fitting procedure. The strain tensor decreases from 0.433 % to 0.373 % with increasing argon pressure. Thus, the variation in the distance between the lattice planes is reduced. It can be concluded, that a high degree of epitaxy is induced by increasing the argon pressure during the sputtering of the FePt.

The magnetic behavior of the samples has been investigated. The applied external magnetic field was perpendicular to the film plane. Figure 54 shows the magnetization in dependence of the external magnetic field for the samples sputtered with different p. All samples exhibit a sharp magnetic switching. This indicates a nucleation barrier for the formation of oppositely magnetized domains. For p<10·10^{-3} mbar the nucleation of the oppositely magnetized domains occurs before the external field is reduced to zero because of an perpendicular demagnetizing field. For p=10·10^{-3} mbar a higher nucleation barrier exists and the nucleation is delayed until the external field has become negative and aids the demagnetization field.

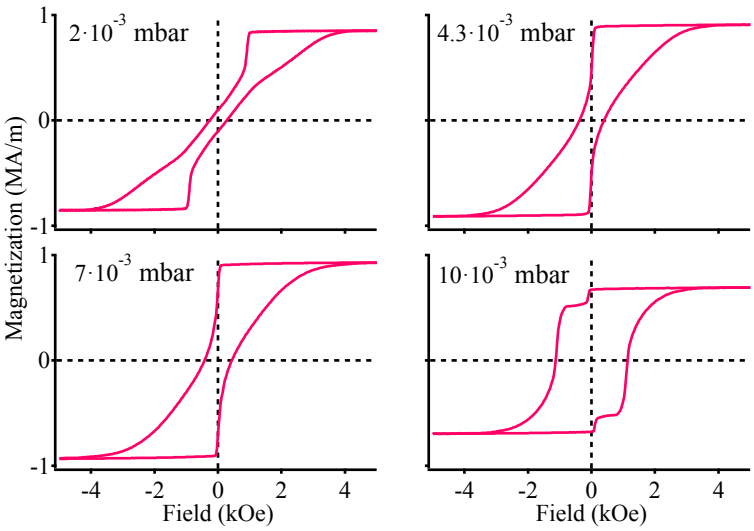

Figure 54: AGM measurements of the samples MgO substrate/MgO 5/Fe 1/Pt 20 /FePt 20/MgO 2.1 for different argon pressures p during the sputtering of the FePt layer. The thickness of the FePt layer, the substrate temperature during the sputtering process of the FePt, and the Fe content remained unchanged at X=20 nm and T_s=550 °, and c=50 at. %, respectively.

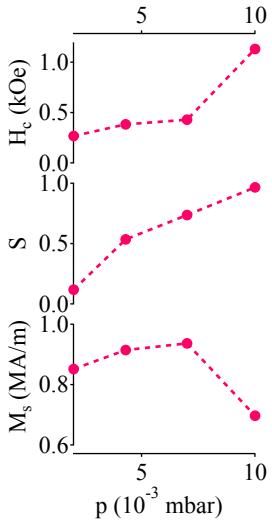

Figure 55: Coercivity H_c, squareness S, and saturation magnetization M_s dependent on the argon pressure p.

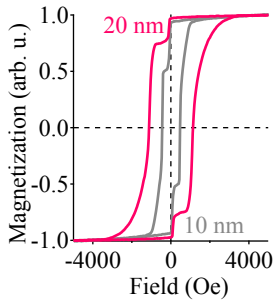

Figure 56: Normalized hysteresis curves of samples with different FePt thicknesses. The buffer layer thickness remains unchanged for the both samples.

[116] M. Sakurai, Phys. Rev. B **50**, 3761 (1994)

[117] S. Okamoto et al., Phys. Rev. B **66**, 024413 (2002)

In figure 55 the saturation magnetization M_s, the squareness $S{=}M_r/M_s$, where M_r is the remanent magnetization, and the coercivity H_c determined by the magnetization measurements are summarized. The saturation magnetization M_s stays roughly constant in the range of 0.7 MA/m to 0.9 MA/m. The coercivity H_c increases from about 270 Oe to about 1130 Oe. The squareness S increases from about 0.12 at $2{\cdot}10^{-3}$ mbar to about 0.97 at $10{\cdot}10^{-3}$ mbar. The sample sputtered at $10{\cdot}10^{-3}$ mbar has perpendicular magnetic anisotropy, as the nucleation of oppositely magnetized domains occurs not before the external field reaches zero and thus, S is larger than 0.9.

The step in the hystereses curve of the sample sputtered with $p{=}10{\cdot}10^{-3}$ mbar is supposed to be due to the Fe buffer layer, which is separated by a 20 nm Pt layer from the FePt. If the FePt layer has strong perpendicular magnetic anisotropy, the magnetization of the Fe layer is influenced and turns out of plane, too. In particular, the Fe/Pt interface already has the tendency to form a perpendicular contribution to the magnetization.[116] Samples with different FePt thickness and constant Fe buffer layer thickness are prepared to prove this assumption. T_s, p, and c remain unchanged at 550 °C, $10{\cdot}10^{-3}$ mbar, and 50 at. %. Figure 56 shows the normalized hysteresis curves for 20 nm and 10 nm FePt. The coercivity H_c increases from about 1130 Oe to about 2860 Oe. The height of the step in the magnetization curve changes from 12 % of the total magnetization to 22 % of the total magnetization by decreasing the FePt thickness. The contribution of the FePt to the total magnetization is reduced, while the contribution of the Fe is enhanced by using less FePt but the same Fe buffer layer thickness. Thus, the increase of the height of the step with decreasing FePt thickness confirms the supposition that the step is due to the magnetization of the Fe buffer.

SUMMARIZING, the increase of the pressure leads to a higher degree of tetragonality as the out of plane lattice constant decreases and the in-plane lattice constants increases. An improvement of the pMA has been attained by imposing a strong internal strain/stress to thin films via the high argon pressure. Okamoto et al.[117] reported about a similar behavior of FePt films. A high

grade of epitaxy and the perpendicular magnetic anisotropy, that are strongly correlated to the $L1_0$ structure of the FePt, are induced by increasing the argon pressure. Similar behavior was observed by Hsiao et al.[118] They reported about the enhancement of the $L1_0$ ordering due to high argon pressure. A further increase of the argon pressure during the sputtering of the FePt layer is not possible, as the stoichiometry of the FePt cannot be controlled. All further samples are prepared with p=10·10^{-3} mbar during the sputtering of the FePt layer.

[118] S. N. Hsiao et al., Appl. Phys. Lett. **94**, 232505 (2009)

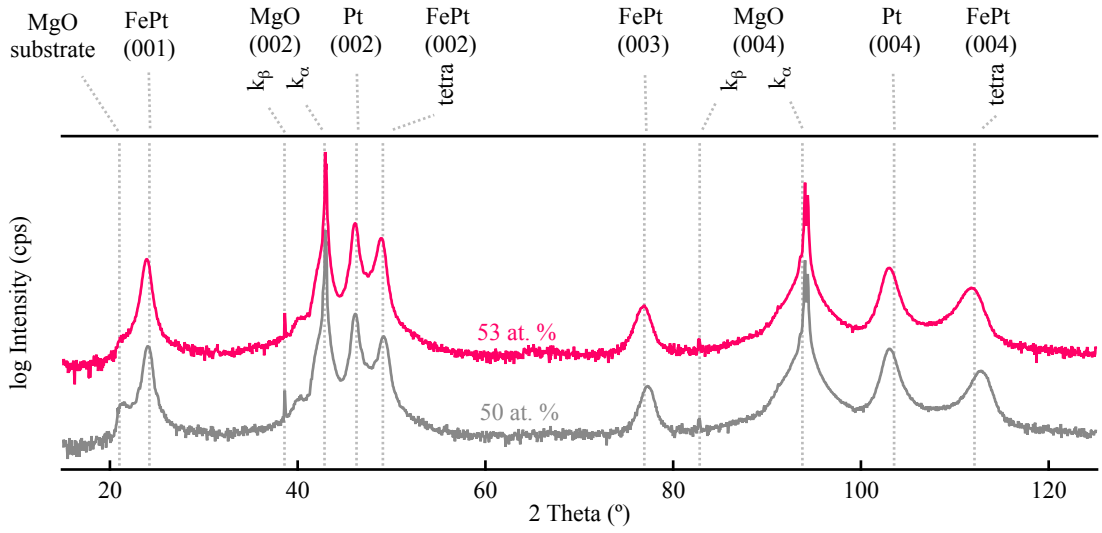

Figure 57: XRD measurements of the samples MgO substrate/MgO 5/Fe 1/Pt 20 /FePt 20/MgO 2.1 for different Fe contents of the FePt layer.

The stoichiometry of the FePt has been changed from 50 at. % to 53 at. % in order to further optimize the properties of the samples. The stoichiometry of 50 at. % has been used so far for the optimization of the buffer layer, the substrate temperature, and the argon pressure. The stoichiometry was determined by using a combined x-ray reflectivity and x-ray fluorescence technique. The variation in the stoichiometry was regulated by the power of the sputtering guns as Fe and Pt are sputtered from two independent sputtering guns simultaneously. A statistical error of ± 1 at. % in the stoichiometry is assumed.

In figure 57 the XRD measurements for the different Fe contents are shown. The FePt (00n) peaks are shifted to smaller angles if

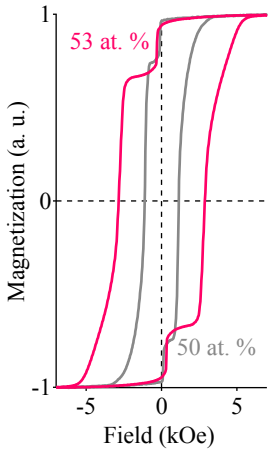

Figure 58: AGM measurements of the samples with different Fe contents of the FePt layer.

the Fe content is increased from 50 at. % to 53 at. %. This means, that the lattice constant c changes from about 3.69 Å at 50 at. % Fe to about 3.71 Å at 53 at. % Fe. Please note, that even though the values for 53 at. % Fe are closer to the literature values of the tetragonal $L1_0$ phase, higher peak positions (and thus larger c), as measured for 50 at. % Fe, are desirable. A larger c corresponds to a higher degree of tetragonality if the in-plane lattice constant is assumed to be unchanged. In figure 58 the AGM measurements of the samples with perpendicular magnetic field are shown. The coercivity changes from about 1130 Oe to about 2860 Oe. The value of 2860 Oe is consistent with literature values for H_c of epitaxial $L1_0$ FePt thin films.[119] The step at about 250 Oe due to the Fe buffer layer is not affected by the change in the stoichiometry of the FePt layer.

In summary, an increase of the Fe content from 50 at. % to 53 at. % in the FePt layer leads to a smaller out of plane lattice constant c and a larger coercivity in the magnetization measurements. Similar behavior was presented by Barmak et al. They investigated the stoichiometry-anisotropy connections in epitaxial $L1_0$ FePt (001) films and showed that the order parameter has a maximum for the film composition closest to equiatomic, whereas the anisotropy shows an increase as the Fe content is increased from below to slightly above the equiatomic composition.[120] It is supposed that a slight excess of Fe increases the anisotropy of the $L1_0$ phase without considerably degrading the long-range chemical order.

SUMMARIZING THE WHOLE OPTIMIZATION PROCESS of the FePt electrode, a high degree of epitaxy in the tetragonal distorted system and a high perpendicular magnetic anisotropy, strongly correlated to the $L1_0$ structure of FePt, could successfully be reached by a careful variation of the different parameters. The optimum conditions were found to be a substrate temperature of T_s=550 °C and an argon pressure of p=10·10^{-3} mbar. If desired, the coercivity can be raised by increasing the Fe content from 50 at. % to 53 at. %.

[119] C. C. Chiang et al., Appl. Phys. Lett. **88**, 152508 (2006); and M. H. Hong et al., J. Appl. Phys. **84**, 4403 (1998)

[120] K. Barmak et al., J. Appl. Phys. **95**, 7501 (2004); and K. Barmak et al., J. Appl. Phys. **98**, 033904 (2005)

pMTJ: A combination of Co/Pt multilayers and FePt

The optimized FePt layer can now be integrated as the lower electrode into a pMTJ. As shown in the last section, the substrate and the buffer layers are important for the growth, and, therefore, for the perpendicular magnetic anisotropy of the FePt. It is obviously not possible to generate perpendicular magnetic anisotropy in the FePt in the same way, if it is used as the upper electrode. Thus, Co/Pt multilayers are used as the upper electrode. The resulting sample stack is MgO substrate/MgO 5/Fe 1/Pt 20/FePt 20/Fe 1/Mg 0.5/MgO 2.1/Fe 1/(Co 0.6/Pt 1.8)$_9$/protection layers and is shown in figure 59. The Fe layer is inserted at the MgO interface, as the lattice mismatch between the MgO and the tetragonal FePt is about 9.85 %. This is probably to high for an epitaxial growth of a MgO (001) barrier directly on the FePt. The samples were prepared in a magnetron sputter system with a base pressure of $5{\cdot}10^{-10}$ mbar. The stack was patterned by laser lithography and ion beam etching. The resulting patterns are squares of $7.5{\times}7.5\,\mu m^2$ and $12.5{\times}12.5\,\mu m^2$. These structures were capped with gold contact pads. The transport measurements have been done by a conventional two-probe technique with a 10 mV bias voltage in a perpendicular magnetic field. Figure 60 shows

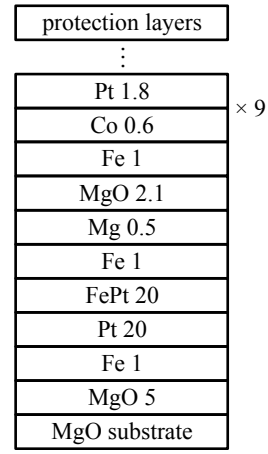

Figure 59: Stack of a pMTJ. A combined FePt and Co/Pt-multilayer system.

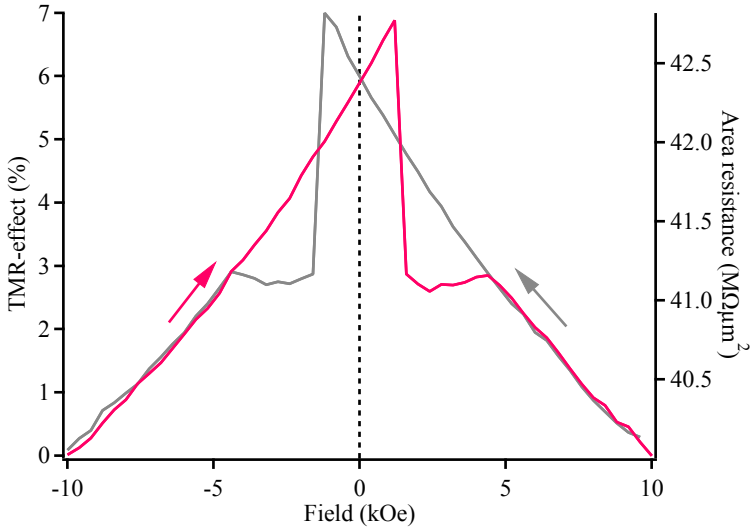

Figure 60: TMR-effect and area-resistance product of the sample MgO substrate/MgO 5/Fe 1/Pt 20/FePt 20/Fe 1/Mg 0.5/MgO 2.1/Fe 1/(Co 0.6/Pt 1.8)$_9$/protection layers. The values measured with increasing external magnetic field (from negative to positive) are marked in pink and the values measured with decreasing external magnetic field (from positive to negative) are marked in grey. The arrows indicate the field change directions.

the measurement of the TMR-effect as well as the area-resistance product. The values measured with increasing external magnetic field (from negative to positive) are marked in pink and the values measured with decreasing external magnetic field (from positive to negative) are marked in grey. The arrows indicate the corresponding field change directions. The TMR-effect of the sample is about 7 % at room-temperature and the area resistance-product is about 40 $M\Omega\mu m^2$. The observed sharp switching at about 2000 Oe is near the coercivity value of 2860 Oe of the optimized FePt layer. Thus, the sharp switching is considered to be due to the lower FePt electrode which has perpendicular magnetic anisotropy. The upper Co/Pt electrode has no sharp switching if measured with an external magnetic field in perpendicular direction. The magnetization of the electrode can not be saturated with the available magnetic field of 10 kOe at the TMR-measurement setup. It is considered, that the Co/Pt electrode has in-plane anisotropy. Please note, that even if the Co/Pt multilayer system has pMA with a Squareness > 0.9 (see chapter "*Co/Pt multilayers*"), the system has soft magnetic properties and a low perpendicular coercivity. The coercivity for the multilayer system (Co 0.6/Pt 1.8)$_9$ as used here as upper electrode is only 260 Oe. Thus, the coupling to the Fe layer, which alone would have in-plane anisotropy, can easily turn the magnetization of the Co/Pt multilayer electrode into the film plane. Samples with different Fe interface layer thickness and without Fe interface layer were prepared to minimize the in-plane component, but no tunneling was observed. It is possible that the decrease of the Fe thickness causes defects in the MgO barrier. Similar behavior was observed by Yoshikawa et al.[121] They showed that the quality of the MgO barrier is improved by the insertion of a Fe interfacial layer.

[121] M. Yoshikawa et al., IEEE Trans. Magn. **44**, 2573 (2008)

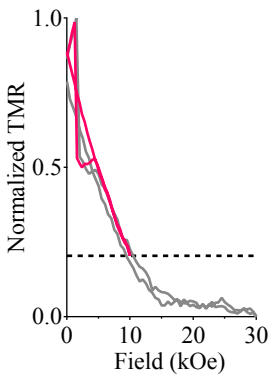

Figure 61: Normalized TMR with maximum magnetic field of 10 kOe (pink) and 30 kOe (grey).

The room-temperature TMR-effect of the sample with 1 nm Fe was measured in a ^{3}He Cryostat because the available magnetic field in this measurement setup is 40 kOe. Figure 61 shows the TMR-effect of the sample, saturated with an external magnetic field of 30 kOe (grey line). The measurement with a maximum external field of 10 kOe, as also shown in figure 60, is marked in pink. The values are normalized as the TMR varies depending on the element on the sample. It was not possible to measure

exactly the same elements in both setups as the sample has to be bonded on different sockets for the measurements. It is assumed that the switching behavior would be the same in the two different measurements if it is possible to saturate. As the TMR-effect is about 7 % with a maximum field of 10 kOe, it can be supposed by comparing both measurements, that the room-temperature TMR-effect is about 9 % if saturated.

In summary, this chapter deald with the investigation of the material FePt. The properties have successfully been optimized in order to induce a tetragonal lattice structure, which is strongly correlated with a perpendicular magnetic anisotropy of the system. The lattice structure and the magnetic behavior of the FePt samples have been investigated in dependence of various preparation parameters, such as the substrate temperature, the argon pressure during the sputtering process, and the Fe content in the FePt layer. The phase transition from the chemical disordered cubic $A1$ structure to the chemical ordered tetragonal fcc $L1_0$ structure has been attained by imposing a strong internal strain/ stress to the thin films via a high argon pressure and temperatures between 500 °C and 600 °C. This phase transition goes along with an improvement of the perpendicular magnetic anisotropy. The argon pressure dependence of the coherence length and of the strain tensor's averaged [001] component emphasizes the improvement of the structure with increasing pressure. The calculated coherence length matches the sputtered film thickness quite well and an increasing amount of epitaxy with increasing argon pressure is concluded from the analysis of the strain tensor. The possibility of controlling the coercivity is of large importance for practical applications of the material. In this work, the coercivity of the FePt could be manipulated by a slight variation of the Fe content compared to the equiatomic composition.

The optimized FePt layer was successfully integrated as lower electrode into a magnetic tunnel junction. The $L1_0$ structure of FePt with (001) orientation is very promising for the use as perpendicularly magnetized electrode in tunnel junctions. The large perpendicular magnetic anisotropy with (001) easy axis and a lattice mismatch with the MgO (001) plane of less than 10 % are im-

portant conditions for the fabrication of fully epitaxial junctions with a (001) orientated crystalline MgO barrier, and, therefore high TMR-ratios. The FePt layer has been integrated as the lower electrode into a perpendicular magnetic tunnel junction. The upper electrode is a Co/Pt multilayer system as the FePt cannot grow in the $L1_0$ structure if used as upper electrode. The room-temperature TMR-effect of this system is about 9 %.

Ferrimagnetic Co-Fe-Tb

In this chapter, the material Co-Fe-Tb is investigated. A perpendicular magnetic anisotropy with a rectangular hysteresis loop is generated by varying the Tb content in the Co-Fe-Tb layer. The results of the magnetization measurements in dependence of the Tb content and in dependence of the Co-Fe-Tb thickness show an optimum pMA for a Tb content between 13 at. % and 21 at. %, and a layer thickness larger than 10 nm. The Co-Fe-Tb layers are integrated as electrodes into magnetic tunnel junctions with an MgO barrier. A TMR-effect of 16 % at 360 K and 30 % at 13 K is attained. The transport properties of the Co- Fe-Tb based samples show no significant change compared to a reference sample with Co-Fe-B electrodes and in-plane anisotropy. It is supposed here, that the available measurement temperature range between 13 K and 360 K is not close to the compensation point temperature of the Co-Fe-Tb electrodes.

Some properties of the Co-Fe-Tb alloy

Rare earth transition metal (RE-TM) alloys, such as Co-Fe-Tb, Fe-Tb, Co-Fe-Gd, have attained considerable attention in the last decade as they open the way for a magneto-optic recording media. This application might be realized due to the ferrimagnetic properties combined with a large perpendicular magnetic anisotropy of $5{\cdot}10^7$-$20{\cdot}10^7$ erg/cm^3 of a RE-TM alloy.[122]

The first investigations concerning thin films of RE-TM alloys were made in 1972 on samples of Gd and Fe.[123] About one year later it was reported about the formation of stripe and cylindrical domains in these materials, indicating a perpendicular magnetic anisotropy and the possibility of using these materials as magneto-optic recording media was introduced for the first time.[124]

[122] D. Weller et al., IEEE Trans. Magn. **36**, 10 (2000)

[123] J. Orehotsky et al., J. Appl. Phys. **43**, 2413 (1972)

[124] P. Chaudhari et al., Appl. Phys. Lett. **22**, 337 (1973)

The RE-TM alloy films are pure, uniform, amorphous and without a microcrystalline structure, as has been shown by a structural and a compositional analysis.[125] A lot of research has focused on the investigation of the magnetic properties of the RE-TM alloys.[126] These materials turned out to be ferrimagnets with the rare-earth and transition-metals having antiparallel moments. The moments are aligned perpendicular to the sample surface and a perpendicular magnetic anisotropy results. The microscopic origin of the pMA has caused a lot of discussions, and several mechanisms have been proposed for a possible explanation.[127] Dover et al. suppose, that the reason for the occurrence of the pMA is some sort of short-range order on the nearest neighbor atomic scale.[128]

The net magnetization of a RE-TM alloy results from the difference between the magnetization of the rare earth and the transition metal. The direction of the net magnetization is perpendicular to the film surface if the magnetic anisotropy constant K_u is larger than the demagnetization energy. Figure 62 shows a sketch of the subnetwork magnetizations and the resulting net magnetization of a RE-TM alloy in dependence of the temperature. The net magnetization of a RE-TM alloy vanishes at a certain point due to the antiferromagnetic coupling between the magnetic moments of the rare earth material and the transition metal. A so-called compensation point temperature T_{comp} results for a fixed stoichiometry of the system. Otherwise, the compensation point can be easily manipulated by varying the stoichiometry of the alloy. In general, the compensation point temperature is in the range of 40 K to 500 K.[129]

Most of the studies concerning RE-TM alloys report about the use of these materials as magneto-optic recording media. Nevertheless, these materials have also been integrated as perpendicularly magnetized electrodes into magnetic tunnel junctions. A current induced switching of electrodes in a pMTJ could be realized for the first time by using RE-TM alloy based electrodes.[130] The free layer of the junction was switched by a 100 ns pulse current with a current density of 4.7 MA/cm^2. TMR-ratios of about 50 % at room-temperature have been reported for magnetic tunnel junctions with an alumina barrier and electrodes that are based

[125] G. S. C. III et al., AIP Conf. Proc. **31**, 339 (1976); S. S. Nandra et al., J. Phys. F. **7**, 207 (1977); and A. Ali et al., Phil. Mag. B **37**, 353 (1978)

[126] Y. Mimura et al., J. Appl. Phys. **49**, 1208 (1978); M. Mansuripur et al., J. Appl. Phys. **69**, 4844 (1991); A. Lyberatos et al., Phys. Rev. B **53**, 5493 (1996); and F. Hellman et al., J. Appl. Phys. **86**, 1047 (1999)

[127] X. Yan et al., Phys. Rev. B **43**, 9300 (1991); and F. Hellman et al., Phys. Rev. Lett. **68**, 1391 (1992)

[128] R. B. van Dover et al., J. Appl. Phys. **57**, 3897 (1985)

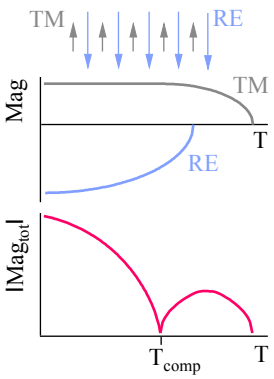

Figure 62: Subnetwork magnetizations of a rare earth element (RE) and a transition metal (TM), and the resulting net magnetization Mag_{tot} of the RE-TM alloy in dependence of the temperature T.

[129] P. Chaudhari et al., Appl. Phys. Lett. **22**, 337 (1973)

[130] M. Nakayama et al., J. Appl. Phys. **103**, 07A710 (2008)

on Co-Fe-Tb and Gd-Fe-Co.[131] This value is comparable to the recent results for alumina based magnetic tunnel junctions with in-plane anisotropy.[132] Finally, the difficulties of using RE-TM alloys in combination with an MgO (100) tunneling barrier have been overcome and a TMR-effect of 64 % at room-temperature has been attained.[133] However, since a high temperature treatment may cause a degradation of the perpendicular magnetic anisotropy of RE-TM films,[134] these pMTJs are not easy to fabricate because of the requirement of the high temperature process[135] to attain MgO (100) textured films and a detailed optimization and characterization of these junctions is still missing.

[131] N. Nishimura et al., J. Appl. Phys. **91**, 5246 (2002)

[132] H. X. Wei et al., J. Appl. Phys. **101**, 09B501 (2007); and D. Wang et al., IEEE Trans. Magn. **40**, 2269 (2004)

[133] H. Ohmori et al., J. Appl. Phys. **103**, 07A911 (2008)

[134] T. Katayama et al., J. Appl. Phys. **49**, 1759 (1978)

[135] D. D. Djayaprawira et al., Appl. Phys. Lett. **86**, 092502 (2005)

The electrodes

In the first section of this chapter, the magnetic behavior of a RE-TM alloy layer is investigated with the aim to tailor a perpendicular magnetic anisotropy. Afterwards, the optimized layers are integrated as electrodes into a pMTJ. In this thesis, Co-Fe is used as the transition metal and Tb as the rare earth material as particularly this combination shows a large magnetic anisotropy[136] and, furthermore, a large TMR-effect is predicted by using Fe or Co-Fe electrodes together with an MgO tunneling barrier.[137]

The stoichiometry of the Co-Fe-Tb might be a sensitive parameter concerning the perpendicular magnetic anisotropy of the system, as the pMA in a RE-TM alloy results from the antiferromagnetic coupling of the individual magnetic moments. Thus, the first samples have been prepared with different Tb contents x in the Co-Fe-Tb layer, ranging from 10 at. % to 24 at. %. The sample layer structure is Si wafer/SiO/Ta 5/$(CoFe)_{1-x}Tb_x$ 30/MgO 2.1. The layer stack is sketched in figure 63. The samples have been prepared in a magnetron sputter system with a base pressure of $5 \cdot 10^{-10}$ mbar. The Co-Fe-Tb layer was prepared by sputtering Co-Fe and Tb from two independent sputtering guns simultaneously. The relative concentration of Co to Fe has been kept constant, as a $Co_{70}Fe_{30}$ target was used. Elemental targets of 99.99 % purity were used. The atomic concentration of Tb and Co-Fe in the Co-Fe-Tb layer has been controlled by the power of the corresponding sputtering guns. The sputter power ratios to obtain the desired

[136] F. Hellman et al., J. Appl. Phys. **86**, 1047 (1999)

[137] S. Yuasa et al., Nat. Mater. **3**, 868 (2004); and S. S. P. Parkin et al., Nat. Mater. **3**, 862 (2004)

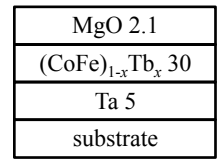

Figure 63: Stack of the CoFeTb samples. The Tb content in the Co-Fe-Tb layer is varied.

amount of Co-Fe and Tb were determined by using a combined x-ray reflectivity and x-ray fluorescence technique. The magnetization measurements have been carried out with an alternating gradient magnetometer (AGM) with an external magnetic field perpendicular to the sample surface. Figure 64 shows the magnetization measurements of the samples with different Tb contents x in the Co-Fe-Tb layer. The step in the hysteresis at about zero Oe is supposed to be due to two different processes in the magnetization reversal. In general, materials with pMA show a process of domain nucleation followed by the domain growth in the magnetization reversal process. It can be distinguished between the nucleation coercivity H_n and the wall-motion coercivity H_w. A rectangular hysteresis results if these coercivities are in the same range, or even $H_n > H_w$.

This is the case for a Tb content x between 13 at. % and 21 at. % of the samples that are used here. A high nucleation barrier exists and the nucleation of the domains is delayed until the external field has become negative and aids the demagnetization field. For $x<13$ at. % the nucleation of the oppositely magnetized domain occurs before the external field is reduced to zero because of a perpendicular demagnetizing field. For the samples with a Tb content of more than 21 at. %, the domain wall coercivity H_w exceeds the nucleation coercivity H_n and the step in the hysteresis is pronounced. The existence of this finite domain-wall coercivity might be due to the existence of nanoscale structural and magnetic inhomogeneities that act as pinning centers. Fu et al. reported about a similar behavior in RE-TM alloys.[138]

[138] H. Fu et al., Comput. Phys. **6**, 610 (1992)

The saturation and remanent magnetization M_s and M_r, the squareness $S = M_r / M_s$, and the coercivity H_c of the samples are summarized in dependence of x as shown in the last three graphs of figure 64. The saturation magnetization decreases from about 0.69 MA/m at x=10 at. % to 0.02 MA/m at x=24 at. %, indicating a compensation point near room-temperature for x=24 at. %. The remanent magnetization increases from 0.15 MA/m at x=10 at. % to 0.59 MA/m at x=13 at. %. After reaching this maximum, M_r decreases again to about 5.6 kA/m. The behavior, as well as the absolute values of M_s and M_r are very similar in the range between x=13 at. % and x=21 at. %. Thus, the squareness S is larger or equal

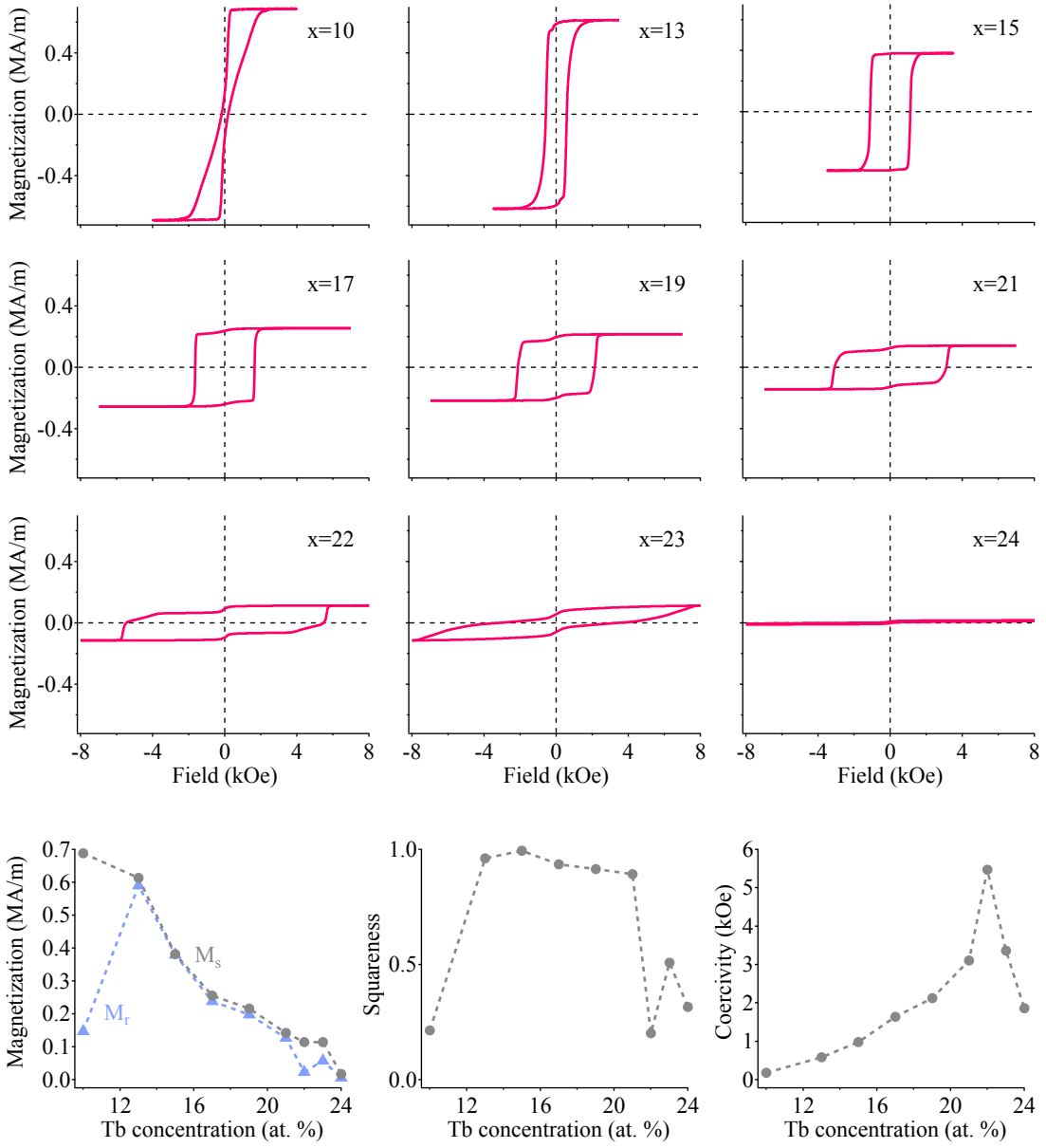

Figure 64: Magnetization measurements of the samples Si wafer/SiO/Ta 5/$(CoFe)_{1-x}Tb_x$ 30/MgO 2.1 (numbers in nm) with different Tb contents x in the Co-Fe-Tb layer. The saturation and remanent magnetization, the squareness, and the coercivity of the samples are summarized in dependence of x in the last three graphs.

to 0.9 in this range and a perpendicular magnetic anisotropy is successfully generated. The coercivity first increases from 182 Oe at x=10 at. % to 5473 Oe at x=22 at. %. After reaching this maximum, H_c decreases again to about 1870 Oe. The coercivity can thus be easily controlled by changing the Tb content in the Co-Fe-Tb layer. This is a straightforward method to generate two different switching fields of the electrodes in a pMTJ.

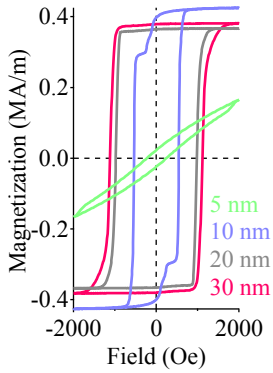

Figure 65: Magnetization measurements of the samples Si wafer/SiO/Ta 5/$(CoFe)_{85}Tb_{15}$ t/MgO 2.1 (numbers in nm) with different Co-Fe-Tb layer thickness.

THE THICKNESS t of the Co-Fe-Tb layer can give an additional parameter for tailoring different switching fields of the two electrodes in a pMTJ. Here, t has been varied between 5 nm and 30 nm. The Tb content has been kept constant at 15 at. %.

Figure 65 shows the AGM measurements for the Co-Fe-Tb samples with different t. The coercivity increases from about 231 Oe at t=5 nm to about 1119 Oe at t=30 Oe. The saturation magnetization stays in the same range for the investigated thicknesses. A slow magnetization reversal occurs for t=5 nm. A perpendicular magnetic anisotropy cannot be concluded from this measurement. A sharp switching is generated by increasing the thickness t and a rectangular hysteresis is observed for t larger than 10 nm. This behavior might be due to the formation of nanoscale structural and magnetic inhomogeneities with increasing t. These inhomogeneities may act as pinning centers and reduce the wall-motion coercivity H_w. Thus, the nucleation coercivity H_n exceeds the wall-motion coercivity H_w and a rectangular hysteresis results.

protection layers
$(CoFe)_{79}Tb_{21}$ 10
CoFeB 1
MgO 2.1
Mg 0.5
CoFeB 1
$(CoFe)_{79}Tb_{21}$ 30
Ta 20
substrate

Figure 66: Stack of a pMTJ. CoFeTb layers with different thickness are integrated as electrodes.

Co-Fe-Tb integrated into a pMTJ

The Co-Fe-Tb layers have been integrated as the electrodes into a MgO based pMTJ. The Tb content in both electrodes has been kept constant at 21 at.%, as the sample with this content showed good pMA with a squareness larger than 0.9 and a large coercivity of about 3106 Oe. Different switching fields have been generated by varying the thickness of the electrodes. The thickness in the lower electrode is larger than in the upper electrode. This means, that the lower electrode is the hard one. The sample stack is SiO_2/Ta 20/$(CoFe)_{79}Tb_{21}$ 30/CoFeB 1/Mg 0.5/MgO 2.1/CoFeB 1/$(CoFe)_{79}Tb_{21}$ 10/protection layers, as shown in figure 66.

Transport measurements of this sample have been performed at different measurement temperatures T. The measurements have been carried out in a closed-cycle helium cryostat with a temperature range of 13 K to 360 K.

The electrodes of the pMTJ cannot be completely saturated at room-temperature with the available magnetic field of 10 kOe at the measurement setup. The sample has been carefully heated in small steps to align the magnetization as the coercivity of the Co-Fe-Tb decreases with the temperature.[139] A saturation of the magnetization in both electrodes is possible with the available magnetic field of 10 kOe at a temperature of 360 K. Figure 67 shows

[139] This will be shown later

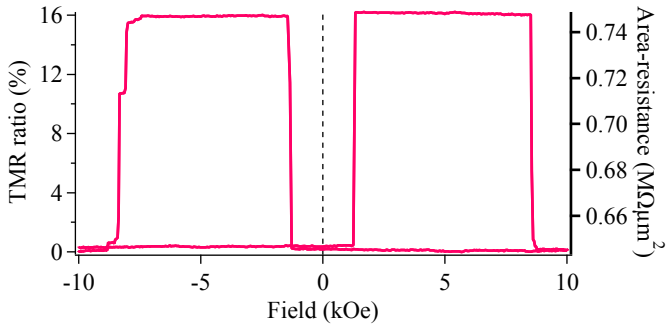

Figure 67: Major loop of the sample .../$(CoFe)_{79}Tb_{21}$ 30/ CoFeB 1/Mg 0.5/MgO 2.1/ CoFeB 1/$(CoFe)_{79}Tb_{21}$ 10/... measured at 360 K. Both electrodes can be saturated at this temperature.

the major loop of the sample measured at 360 K. The TMR-effect is about 16.2 % with an area-resistance in the parallel state of 0.64 $M\Omega\mu m^2$. A sharp switching of both electrodes is observed and the antiparallel alignment of the magnetization is observed in the field range between 1326 Oe and 8510 Oe.

After saturating both electrodes into one direction by heating up to 360 K, transport measurements with increasing measurement temperature T have been performed. Minor loops have been measured as the coercivity of the hard magnetic electrode is large and cannot be switched at temperatures lower than 360 K. The measurements are shown in figure 68. A sharp switching and two well-defined states of the magnetization at zero field are observed for all measurement temperatures. The switching field of the soft electrode increases from about 1326 Oe at 360 K to about 9000 Oe at 190 K. A direct measurement of a TMR minor loop with a temperature lower than 190 K is not possible, as the available magnetic field of 10 kOe is to small to switch the "soft" electrode any more.

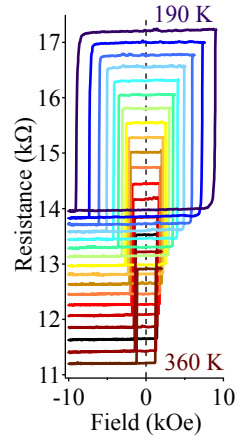

Figure 68: Minor loops of the sample .../$(CoFe)_{79}Tb_{21}$ 30/ CoFeB 1/Mg 0.5/MgO 2.1/ CoFeB 1/$(CoFe)_{79}Tb_{21}$ 10/... at different temperatures.

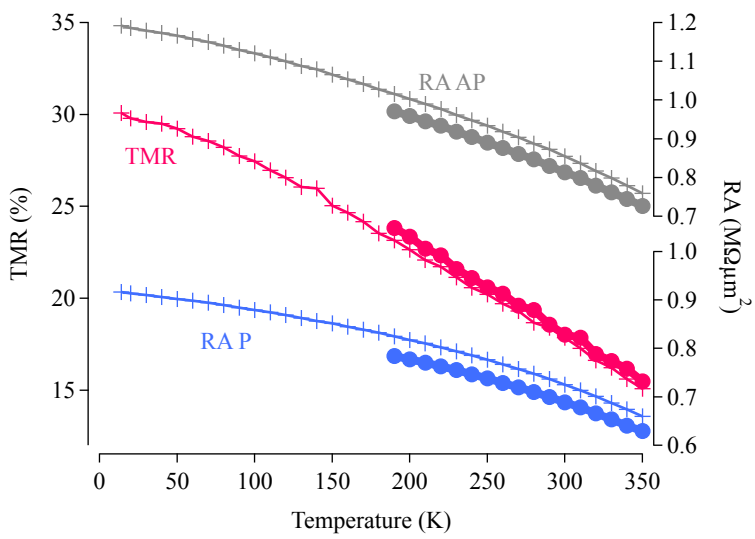

Figure 69: Results of the temperature dependent transport measurement of the sample .../$(CoFe)_{79}Tb_{21}$ 30/ CoFeB 1/Mg 0.5/MgO 2.1/ CoFeB 1/$(CoFe)_{79}Tb_{21}$ 10/...

Figure 69 shows the temperature dependence of the TMR and of the area resistance products RA in the parallel state P and in the antiparallel state AP. The results of the minor loop measurements, that have already been discussed, are marked with points.

Another kind of measurement has been performed in order to determine the TMR-effect of the sample at temperatures lower than 190 K. One defined orientation of the magnetization, parallel or antiparallel, has been adjusted with the external magnetic field at 360 K prior to the measurement. The sample has been cooled down twice and the resistance was obtained. The first cooling process has been done with the parallel, and the second one with the antiparallel orientation of the magnetization in the electrodes. Therefore, the external magnetic field, adjusted at 360 K for a defined state of the magnetization, has not been changed during the temperature dependent measurement. The results of these measurements are marked with crosses in figure 69. The TMR-effect is calculated from the temperature dependent resistances of the sample in the parallel and antiparallel state.

The RA in the P state changes from 0.73 $M\Omega\mu m^2$ at 300 K to 0.92 $M\Omega\mu m^2$ at 13 K, this is a change of 26 % with the temperature. The RA in the AP state changes by 39 %, which changes the TMR-ratio by a factor of 1.7 to 30 % at 13 K.

This temperature dependent behavior is compared to the behavior of a reference sample with Co-Fe-B electrodes and in-plane anisotropy. The MgO barrier of the pMTJ is not considered to be textured as the TMR-values are not close to that in the coherent tunneling scheme.[140] Thus, amorphous alumina is chosen as the barrier material for the reference sample. The layer stack of the reference sample is Si wafer/SiO/Ta 5/Cu 30/Ta 5/Cu 5/Mn-Ir 12/Co-Fe-B 4/Al 1.2+Oxidation/Co-Fe-B 4/Ni-Fe 3/Ta 5/Cu 20/Au 20 as shown in figure 70. The reference sample was annealed at 275°C and shows a TMR-effect of 110 % at 10 mV and 13 K.

The normalized TMR-effects of the Co-Fe-Tb based pMTJ and of the reference sample are shown in figure 71 in dependence of the measurement temperature. The TMR of the pMTJ changes by a factor of 1.7 if cooled to 13 K, whereas the reference sample changes by a factor of 1.6. This is no fundamental change in the temperature dependence of the samples.

[140] D. D. Djayaprawira et al., Appl. Phys. Lett. **86**, 092502 (2005); and S. Ikeda et al., Appl. Phys. Lett. **93**, 082508 (2008)

protection layers
NiFe 3
CoFeB 4
Al 1.2 + Ox
CoFeB 4
MnIr 12
Cu 5
Ta 5
Cu 30
Ta 5
substrate

Figure 70: Stack of the reference sample. An Alumina based system with in-plane anisotropy.

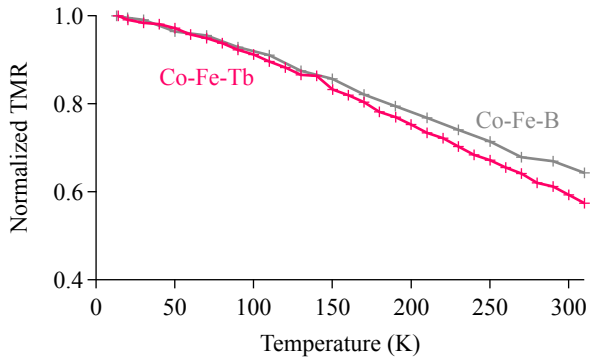

Figure 71: Normalized TMR of the Co-Fe-Tb based pMTJ and of a reference sample with Co-Fe-B electrodes and in-plane anisotropy in dependence of the measurement temperature.

A difference in the temperature dependence of MTJs based on electrodes of rare earth transition metal alloys compared to samples with the "usual" in-plane magnetized electrodes is expected. The magnetization of RE-TM alloys shows a strong temperature dependence for temperatures near the compensation point temperature T_{comp}, resulting from the ferrimagnetic coupling between the RE and TM subnetworks.[141]

RE-TM alloys at the temperature dependent compensation concentration can have zero total magnetization but still exhibit a strongly spin-polarized current. This is a consequence of the ferrimagnetic structure: The spin polarization of the tunneling cur-

[141] This behavior has been sketched in figure 62.

rent from the transition metal can be much higher as compared to the rare-earth metal component combined with a much higher magnetic moment of the latter.[142] As the measured temperature dependence of the Co-Fe-Tb based pMTJ shows no fundamental change compared to the reference sample, it can be concluded, that the available measurement temperature range between 13 K and 360 K is not close to the compensation point temperature of the Co-Fe-Tb electrodes. The compensation point temperature could be manipulated by varying the Tb content in the Co-Fe-Tb layer.[143] Nevertheless, in this study, the electrodes have been designed for the use as electrodes in MTJs and the aim was to tailor a large pMA and a maximum TMR-effect. As these important conditions are now successfully fulfilled, it might be possible to obtain information about the interaction of the antiferromagnetically coupled subnetworks of Tb and Co-Fe by investigating the measurement temperature dependent TMR-effect with respect to different Tb contents in the electrode.

[142] C. Kaiser et al., Phys. Rev. Lett. **95**, 047202 (2005)

[143] P. Chaudhari et al., Appl. Phys. Lett. **22**, 337 (1973)

In Summary, Co-Fe-Tb layers for the use as electrodes in MTJs have been investigated. A perpendicular magnetic anisotropy with a rectangular hysteresis loop has been successfully generated by carefully varying the Tb content in the Co-Fe-Tb layer. Furthermore, the magnetic behavior of the samples was investigated in dependence of the Co-Fe-Tb thickness. The optimum conditions for a pMA are a Tb content between 13 at. % and 21 at. % and a layer thickness larger than 10 nm.

The Co-Fe-Tb layers have successfully been integrated as electrodes into magnetic tunnel junctions with an MgO barrier. A TMR-effect of 18 % at 300 K and 30 % at 13 K has been obtained. The transport properties of the Co-Fe-Tb based samples show no significant change compared to a reference sample with Co-Fe-B electrodes and in-plane anisotropy. Thus, the available measurement temperature range between 13 K and 360 K is not close to the compensation point temperature of the Co-Fe-Tb electrodes.

Summary and Outlook

In this work, various materials for the use as electrodes in perpendicular magnetic tunnel junctions have been investigated. The aim was to tailor a large perpendicular magnetic anisotropy in the systems, to integrate them as electrodes in magnetic tunnel junctions, and, finally, to maximize the tunneling magneto resistance-effect. The generation of a large tunneling magneto resistance-effect in magnetic tunnel junctions combined with a perpendicular magnetic anisotropy in the electrodes is of exceptional importance, as the resulting structures are the most promising candidates for a future commercialization as magnetic random access memory-devices. The advantages of using perpendicular magnetic tunnel junctions compared to devices with in-plane magnetic anisotropy are a higher memory density and thermal stability, a better scalability at sub-micron dimensions, and a lower operation current density.

The challenge of inducing an anisotropy perpendicular to the film plane in a layered structure with only some nanometers in height,[144] has successfully been overcome in this work by carefully varying the preparation parameters of the different materials.

[144] As it is necessary for the use of these structures in a magnetic tunnel junction.

In the first and in the second chapter, structures of alternating Co and Pd or Pt layers have been investigated, respectively. The Co layer thickness in these multilayers has been varied carefully as the perpendicular magnetic anisotropy is a result of a broken symmetry between the nonmagnetic and the magnetic layers. For every Co layer thickness, a detailed investigation of the annealing temperature dependence has been carried out. This is of large importance as the interface anisotropy, the surface anisotropy, the

critical Co thickness, where the perpendicular anisotropy turns into in-plane anisotropy, as well as the interface magnetization have been calculated from the results.

The Co thickness- and annealing temperature-dependence of the saturation magnetization M_s and the remanent magnetization M_r, as well as their absolute values are very similar for all of the investigated samples with Pd as the nonmagnetic layer. Thus, the squareness (M_r/M_s) is nearly one for all of the investigated samples. This shows the very strong perpendicular magnetic anisotropy and good quality of the Co/Pd based superlattices. The anisotropies increase exponentially with the annealing temperature, and the critical Co thickness stays roughly constant.

In the second chapter, Pt has been integrated as non-magnetic material in the multilayer system instead of Pd. The saturation magnetization is in the same range for Co/Pd and for Co/Pt because the magnetic material in the multilayers is the same for both systems. The coercivity of the Co/Pt is about a factor of 10 smaller compared to the Co/Pd. This is due to a rougher surface of the Pt layers compared to the Pd layers. The domain-wall pinning effect is not so serious in Co/Pt films and causes the reduced coercivity of Co/Pt compared to Co/Pd. The annealing temperature behavior of the anisotropies is similar for Pt and Pd as the nonmagnetic material, but the absolute values are smaller for Co/Pt since they are a result from M_s and from H_c. The Co thickness-range with a squareness larger or equal to 0.9, and therefore perpendicular magnetic anisotropy, is shifted to larger values for the Co/Pt compared to the Co/Pd multilayers. This shift is also explained by the rougher surface of the Pt.

In the third chapter, the material FePt has been investigated. The properties of this material have successfully been optimized in order to induce a tetragonal lattice structure, which is strongly correlated with a perpendicular magnetic anisotropy of the system. The lattice structure and the magnetic behavior of the FePt samples have been investigated in dependence of various preparation parameters, such as the substrate temperature, the argon pressure during the sputtering process, and the Fe content in the FePt layer. A phase transition from the chemical disordered cubic $A1$ structure to the ordered face centered tetragonal $L1_0$ struc-

ture has been realized by imposing a strong internal strain/stress to the thin films via a high argon pressure and temperatures between 500 ° C and 600 ° C. This goes along with an improvement of the perpendicular magnetic anisotropy. The argon pressure dependence of the coherence length and of the strain tensor's averaged [001] component emphasizes the improvement of the structure with increasing pressure. The calculated coherence length matches the sputtered film thickness quite well and an increasing amount of epitaxy with increasing argon pressure is concluded from the analysis of the strain tensor. The possibility of controlling the coercivity is of large importance for practical applications of the material. In this work, the coercivity of the FePt could be manipulated by a slight variation of the Fe content compared to the equiatomic composition.

The last material, that has been investigated in this work, is the rare-earth transition-metal alloy Co-Fe-Tb. This is a ferrimagnet with the rare-earth and the transition-metals having antiparallel magnetic moments. The moments are aligned perpendicular to the sample surface and a perpendicular magnetic anisotropy results. The reason for the occurrence of this perpendicular anisotropy is a short-range order on the nearest neighbor atomic scale. A perpendicular magnetic anisotropy with a rectangular hysteresis loop has been successfully generated by carefully varying the Tb content in the Co-Fe-Tb layer. Furthermore, the magnetic behavior of the samples has been investigated in dependence of the Co-Fe-Tb thickness. The optimum conditions for a perpendicular magnetic anisotropy are a Tb content between 13 at. % and 21 at. % and a layer thickness larger than 10 nm.

Finally, the perpendicular magnetic anisotropy with a squareness larger than 0.9 and a rectangular hysteresis loop could be generated in all the different systems by a thoughtful treatment of the respective preparation parameters. In the second section of each chapter, the optimized materials have been used as electrodes in magnetic tunnel junctions. The integration of materials with perpendicular magnetic anisotropy in a magnetic tunnel junction bears a lot of challenges, as two electrodes are necessary. The behavior of one electrode can be strongly influenced by the other

one, as the stray fields are perpendicular to the film plane. The layers cannot be treated as being independent from each other anymore and the antiparallel alignment of the magnetization in the electrodes becomes difficult to realize. In this work, all the investigated materials have been integrated into MgO based magnetic tunnel junctions. The interaction of the electrodes could successfully be controlled by the preparation parameters and measurement conditions.

The multilayer based electrodes are promising materials for the use as electrodes in tunnel junctions, as a lot of parameters are accessible and thus, the interaction of the electrodes can be controlled in several ways.

In the first chapter, the Co/Pd layers have been used as the electrodes. The Co thickness in the electrodes, the material at the barrier interface, the number of multilayers, and the annealing temperature have been investigated in order to maximize the tunneling magneto resistance. The in-plane components of the magnetization, the stray field coupling of the individual electrodes and a diffusion of the Pd to the MgO barrier have been influenced, or rather suppressed. The optimized sample shows a maximum tunneling magneto resistance-ratio of about 11 % at room-temperature with two well-defined switching fields. A rectangular minor loop with two separated magnetic states at zero field has been observed. The tunneling magneto resistance-ratio changes by a factor of 1.7 to 18.5 % at 13 K. This is the highest value reported for magnetic tunnel junctions with Co/Pd multilayers as perpendicular magnetized electrodes.

In the second chapter, the Pd of the multilayers is replaced by Pt, as the Pd turned out to be diffusing to the barrier of the tunnel junction at high annealing temperatures. The annealing temperature dependence of the tunneling magneto resistance-effect has again been investigated. It has been shown that, in contrast to the Pd, no diffusion takes place for the Pt based multilayer electrodes. Tunneling magneto resistance-ratios of about 19 % at room temperature and two well-defined switching fields were observed. The tunneling magneto resistance-effect changes by a factor of 1.9 if cooled to 13 K. The magnetic coupling behavior of both Co/Pt multilayer electrodes has a stronger influence on the annealing-

and measurement-temperature dependence of the tunneling magneto resistance-effect, than reported for Co/Pd based samples.

The optimized FePt layer has also been used as an electrode in a perpendicular magnetic tunnel junction. This has been discussed in the third chapter of this thesis. The $L1_0$ structure of FePt with (001) orientation is very promising for the use as perpendicularly magnetized electrode in tunnel junctions. The large perpendicular magnetic anisotropy with (001) easy axis and a lattice mismatch with the MgO (001) plane of less than 10 % are important conditions for the fabrication of fully epitaxial junctions with a (001) orientated crystalline MgO barrier, and, therefore, high tunneling magneto resistance-ratios. The FePt layer has been integrated as the lower electrode into a perpendicular magnetic tunnel junction. The upper electrode is a Co/Pt multilayer system as the FePt cannot grow in the $L1_0$ structure if used as upper electrode. The room-temperature tunneling magneto resistance-effect of this system is about 9 %.

For the samples with Co-Fe-Tb layers as electrodes, a TMR-effect of 18 % at 300 K and 30 % at 13 K has been attained. This has been shown in the last chapter of the presented thesis. The transport properties of the Co-Fe-Tb based samples showed no significant change compared to a reference sample with Co-Fe-B electrodes and in-plane anisotropy. Thus, the available measurement temperature range between 13 K and 360 K is not close to the compensation point temperature of the Co-Fe-Tb electrodes. An interesting outlook concerning the Co-Fe-Tb based tunnel junction is the investigation of the measurement temperature dependent tunneling magneto resistance-effect with respect to different Tb contents in the electrode. These measurements might give information about the basic physics concerning the interaction of the antiferromagnetically coupled subnetworks of Tb and Co-Fe.

Structures of less than 10 nm are necessary for the final realization of spin torque switched high-density devices with a long time data retention. The only way to reach the commercialization is to combine the large perpendicular magnetic anisotropy of the electrode material with a low damping constant. A low damping in a magnetic tunnel junction leads to the required low current den-

sity for the spin torque switching. A large perpendicular magnetic anisotropy and a low damping constant as parameters of one material are predicted for a special class of ferrimagnetic compounds. The results of this work already exhibit an important basis for the future development of magnetic tunnel junctions as memory devices. An important progress has been done as a perpendicular magnetic anisotropy has been tailored in various materials and a successful integration into magnetic tunnel junctions has been realized.

References

P. Auger, 'Sur L'effet Photoelectrique Compose', J. Phys. Radium **6**, 205 (1925). **A**

P. Auger, 'Sur les rayons β secondaires produits dans un gaz par des rayons', Comptes Rendus **180**, 65 (1925).

A. Ali, W. A. Grant, and P. J. Grttndy, 'A microstructural study of some amorphous transition metal-metalloid surface alloys formed by ion implantation', Phil. Mag. B **37**, 353 (1978).

S. Bader and S. Parkin, 'Spintronics', Annu. Rev. Condens. Matter Phys. **1**, 71 (2010). **B**

K. Barmak, J. Kim, L. H. Lewis, K. R. Coffey, M. F. Toney, A. J. Kellock, and J.-U. Thiele, 'Stoichiometry–anisotropy connections in epitaxial $L1_0$ FePt(001) films', J. Appl. Phys. **95**, 7501 (2004).

K. Barmak, J. Kim, L. H. Lewis, K. R. Coffey, M. F. Toney, A. J. Kellock, and J.-U. Thiele, 'On the relationship of magnetocrystalline anisotropy and stoichiometry in epitaxial $L1_0$ CoPt (001) and FePt (001) thin films', J. Appl. Phys. **98**, 033904 (2005).

L. Berger, 'Emission of spin waves by a magnetic multilayer traversed by a current', Phys. Rev. B **54**, 9353 (1996).

W. H. Bragg and W. L. Bragg, 'The Reflection of X-rays by Crystals', Proc. R. Soc. A **88**, 428 (1913).

W. L. Bragg, 'The Diffraction of Short Electromagnetic Waves by a Crystal', Proc. Cambridge Philos. Soc. **17**, 43 (1913).

F. J. A. den Broeder, W. Hoving, and P. Bloemen, 'Magnetic anisotropy of multilayers', J. Magn. Magn. Mater. **93**, 562 (1991).

F. J. A. den Broeder, D. Kuiper, A. P. van de Mosselaer, and W. Hoving, 'Perpendicular Magnetic Anisotropy of Co-Au Multilayers Induced by Interface Sharpening', Phys. Rev. Lett. **60**, 2769 (1988).

P. Bruno, 'Tight-binding approach to the orbital magnetic moment and magnetocrystalline anisotropy of transition-metal monolayers', Phys. Rev. B **39**, 865 (1989).

P. Bruno and J. P. Renard, 'Magnetic surface anisotropy of transition metal ultrathin films', Appl. Phys. A: Mater. Sci. Process. **49**, 499 (1989).

W. H. Butler, X.-G. Zhang, T. C. Schulthess, and J. M. MacLaren, 'Spin-dependent tunneling conductance of $Fe|MgO|Fe$ sandwiches', Phys. Rev. B **63**, 054416 (2001).

C P. F. Carcia, A. D. Meinhaldt, and A. Suna, 'Perpendicular magnetic anisotropy in Pd/Co thin film layered structures', Appl. Phys. Lett. **47**, 178 (1985).

B. Carvello, C. Ducruet, B. Rodmacq, S. Auffret, E. Gautier, G. Gaudin, and B. Dieny, 'Sizable room-temperature magnetoresistance in cobalt based magnetic tunnel junctions with out-of-plane anisotropy', Appl. Phys. Lett. **92**, 102508 (2008).

P. Chaudhari, J. Cuomo, and R. Gambino, 'Amorphous metallic films for magneto-optic applications', Appl. Phys. Lett. **22**, 337 (1973).

J. S. Chen, Y. Xu, and J. P. Wang, 'Effect of Pt buffer layer on structural and magnetic properties of FePt thin films', J. Appl. Phys. **93**, 1661 (2003).

C. C. Chiang, C.-H. Lai, and Y. C. Wu, 'Low-temperature ordering of $L1_0$ FePt by PtMn underlayers', Appl. Phys. Lett. **88**, 152508 (2006).

K. Coffey, M. Parker, and J. Howard, 'High anisotropy $L1_0$ thin films for longitudinal recording', IEEE Trans. Magn. **31**, 2737 (1995).

T. Devolder, S. Pizzini, J. Vogel, H. Bernas, C. Chappert, V. Mathet, and M. Borowski, 'X-ray absorption analysis of sputter-grown Co/Pt stackings before and after helium irradiation', Z. Phys. B **22**, 193 (1975). **D**

Y. Ding, J. Chen, E. Liu, and L. Li, '$L1_0$ FePt films epitaxially grown on MgO substrates with or without a Cr underlayer', J. Magn. Magn. Mater. **303**, e238 (2006).

D. D. Djayaprawira, K. Tsunekawa, M. Nagai, H. Maehara, S. Yamagata, N. Watanabe, S. Yuasa, Y. Suzuki, and K. Ando, '230% room-temperature magnetoresistance in CoFeB/MgO/CoFeB magnetic tunnel junctions', Appl. Phys. Lett. **86**, 092502 (2005).

R. B. van Dover, M. Hong, E. M. Gyorgy, J. J. F. Dillon, and S. D. Albiston, 'Intrinsic anisotropy of Tb-Fe films prepared by magnetron Co sputtering', J. Appl. Phys. **57**, 3897 (1985).

H. Draaisma, W. de Jonge, and F. den Broeder, 'Magnetic interface anisotropy in Pd/Co and Pd/Fe multilayers', J. Magn. Magn. Mater. **66**, 351 (1987).

V. Drewello, J. Schmalhorst, A. Thomas, and G. Reiss, 'Evidence for strong magnon contribution to the TMR temperature dependence in MgO based tunnel junctions', Phys. Rev. B **77**, 014440 (2008).

Y. Endo, N. Kikuchi, O. Kitakami, and Y. Shimada, 'Lowering of ordering temperature for fct Fe–Pt in Fe/Pt multilayers', J. Appl. Phys. **89**, 7065 (2001). **E**

B. N. Engel, C. D. England, R. A. Van Leeuwen, M. H. Wiedmann, and C. M. Falco, 'Interface magnetic anisotropy in epitaxial superlattices', Phys. Rev. Lett. **67**, 1910 (1991).

G. Feng, H. C. Wu, J. F. Feng, and J. M. D. Coey, 'Temperature dependent coercivity crossover in pseudo-spin-valve magnetic tunnel junctions with perpendicular anisotropy', Appl. Phys. Lett. **99**, 042502 (2011). **F**

M. E. Fisher and A. Aharony, 'Dipolar Interactions at Ferromagnetic Critical Points', Phys. Rev. Lett. **30**, 559 (1973).

H. Fu, R. Giles, M. Mansuripur, and G. Patterson, 'Investigation of the effects of nanostructure on the observable behavior of magnetic thin film using large-scale computer simulation', Comput. Phys. **8**, 80 (1994).

G F. Garcia, G. Casali, S. Auffret, B. Rodmacq, and B. Dieny, 'Exchange bias in $(Pt/Co_{0.9}Fe_{0.1})_n$/FeMn multilayers with perpendicular magnetic anisotropy', J. Appl. Phys. **91**, 6905 (2002).

F. Garcia, F. Fettar, S. Auffret, B. Rodmacq, and B. Dieny, 'Exchange-biased spin valves with perpendicular magnetic anisotropy based on (Co/Pt) multilayers', J. Appl. Phys. **93**, 8397 (2003).

H U. Hartmann, 'Magnetic force microscopy', Annu. Rev. Mater. Sci. **29**, 53 (1999).

J. V. Harzer, B. Hillebrands, R. L. Stamps, G. Guntherodt, C. D. England, and C. M. Falco, 'Magnetic properties of Co/Pd multilayers determined by Brillouin light scattering and SQUID magnetometry', J. Appl. Phys. **69**, 2448 (1991).

S. Hashimoto and Y. Ochiai, 'Co/Pt and Co/Pd multilayers as magneto-optical recording materials', J. Magn. Magn. Mater. **88**, 211 (1990).

S. Hashimoto, Y. Ochiai, and K. Aso, 'Perpendicular magnetic anisotropy and magnetostriction of sputtered Co/Pd and Co/Pt multilayered films', J. Appl. Phys. **66**, 4909 (1989).

J. O. Hauch, M. Fonin, M. Fraune, P. Turban, R. Guerrero, F. G. Aliev, J. Mayer, U. Rüdiger, and G. Güntherodt, 'Fully epitaxial Fe(110)/MgO(111)/Fe(110) magnetic tunnel junctions: Growth, transport, and spin filtering properties', Appl. Phys. Lett. **93**, 083512 (2008).

R. M. Hazeni and A. Navrotzky, 'Effects of pressure on order-disorder reactions', Am. Mineral. **81**, 1021 (1996).

F. Hellman and E. M. Gyorgy, 'Growth-induced magnetic anisotropy in amorphous Tb-Fe', Phys. Rev. Lett. **68**, 1391 (1992).

F. Hellman, M. Messer, and E. N. Abarra, 'Coercivity in amorphous Tb–Fe alloys', J. Appl. Phys. **86**, 1047 (1999).

M. H. Hong, K. Hono, and M. Watanabe, 'Microstructure of FePt/Pt magneticthin films with high perpendicular coercivity', J. Appl. Phys. **84**, 4403 (1998).

S. N. Hsiao, F. T. Yuan, H. W. Chang, H. W. Huang, S. K. Chen, and H. Y. Lee, 'Effect of initial stress/strain state on order-disorder transformation of FePt thin films', Appl. Phys. Lett. **94**, 232505 (2009).

Y.-N. Hsu, S. Jeong, D. E. Laughlin, and D. N. Lambeth, 'Effects of Ag underlayers on the microstructure and magnetic properties of epitaxial FePt thin films', J. Appl. Phys. **89**, 7068 (2001).

S. Ikeda, J. Hayakawa, Y. Ashizawa, Y. M. Lee, K. Miura, H. Hasegawa, M. Tsunoda, F. Matsukura, and H. Ohno, 'Tunnel magnetoresistance of 604% at 300 K by suppression of Ta diffusion in CoFeB/MgO/CoFeB pseudo-spin-valves annealed at high temperature', Appl. Phys. Lett. **93**, 082508 (2008). **I**

S. Ikeda, J. Hayakawa, Y. M. Lee, F. Matsukura, Y. Ohno, T. Hanyu, and H. Ohno, 'Magnetic Tunnel Junctions for Spintronic Memories and Beyond', IEEE Trans. Electr. Dev. **54**, 991 (2007).

S. Ikeda, K. Miura, H. Yamamoto, K. Mizunuma, H. D. Gan, M. Endo, S. Kanai, J. Hayakawa, F. Matsukura, and H. Ohno, 'A perpendicular-anisotropy CoFeB-MgO magnetic tunnel junction', Nat. Mater. **9**, 721 (2010).

G. S. C. III and S. Kirkpatrick, 'Structural ordering in some amorphous metals and alloys', AIP Conf. Proc. **31**, 339 (1976).

M. T. Johnson, P. J. H. Bloemen, F. J. A. den Broeder, and J. J. de Vries, 'Magnetic anisotropy in metallic multilayers', Rep. Prog. Phys. **59**, 1409 (1996). **J**

Joint Committee on Powder Diffraction Standards, *JCPDS-ICDD Powder Diffraction Database (2000)*, card No. 29-718.

Joint Committee on Powder Diffraction Standards, *JCPDS-ICDD Powder Diffraction Database (2000)*, card No. 43-1359.

M. Julliere, 'Tunneling between ferromagnetic films', Phys. Lett. A **54**, 225 (1975).

K C. Kaiser, A. F. Panchula, and S. S. P. Parkin, 'Finite Tunneling Spin Polarization at the Compensation Point of Rare-Earth-Metal–Transition-Metal Alloys', Phys. Rev. Lett. **95**, 047202 (2005).

S. Kämmerer, A. Thomas, A. Hütten, and G. Reiss, 'Co_2MnSi Heusler alloy as magnetic electrodes in magnetic tunnel junctions', Appl. Phys. Lett. **85**, 79 (2004).

T. Katayama, K. Hasegawa, K. Kawanishi, and T. Tsushima, 'Annealing effects on magnetic properties of amorphous GdCo, GdFe, and GdCoMo films', J. Appl. Phys. **49**, 1759 (1978).

G. Kim, Y. Sakuraba, M. Oogane, Y. Ando, and T. Miyazaki, 'Tunneling magnetoresistance of magnetic tunnel junctions using perpendicular magnetization $L1_0$-CoPt electrodes', Appl. Phys. Lett. **92**, 172502 (2008).

K. Kobayashi and H. Akimoto, 'TMR Film and Head Technologies', FUJITSU Sci. Tech. J. **42**, 139 (2006).

U. F. Kocks, C. N. Tomé, and H. R. Wenk, *Texture and anisotropy* (Camebridge university press, 1998).

K. Kopitzki and P. Herzog, *Einführung in die Festkörperphysik* (G. B. Teubner Verlag, 2004).

Z. Kugler, V. Drewello, M. Schäfers, J. Schmalhorst, G. Reiss, and A. Thomas, 'Temperature and bias voltage dependence of Co/Pd multilayer-based magnetic tunnel junctions with perpendicular magnetic anisotropy', J. Magn. Magn. Mater. **323**, 198 (2011).

Z. Kugler, J.-P. Grote, V. Drewello, O. Schebaum, G. Reiss, and A. Thomas, 'Co/Pt multilayer-based magnetic tunnel junctions with perpendicular magnetic anisotropy', J. Appl. Phys. **111**, 07C703 (2012).

C. M. Kuo, P. C. Kuo, H. C. Wu, Y. D. Yao, and C. H. Lin, 'Magnetic hardening mechanism study in FePt thin films', J. Appl. Phys. **85**, 4886 (1999).

L R. Law, R. Sbiaa, T. Liew, and T. C. Chong, 'Effects of Ta seed layer and annealing on magnetoresistance in CoFe/Pd-based

pseudo-spin-valves with perpendicular anisotropy', Appl. Phys. Lett. **91**, 242504 (2007).

Y. M. Lee, J. Hayakawa, S. Ikeda, F. Matsukura, and H. Ohno, 'Giant tunnel magnetoresistance and high annealing stability in CoFeB/MgO/CoFeB magnetic tunnel junctions with synthetic pinned layer', Appl. Phys. Lett. **89**, 042506 (2006).

Y. M. Lee, J. Hayakawa, S. Ikeda, F. Matsukura, and H. Ohno, 'Effect of electrode composition on the tunnel magnetoresistance of pseudo-spin-valve magnetic tunnel junction with a MgO tunnel barrier', Appl. Phys. Lett. **90**, 212507 (2007).

D. Lim, S. Kim, and S.-R. Lee, 'Magnetoresistance behavior of a magnetic tunnel junction with perpendicularly magnetized Co/Pd multilayers', J. Appl. Phys. **97**, 10C902 (2005).

S. Lim, S. Han, K. Shin, and H. Kim, 'Size effects on characteristic magnetic fields of a spin-valve multilayer by computer simulation', J. Magn. Magn. Mater. **223**, 192 (2001).

A. Lyberatos, J. Earl, and R. W. Chantrell, 'Model of thermally activated magnetization reversal in thin films of amorphous rare-earth-transition-metal alloys', Phys. Rev. B **53**, 5493 (1996).

T. Maeda, T. Kai, A. Kikitsu, T. Nagase, and J. ichi Akiyama, 'Reduction of ordering temperature of an FePt-ordered alloy by addition of Cu', Appl. Phys. Lett. **80**, 2147 (2002). **M**

S. Mangin, D. Ravelosona, J. A. Katine, M. J. Carey, B. D. Terris, and E. E. Fullerton, 'Current-induced magnetization reversal in nanopillars with perpendicular anisotropy', Nat. Mater. **5**, 210 (2006).

M. Mansuripur, R. Giles, and G. Patterson, 'Coercivity of domain-wall motion in thin films of amorphous rare-earth–transition-metal alloys', J. Appl. Phys. **69**, 4844 (1991).

T. B. Massalski, *Binary Alloy Phase Diagrams* (ASM International, 2nd ed., 1990).

J. Mathon and A. Umerski, 'Theory of tunneling magnetoresistance of an epitaxial Fe/MgO/Fe(001) junctions', Phys. Rev. B **63**, 220403 (2001).

M. A. McCord and M. J. Rooks, *Handbook of Microlithography, Micromachining and Microfabrication* (SPIE Optical Engineering Press, 1997).

H. Meng and J.-P. Wang, 'Spin transfer in nanomagnetic devices with perpendicular anisotropy', Appl. Phys. Lett. **88**, 172506 (2006).

Y. Mimura, N. Imamura, T. Kobayashi, A. Okada, and Y. Kushiro, 'Magnetic properties of amorphous alloy films of Fe with Gd, Tb, Dy, Ho, or Er', J. Appl. Phys. **49**, 1208 (1978).

T. Miyazaki and N. Tezuka, 'Giant magnetic tunneling effect in $Fe/Al_2O_3/Fe$ junctions', J. Magn. Magn. Mater. **139**, L231 (1995).

K. Mizunuma, S. Ikeda, J. H. Park, H. Yamamoto, H. Gan, K. Miura, H. Hasegawa, J. Hayakawa, F. Matsukura, and H. Ohno, 'MgO barrier-perpendicular magnetic tunnel junctions with CoFe/Pd multilayers and ferromagnetic insertion layers', Appl. Phys. Lett. **95**, 232516 (2009).

K. Mizunuma, M. Yamanouchi, S. Ikeda, H. Sato, H. Yamamoto, H.-D. Gan, K. Miura, J. Hayakawa, F. Matsukura, and H. Ohno, 'Pd Layer Thickness Dependence of Tunnel Magnetoresistance Properties in CoFeB/MgO-Based Magnetic Tunnel Junctions with Perpendicular Anisotropy CoFe/Pd Multilayers', Appl. Phys. Express **4**, 023002 (2011).

J. S. Moodera, L. R. Kinder, T. M. Wong, and R. Meservey, 'Large Magnetoresistance at Room Temperature in Ferromagnetic Thin Film Tunnel Junctions', Phys. Rev. Lett. **74**, 3273 (1995).

N N. Nakajima, T. Koide, T. Shidara, H. Miyauchi, H. Fukutani, A. Fujimori, K. Iio, T. Katayama, M. Nývlt, and Y. Suzuki, 'Perpendicular Magnetic Anisotropy Caused by Interfacial Hybridization via Enhanced Orbital Moment in Co/Pt Multilay-

ers: Magnetic Circular X-Ray Dichroism Study', Phys. Rev. Lett. **81**, 5229 (1998).

M. Nakayama, T. Kai, N. Shimomura, M. Amano, E. Kitagawa, T. Nagase, M. Yoshikawa, T. Kishi, S. Ikegawa, and H. Yoda, 'Spin transfer switching in TbCoFe /CoFeB /MgO /CoFeB/ TbCoFe magnetic tunnel junctions with perpendicular magnetic anisotropy', J. Appl. Phys. **103**, 07A710 (2008).

S. S. Nandra and P. J. Grundy, 'An investigation of the atomic arrangements in some amorphous rare earth-transition metal alloys', J. Phys. F. **7**, 207 (1977).

L. Néel, 'Anisotropie magnétique superficielle et surstructures d'orientation', J. Phys. Radium **15**, 225 (1954).

N. Nishimura, T. Hirai, A. Koganei, T. Ikeda, K. Okano, Y. Sekiguchi, and Y. Osada, 'Magnetic tunnel junction device with perpendicular magnetization films for high-density magnetic random access memory', J. Appl. Phys. **91**, 5246 (2002).

Y. Ochiai, S. Hashimoto, and K. Aso, 'Co/Pt and Co/Pd ultrathin-multilayered films as new magneto-optical recording materials', IEEE Trans. Magn. **25**, 3755 (1989).

H.-S. Oh and S.-K. Joo, 'Enhancement of coercivity by underlayer control in Co/Pd and Co/Pt multilayers', IEEE Trans. Magn. **32**, 4061 (1996).

H. Ohmori, T. Hatori, and S. Nakagawa, 'Perpendicular magnetic tunnel junction with tunneling magnetoresistance ratio of 64% using MgO (100) barrier layer prepared at room temperature', J. Appl. Phys. **103**, 07A911 (2008).

M. Ohring, *Materials Science of Thin Films, Deposition and Structure* (Academic Press, San Diego u.a., 2002).

S. Okamoto, N. Kikuchi, O. Kitakami, T. Miyazaki, Y. Shimada, and K. Fukamichi, 'Chemical-order-dependent magnetic anisotropy and exchange stiffness constant of FePt (001) epitaxial films', Phys. Rev. B **66**, 024413 (2002).

O

T. Onoue, J. Kawaji, K. Kuramochi, T. Asahi, and T. Osaka, 'Effect of underlayers on magnetic properties of Co/Pd multilayer perpendicular magnetic recording media', J. Magn. Magn. Mater. **235**, 82 (2001).

J. Orehotsky and K. Schröder, 'Magnetic Properties of Amorphous Fe_xGd_y Alloy Thin Films', J. Appl. Phys. **43**, 2413 (1972).

P J.-H. Park, C. Park, T. Jeong, M. T. Moneck, N. T. Nufer, and J.-G. Zhu, 'Co/Pt multilayer based magnetic tunnel junctions using perpendicular magnetic anisotropy', J. Appl. Phys. **103**, 07A917 (2008).

W. Park, I. J. Hwang, T. Kim, K. J. Lee, and Y. K. Kim, 'Anomalous switching in submicrometer magnetic tunnel junction arrays arising from magnetic vortex and domain wall pinning', J. Appl. Phys. **96**, 1748 (2004).

S. S. P. Parkin, C. Kaiser, A. Panchula, P. M. Rice, B. Hughes, M. Samant, and S. H. Yang, 'Giant tunnelling magnetoresistance at room temperature with MgO (100) tunnel barriers', Nat. Mater. **3**, 862 (2004).

Peter and Sigmund, 'Mechanisms and theory of physical sputtering by particle impact', Nucl. Instrum. Meth. Phys. Res. B **27**, 1 (1987).

G. A. Prinz, 'Magnetoelectronics', Science **282**, 1660 (1998).

R M. T. Rahman, A. Lyle, G. Hu, W. J. Gallagher, and J. ping Wang, 'High temperature annealing stability of magnetic properties in MgO-based perpendicular magnetic tunnel junction stacks with CoFeB polarizing layer', J. Appl. Phys. **109**, 07C709 (2011).

D. Ravelosona, C. Chappert, V. Mathet, and H. Bernas, 'Chemical order induced by ion irradiation in FePt (001) films', Appl. Phys. Lett. **76**, 236 (2000).

R. A. Ristau, K. Barmak, L. H. Lewis, K. R. Coffey, and J. K. Howard, 'On the relationship of high coercivity and $L1_0$ ordered phase in CoPt and FePt thin films', J. Appl. Phys. **86**, 4527 (1999).

S

A. Sakuma, 'First Principle Calculation of the Magnetocrystalline Anisotropy Energy of FePt and CoPt Ordered Alloys', J. Phys. Soc. Jpn. **63**, 3053 (1994).

M. Sakurai, 'Magnetic anisotropy of epitaxial Fe/Pt(001) multilayers', Phys. Rev. B **50**, 3761 (1994).

M. Sakurai, T. Takahata, and I. Moritani, 'Magnetic and magneto-optical properties of Co/Ru multilayers', J. Magn. Soc. Japan **15**, 411 (1991).

O. Schebaum, PhD thesis, Universität Bielefeld, 2011.

J. Schmalhorst, A. Thomas, S. Kämmerer, O. Schebaum, D. Ebke, M. D. Sacher, G. Reiss, A. Hütten, A. Turchanin, A. Gölzhäuser, and E. Arenholz, 'Transport properties of magnetic tunnel junctions with Co_2MnSi electrodes: The influence of temperature-dependent interface magnetization and electronic band structures', Phys. Rev. B **75**, 014403 (2007).

S. Seal, *Functional Nanostructures: Processing, Characterization, and Application* (Springer US, 2007).

T. Seki, T. Shima, K. Takanashi, Y. Takahashi, E. Matsubara, and K. Hono, '$L1_0$ ordering of off-stoichiometric FePt (001) thin films at reduced temperature', Appl. Phys. Lett. **82**, 2461 (2003).

T. Seki, T. Shima, K. Takanashi, Y. Takahashi, E. Matsubara, Y. K. Takahashi, and K. Hono, 'Influence of the buffer layers on magnetic properties of FePt (001) films sputter-deposited at reduced temperature', J. Appl. Phys. **96**, 1127 (2004).

T. Shima, T. Moriguchi, S. Mitani, and K. Takanashi, 'Low-temperature fabrication of $L1_0$ ordered FePt alloy by alternate monoatomic layer deposition', Appl. Phys. Lett. **80**, 288 (2002).

J. Slonczewski, 'Current-driven excitation of magnetic multilayers', J. Magn. Magn. Mater. **159**, L1 (1996).

R. C. Sousa, J. J. Sun, V. Soares, P. P. Freitas, A. Kling, M. F. da Silva, and J. C. Soares, 'Large tunneling magnetoresistance

enhancement by thermal anneal', Appl. Phys. Lett. **73**, 3288 (1998).

E. C. Stoner and E. P. Wohlfarth, 'A Mechanism of Magnetic Hysteresis in Heterogeneous Alloys', Phil. Trans. R. Soc. A **240**, 599 (1948).

A.-C. Sun, P. C. Kuo, J.-H. Hsu, H. L. Huang, and J.-M. Sun, 'Epitaxial growth mechanism of $L1_0$ FePt thin films on Pt/Cr bilayer with amorphous glass substrate', J. Appl. Phys. **98**, 076109 (2005).

T. Suzuki, K. Harada, N. Honda, and K. Ouchi, 'Preparation of ordered FePt thin films for perpendicular magnetic recording media', J. Magn. Magn. Mater. **193**, 85 (1999).

T. Suzuki, N. Honda, and K. Ouchi, 'Magnetization reversal process in polycrystalline ordered Fe–Pt(001) thin films', J. Appl. Phys. **85**, 4301 (1999).

T Z. R. Tadisina, A. Natarajarathinam, B. D. Clark, A. L. Highsmith, T. Mewes, S. Gupta, E. Chen, and S. Wang, 'Perpendicular magnetic tunnel junctions using Co-based multilayers', J. Appl. Phys. **107**, 09C703 (2010).

Y. Takahashi, M. Ohnuma, and K. Hono, 'Effect of Cu on the structure and magnetic properties of FePt sputtered film', J. Magn. Magn. Mater. **246**, 259 (2002).

N. Tezuka, N. Ikeda, A. Miyazaki, S. Sugimoto, M. Kikuchi, and K. Inomata, 'Tunnel magnetoresistance for junctions with epitaxial full-Heusler $Co_2FeAl_{0.5}Si_{0.5}$ electrodes with $B2$ and $L2_1$ structures', Appl. Phys. Lett. **89**, 112514 (2006).

M. F. Toney, W.-Y. Lee, J. A. Hedstrom, and A. Kellock, 'Thickness and growth temperature dependence of structure and magnetism in FePt thin films', J. Appl. Phys. **93**, 9902 (2003).

K. Tsunekawa, D. D. Djayaprawira, M. Nagai, H. Maehara, S. Yamagata, N. Watanabe, S. Yuasa, Y. Suzuki, and K. Ando, 'Giant tunneling magnetoresistance effect in low-resistance CoFeB/MgO(001)/CoFeB magnetic tunnel junctions for read-head applications', Appl. Phys. Let. **87**, 072503 (2005).

D. Wang, C. Nordman, J. Daughton, Z. Qian, and J. Fink, '70% TMR at room temperature for SDT sandwich junctions with CoFeB as free and reference Layers', IEEE Trans. Magn. **40**, 2269 (2004). **W**

Y. Wang, W. X. Wang, H. X. Wei, B. S. Zhang, W. S. Zhan, and X. F. Han, 'Effect of annealing on the magnetic tunnel junction with Co/Pt perpendicular anisotropy ferromagnetic multilayers', J. Appl. Phys. **107**, 09C711 (2010).

J. Wecker and J. Bangert, *Nichtflüchtige Datenspeicherund mit magnetischen Tunnelelementen: Das Magnetic Random Access Memory (MRAM)* (Forschungszentrum Jülich GmbH: Vorlesungsmanuskripte des 30. IFF-Ferienkurses, 1999).

H. X. Wei, Q. H. Qin, M. Ma, R. Sharif, and X. F. Han, '80% tunneling magnetoresistance at room temperature for thin Al–O barrier magnetic tunnel junction with CoFeB as free and reference layers', J. Appl. Phys. **101**, 09B501 (2007).

M. Weisheit, L. Schultz, and S. Fähler, 'Textured growth of highly coercive $L1_0$ ordered FePt thin films on single crystalline and amorphous substrates', J. Appl. Phys. **95**, 7489 (2004).

D. Weller, A. Moser, L. Folks, M. Best, W. Lee, M. Toney, M. Schwickert, J.-U. Thiele, and M. Doerner, 'High K_u materials approach to 100 Gbits/in^2', IEEE Trans. Magn. **36**, 10 (2000).

G. Williamson and W. Hall, 'X-ray line broadening from filed aluminium and wolfram', Acta Metall. **1**, 22 (1953).

Y. Xu, J. S. Chen, and J. P. Wang, 'In situ ordering of FePt thin films with face-centered-tetragonal (001) texture on $Cr_{100-x}Ru_x$ underlayer at low substrate temperature', Appl. Phys. Lett. **80**, 3325 (2002). **X**

K. Yakushiji, K. Noma, T. Saruya, H. Kubota, A. Fukushima, T. Nagahama, S. Yuasa, and K. Ando, 'High Magnetoresistance Ratio and Low Resistance–Area Product in Magnetic Tunnel Junctions with Perpendicularly Magnetized Electrodes', Appl. Phys. Express **3**, 053003 (2010). **Y**

X. Yan, M. Hirscher, T. Egami, and E. E. Marinero, 'Direct observation of anelastic bond-orientational anisotropy in amorphous $Tb_{26}Fe_{62}Co_{12}$ thin films by x-ray diffraction', Phys. Rev. B **43**, 9300 (1991).

L.-X. Ye, C.-M. Lee, J.-W. Syu, Y.-R. Wang, K.-W. Lin, Y.-H. Chang, and T. ho Wu, 'Effect of annealing and barrier thickness on MgO-based Co/Pt and Co/Pd multilayered perpendicular magnetic tunnel junctions', IEEE Trans. Magn. **44**, 3601 (2008).

I. Yoo, D. kee Kim, and Y. K. Kim, 'Switching characteristics of submicrometer magnetic tunnel junction devices with perpendicular anisotropy', J. Appl. Phys. **97**, 10C919 (2005).

M. Yoshikawa, E. Kitagawa, T. Nagase, T. Daibou, M. Nagamine, K. Nishiyama, T. Kishi, and H. Yoda, 'Tunnel Magnetoresistance over 100% in MgO-Based Magnetic Tunnel Junction Films With Perpendicular Magnetic $L1$ -FePt Electrodes', IEEE Trans. Magn. **44**, 2573 (2008).

S. Yuasa, A. Fukushima, H. Kubota, Y. Suzuki, and K. Ando, 'Giant tunneling magnetoresistance up to 410% at room temperature in fully epitaxial Co/MgO/Co magnetic tunnel junctions with bcc Co(001) electrodes', Appl. Phys. Lett. **89**, 042505 (2006).

S. Yuasa, T. Katayama, T. Nagahama, A. Fukushima, H. Kubota, Y. Suzuki, and K. Ando, 'Giant tunneling magnetoresistance in fully epitaxial body-centered-cubic Co/MgO/Fe magnetic tunnel junctions', Appl. Phys. Lett. **87**, 222508 (2005).

S. Yuasa, T. Nagahama, A. Fukushima, S. Yoshishige, and K. Ando, 'Giant room-temperature magnetoresistance in single-crystal Fe/MgO/Fe magnetic tunnel junctions', Nat. Mater. **3**, 868 (2004).

Z H. Zabel and S. D. Bader, *Magnetic Heterostructures* (Springer, 2008).

138 References in total.

Appendix: Methods

In this chapter the sample preparation and measurement techniques with their physical effects, that have been used in the framework of this thesis, are introduced. The basic principles and the technical properties of the equipment for the fabrication, processing, and for the characterization of the thin films are explained. This chapter should give a background for the previous chapters and can only provide a short overview. Further details can be found in the listed references.

Sample preparation

Sputter deposition, or short sputtering, is an UHV-technique for the fabrication of thin films.[145] The basic mechanism is the momentum exchange between an incident, energetic particle and atoms in a solid target material due to inelastic collisions. Clusters of atoms are ejected out of the target material if the energy of the incident particles is higher than the surface binding energy in the target material.[146]

Normally, Ar^+-ions are used as incident particles. For *DC-sputtering*, an Ar^+-ion plasma is generated by applying a high voltage in between the target (cathode) and the anode in an argon gas atmosphere.

Sputtering with low argon pressure is desirable as more ejected particles can reach the substrate, which is placed above the target. In the special case of *magnetron sputtering*, a torus-shaped magnetic field percolates the target due to permanent magnets, placed under the target. The electrons of the plasma are forced on orbits and the probability for an ionization of the argon atoms is

[145] A detailed overview about sputter deposition can be found in

M. Ohring, *Materials Science of Thin Films, Deposition and Structure* (Academic Press, San Diego u.a., 2002)

[146] Peter et al., Nucl. Instrum. Meth. Phys. Res. B **27**, 1 (1987)

increased. Thus, using lower argon pressure becomes possible for magnetron sputtering.

In the special case of *RF-sputtering* a high-frequency voltage[147] is applied in addition to an offset voltage between the anode and the target. The argon ions are accelerated to the cathode by this offset voltage. They are not influenced by the RF-voltage because of their high mass. In contrast, the electrons of the plasma are accelerated to the target due to the RF-voltage. The target material is not sputtered due to the collisions with the electrons, as the momentum exchange is small. The acceleration of both, ions and electrons, to the target material leads to the fact that an insulating material is not charged by the ions and, in contrast to DC-sputtering, sputtering of insulating materials becomes possible by applying the additional RF-voltage.

[147] Typically 1-100 MHz

In this work, two sputtering systems have been used for the sample preparation. A sample transfer without a vacuum break between the two independent sputtering systems is possible as they are connected via a handler chamber. One sputtering system,[148] with six 4 inch and one 2 inch magnetron sputtering guns reaches a base pressure of $1 \cdot 10^{-7}$ mbar. Three of the 4 inch guns are suitable for conductive and ferromagnetic, two for conductive but not ferromagnetic, and one RF sputtering gun for the deposition of insulating materials. The 2 inch sputtering gun can be used for the deposition of conductive target materials. The other sputtering system,[149] with seven 3 inch magnetron sputtering guns, has a base pressure of $5 \cdot 10^{-10}$ mbar. All guns are appropriate for conductive, ferromagnetic or nonferromagnetic materials and one of the magnetrons is a RF sputtering gun. Co-sputtering from two sputtering guns simultaneously as well as sputtering at substrate temperatures of up to 1000 °C is possible. The sputter rates[150] and thus the stoichiometry of co-sputtered samples can be changed by the power of the respective sputtering gun.

[148] *CLAB 600 Clustertool* from LEYBOLD DRESDEN

[149] From BESTEC BERLIN

[150] The sputter rate describes the thickness of the deposited material per time.

The argon pressure in both systems can be controlled by the pump rate or directly by the argon flow. The pump rate is regulated by the position of a throttle in front of the pump. In this work, the argon flow is kept constant while the throttle position is varied to adjust the desired pressure. Normally, the argon pressure is regulated in the range of $1 \cdot 10^{-1}$ mbar to $1 \cdot 10^{-3}$ mbar.

THE CALIBRATIONS of the sputter rates in the LEYBOLD sputtering system are determined by sputtering a certain material for a defined time and afterwards measuring the resulting layer thickness by x-ray reflectometry. The BESTEC sputtering system possesses an integrated quartz crystal for the determination of the sputtered film thickness. Typical sputter rates are in the range of 0.2 nm/s to 0.7 nm/s.

THE ANNEALING of the samples is done in a vacuum furnace with a base pressure of $1 \cdot 10^{-9}$ mbar and temperatures of up to 550 °C. The annealing process has to be carried out under high vacuum conditions to prevent oxidation effects of the sample materials. It is possible to induce a structural changing of the sample by heating for a certain time.[151] Furthermore, annealing can lead to a healing of defects.[152] Otherwise, using too high temperatures causes a diffusion of the materials in the sample stack.[153] In this work, the annealing is done in the magnetic field of 6500 Oe of a permanent magnet perpendicular to the film plane to increase the perpendicular magnetic anisotropy.

AN OPTICAL LITHOGRAPHY PROCESS of the sputtered samples is necessary to prepare elements of a defined area for the transport measurements.[154] The lithography process consists of several steps that are described in the following paragraph.

First, a positive photo resist[155] is pipetted on the sample surface. Spincoating with 6000 revolutions per minute leads to a homogeneous layer of the photo resist on the sample surface. The sample is baked at 85 °C for about 30 min to harden the resist and, thus, to induce a better adhesion on the sample surface.

In the next step of the lithography process, the desired structures are transmitted to the light-sensitive resist by either using an UV exposure[156] in combination with a contact mask or a laser exposer.[157] The contact mask is placed on the sample surface with the photo resist and exposed with the UV-light, while the desired structures are directly written into the resist by using the laser exposure. The laser scans the sample in single lines and a shutter is opened if the respective areas should be exposed to the light. The lithography with a contact mask and UV-light gives a

[151] S. Kämmerer et al., Appl. Phys. Lett. **85**, 79 (2004); and Y. M. Lee et al., Appl. Phys. Lett. **89**, 042506 (2006)

[152] R. C. Sousa et al., Appl. Phys. Lett. **73**, 3288 (1998)

[153] S. Ikeda et al., Appl. Phys. Lett. **93**, 082508 (2008)

[154] A detailed overview about lithography can be found in

M. A. McCord et al., *Handbook of Microlithography, Micromachining and Microfabrication* (SPIE Optical Engineering Press, 1997)

[155] *AR-P 5350* from ALL RESIST

[156] from OXFORD INSTRUMENTS.

[157] *DWL 66* from HEIDELBERG INSTRUMENTS

fast and easy method for the lithography, while the laser lithography is more accurate and provides more flexibility with respect to the desired structures. In this work, the exposed structures are squares of $7.5\times7.5\,\mu m^2$ or $12.5\times12.5\,\mu m^2$.

The solubility of the resist is increased due to the exposure with light. In the next step of the lithography, the development, the resist can be removed on the exposed areas by using an developer[158] diluted with water in a ratio of 1:2.

[158] *AR 300-35* from ALL RESIST

The transfer of the exposed patterns on the layer system is the following lithography step and is done by ion beam etching. Argon ions are accelerated to the sample surface. Thus, the uncovered areas of the sample, where the resist has been removed, are sputtered. The areas that have not been exposed to the light are still protected against the ion beam by the remaining resist. A depth profile can be measured during the etching process by mass spectrometry. Thus, a defined stop of the etching process in a desired layer of the sample stack is possible. The argon pressure is regulated to $5\cdot10^{-4}$ mbar. The sample rotates under an angle of 30° in the ion beam to prevent inhomogenety and shadow effects on the sample.

After the etching, an insulating material, usually TaO_x, is sputtered on the sample to fill up the etched areas in between the patterned elements.

The next step of the lithography process is the removing[159] of the remaining resist with the TaO_x on top. This is done in an ultrasonic sound bath. The result is a homogeneous surface with the insulating material in between the single elements of the sample. This makes a contacting of the elements for a later measurement very comfortable.

[159] A remover *AR 300-70* from ALL RESIST or alternatively acetone has been used.

As the patterned structures are to small for a direct contacting in some of the measurement setups, they are capped with gold contact pads. Therefore, a second lithography process with every single step has to be carried out. The structure that is exposed to the resist is designed in the way, that afterwards, the whole sample surface is capped with the resist, except the areas on top of the patterned elements that should function as the contact pads. Layers of tantalum and gold are sputtered in this "holes" as the contact pads, and the remaining resist is removed.

A BONDING[160] of the patterned elements is necessary for the transport measurements of the samples at low temperatures or at high magnetic field. The samples are cased in an IC-socket with 24 contacts and the patterned elements of the sample are contacted by a 24.4 μm thick gold wire. The remaining end of the gold wire is connected with one contact of the IC-socket. The contacting results from mechanical friction based on ultrasonic sound at temperatures of about 90 °C. Afterwards, the IC-socket with the bonded sample can be placed in a counter-piece at the measurement setup for the investigation of the sample.

[160] A bonding machine from HYBOND, model *572A* has been used.

Measurement techniques

THE TRANSPORT MEASUREMENTS that have been carried out in this work are the investigation of the TMR-effect on the one hand and measurements of I-V-curves on the other hand. The current is measured with a constant bias voltage in dependence of the external magnetic field for the TMR-measurements. Normally, the applied bias voltage is 10 mV. For the detection of an I-V-curve, the current is measured in dependence of the voltage, but with constant external magnetic field.

The transport measurements are carried out by a conventional two probe DC-technique in a perpendicular magnetic field. The samples are contacted via two gold needles if the element has not been bonded previously. The exact positioning of the gold needles is carried out by using three micrometer controllable tables. A custom-made electrometer with integrated constant-voltage source generates the voltage. Seven different gain ranges from 1 mA/V to 1 nA/V are accessible to measure the resulting current. An output voltage with up to $\pm$10 V is displayed at the output of the box. This output voltage is digitized via a multimeter[161] and recorded with the controlling computer.

[161] *K 2000* from KEITHLEY

Two different measurement setups have been used in this work. The one setup is designed for measurements at room-temperature. The magnetic field originates from two coils with an iron core and reaches a maximum value of about $\pm$3000 Oe. The field is measured by a Gaussmeter,[162] digitized via a multimeter,[163] and

[162] *Bell 6010*

[163] *K 2000* from KEITHLEY

recorded with the controlling computer. A special sample holder has been used to place the sample surface perpendicular to the magnetic field for the measurements of pMTJ.

The other measurement setup used in this work is designed for low-temperature measurements. It is a closed-cycle helium cryostat[164] with a temperature range of 13 K to 360 K. A controller[165] sets the temperatures by electric heating of the cooled sample holder. The IC-socket with the bonded sample can be placed in a counter-piece inside the cryostat. Normally, the cryostat is equipped with a coil which generates a maximum magnetic field of ±1900 Oe. Measurements with perpendicular magnetic field are not possible with this coil as the sample has a fixed orientation inside the cryostat. The first magnet[166] that has been set into operation within this work, generates a maximum magnetic field of about 8 kOe by two water cooled coils with an iron core. The field is measured by a Gaussmeter,[167] digitized via a multimeter[168], and recorded with the controlling computer. Any orientation of the sample surface to the magnetic field direction, especially perpendicular or parallel to the film plane, is possible as the whole cryostat can be placed and rotated in between the two coils. Another magnet[169] has been put into operation to further increase the available magnetic field. The maximum magnetic field is ±10 kOe. This magnet consists of individual permanent magnets that can be rotated. The total magnetic field results from the superposition of the particular fields of the permanent magnets. Thus, any field direction, especially perpendicular to the film plane, can be applied.

[164] *Cryodrive 1.5* from Oxford Instruments

[165] *ITC 503* from Oxford Instruments

[166] *B-M 4* from Bruker

[167] Bell 6010

[168] *K 2000* from Keithley

[169] *Multimag* from Magnetic Solutions Ltd.

The magnetic investigations in this work were carried out with an alternating gradient magnetometer (AGM).[170] It is possible to measure the absolute magnetic moment of a sample with respect to one spatial direction. In general, the AGM consist of two pairs of water cooled coils and a piezo ceramic. The one pair of coils generates a static, homogeneous magnetic field with a maximum value of ±14 kOe, whereas the other one produces a time-variable gradient field. The sample starts to oscillate due to the gradient field if it is placed in between the coils by attaching it to the piezo ceramic. The oscillation is measured by a lock-in-

[170] *Micro Mag 2900* from Princeton Measurements Cooperation

technique via the piezo ceramic. The determination of the magnetic moment of the sample becomes possible as it influences the oscillation. The magnetic moment is measured in dependence of the external magnetic field for the determination of a hysteresis loop.

The magnetization is calculated by the magnetic moment per volume of the measured sample. The volume is determined by taking the weight of the sample, the area density of the substrate, and the sputtered magnetic thickness into account. The magnetization measurements in this work are done on layered, not patterned, magnetic structures.

THE AUGER ELECTRON MICROSCOPY is an element specific characterization method and has been used for the determination of the depth profiles in this work. The basic phenomenon is the auger effect:[171] An electron, the so-called auger electron, is emitted out of an atom due to the transition of another electron of the atom filling in an inner-shell vacancy. A release of energy results from the fall of the electron from the higher energy level into the inner-shell vacancy. This energy can be transferred to the auger electron, which is then ejected from the atom. The difference between the energy of the initial electronic transition and the ionization energy for the electron shell from which the auger electron was ejected corresponds to the kinetic energy of the auger electron. As the energy levels of an atom are element specific, the kinetic energy of the auger electron gives information about the type of atom.

[171] P. Auger, Comptes Rendus **180**, 65 (1925); and P. Auger, J. Phys. Radium **6**, 205 (1925)

The inner-shell vacancies and thus the emission of auger electrons can be generated by bombarding the sample with either x-rays or, as in the system used in this work, by energetic electrons. The auger electron spectroscopy involves the determination of the auger electrons intensity as a function of the energy. The resulting spectra can be used to determine the identity of the emitting atoms.

The depth profile is obtained by etching the samples in many short etching steps and measuring the intensity of the emitted electrons by auger electron spectroscopy in between the etching steps.

X-RAY DIFFRACTION (XRD)[172] has been used in this work in order to investigate the lattice structure and orientation. In a θ-2θ-scan, a beam[173] of x-rays is send to the sample surface under an angle θ and the reflected light is measured under an angle of 2θ. The incident x-rays are diffracted by the lattice atoms of the sample as the wavelength of the x-rays is in the same order as the distance of the atoms. Depending on the exact distance between the atoms, constructive or destructive interference of the diffracted x-rays is possible for a certain angle θ. The peaks in a θ-2θ-scan are caused by positive interference of the diffracted x-rays and can be described by Bragg's law:[174]

$$n \cdot \lambda = 2d \cdot sin\theta$$

where n is an integer, λ is the wavelength of the incident beam, d is the spacing between the planes in the atomic lattice, and θ is the angle between incident ray and the sample surface.

The type of lattice as well as the orientation can be identified from the θ-2θ-scan by comparing the obtained peak positions with the literature values of the materials.

A MAGNETIC FORCE MICROSCOPE (MFM)[175] can be used to image magnetic structures, including the domain walls. A mapping of a domain wall motion with an external magnetic field is possible.[176]

The magnetic force microscopy is a variation of the atomic force microscopy (AFM). In principle, an AFM detects small forces[177] between a small tip and the surface of the sample. The atoms of the tip interact with those of the sample surface if the tip is approached to the sample. The resulting force depends on the distance between the tip and the sample surface. The tip is mounted at the end of a cantilever and the force can be detected via the deflection of the cantilever. The deflection is measured by using a laser beam. The beam is focused on the backside of the cantilever and is reflected to a four area photodetector. The forces in a defined area of the sample can be mapped as the cantilever can be moved in lateral direction and thus, scans the sample in single lines.

In the special case of magnetic force microscopy, the tip (as well as the sample surface) consists of a magnetic material.[178] In this

[172] W. H. Bragg et al., Proc. R. Soc. A **88**, 428 (1913)

[173] K_α-line of Copper, wavelength λ=1.54 Å

[174] W. L. Bragg, Proc. Cambridge Philos. Soc. **17**, 43 (1913)

[175] An MFM from DIGITAL INSTRUMENTS has been used

[176] A nice overview concerning magnetic force microscopy is given in:

U. Hartmann, Annu. Rev. Mater. Sci. **29**, 53 (1999)

[177] typically in the range of some nanonewton

[178] standard (ML3) Co-alloy hard magnetic coated tip from NANO AND MORE GMBH

measurement configuration, the detected forces between the tip and the sample are - among others - of a magnetic origin. Thus, these forces can be used to reconstruct the magnetic structure of the sample surface. Many kinds of magnetic interactions can be measured by MFM, including magnetic dipole-dipole interactions.

Appendix: Publications

First author papers

1. Z. Kugler, J.-P. Grote, V. Drewello, O. Schebaum, G. Reiss, and A. Thomas. Co/Pt multilayer-based magnetic tunnel junctions with perpendicular magnetic anisotropy. Journal of Applied Physics **111**, 07C703 (2012)

2. Z. Kugler, V. Drewello, M. Schäfers, J. Schmalhorst, G. Reiss, and A. Thomas. Temperature and bias voltage dependence of Co/Pd multilayer-based magnetic tunnel junctions with perpendicular magnetic anisotropy. Journal of Magnetism and Magnetic Materials **323**, 198 (2011)

Co-author papers

3. V. Drewello, D. Ebke, M. Schäfers, Z. Kugler, G. Reiss, and A. Thomas. Magnon excitation and temperature dependent transport properties in magnetic tunnel junctions with Heusler compound electrodes. Journal of Applied Physics **111**, 07C701 (2012)

4. D. Ebke, Z. Kugler, P. Thomas, O. Schebaum, M. Schäfers, D. Nissen, J. Schmalhorst, A. Hütten, E. Arenholz, and A. Thomas. X-ray Absorption and Magnetic Circular Dichroism Studies of Co_2FeAl in Magnetic Tunnel Junctions. IEEE Transactions on Magnetics **46**, 1925-1928 (2010)

5. V. Drewello, Z. Kugler, G. Reiss, A. Thomas. Tunneling spectroscopy probing magnetic and nonmagnetic electrodes in tunnel junctions. Prepared for publication, arXiv:1008.0326 (2010)

Presentations

- $L1_0$ ordered $Fe_{50}Pt_{50}$ and Co-based superlattices as perpendicular magnetic electrodes for tunnel junctions. MMM conference 2011, Phoenix
  Best poster award winner
- Temperature and bias voltage dependence of Co/Pd multilayer-based magnetic tunnel junctions with perpendicular magnetic anisotropy. DPG Spring Meeting 2011, Dresden
- Co/Pd multilayer based magnetic tunnel junctions with perpendicular magnetic anisotropy. DPG Spring Meeting 2010, Regensburg
- X-ray absorption spectroscopy of molecular magnets. DPG Spring Meeting 2009, Dresden

Co-author presentations

- Zero bias anomalies and magnon excitation in tunnel junctions with magnetic and nonmagnetic electrodes. DPG Spring Meeting 2012, Berlin
- Temperature and thickness dependent sign change of the Anomalous Hall Effect in Co/Pd multilayers. DPG Spring Meeting 2012, Berlin
- Magnon excitation and temperature-dependent transport properties in magnetic tunnel junctions with Heusler compound electrodes. MMM conference 2011, Phoenix
- The Influence of multilayer structure of Heusler compound electrodes on transport and magnon excitation in MTJs. DPG Spring Meeting 2011, Dresden
- Inelastic electron tunneling spectroscopy on single molecule magnets in MgO based magnetic tunnel junctions. DPG Spring Meeting 2009, Dresden

Journal of Magnetism and Magnetic Materials 323 (2011) 198–201

Contents lists available at ScienceDirect

Journal of Magnetism and Magnetic Materials

journal homepage: www.elsevier.com/locate/jmmm

Temperature and bias voltage dependence of Co/Pd multilayer-based magnetic tunnel junctions with perpendicular magnetic anisotropy

Zoë Kugler *, Volker Drewello, Markus Schäfers, Jan Schmalhorst, Günter Reiss, Andy Thomas

Bielefeld University, Department of Physics, Universitätsstr. 25, 33615 Bielefeld, Germany

ARTICLE INFO

Article history:
Received 23 July 2010
Available online 26 August 2010

Keywords:
Perpendicular anisotropy
Magnetic tunnel junction
Spinelectronic

ABSTRACT

Temperature- and bias voltage-dependent transport measurements of magnetic tunnel junctions (MTJs) with perpendicularly magnetized Co/Pd electrodes are presented. Magnetization measurements of the Co/Pd multilayers are performed to characterize the electrodes. The effects of the Co layer thickness in the Co/Pd bilayers, the annealing temperature, the Co thickness at the MgO barrier interface, and the number of bilayers on the tunneling magneto resistance (TMR) effect are investigated. TMR-ratios of about 11% at room temperature and 18.5% at 13 K are measured and two well-defined switching fields are observed. The results are compared to measurements of MTJs with Co–Fe–B electrodes and in-plane anisotropy.

1. Introduction

The tunneling magnetoresistance (TMR) effect in magnetic tunnel junctions (MTJs) is of interest for applications such as high-density read heads and non-volatile memory devices [1]. A large TMR-ratio was theoretically predicted in 2001 for MTJs with a fully epitaxial (0 0 1) MgO barrier and (0 0 1) bcc Fe, Co, or Co–Fe as electrodes [2–4]. The experimental realization of the large TMR effect is the basis for spin transfer torque (STT) switched high-density magnetic random access memory (MRAM) applications [5,6]. However, remaining challenges for planar MTJs are the increase of thermal stability for further miniaturization of the devices and the shape limitations due to magnetization curling at the edges of a patterned element [7]. MTJs based on magnetic layers with perpendicular magnetic anisotropy (PMA), so-called perpendicular magnetic tunnel junctions (pMTJs), are predicted to have a larger thermal stability as a result of a higher magnetic anisotropy and a lower switching current density for STT switching [8–11] compared to in-plane MTJs. In addition to the size limitations, the shape limitations of MTJ elements are also eliminated because pMTJs have no limit on the cell aspect ratio of patterned elements [12,13]. Promising materials with perpendicular magnetic anisotropy are Co based multilayers, such as Co/Pd or Co/Pt [14]. These materials have been successfully integrated into MTJs [15–20]. In this study, temperature- and bias voltage-dependent transport measurements of MgO-based pMTJs with Co/Pd multilayers as electrodes are presented and compared to measurements of MTJs with $Co_{40}Fe_{40}B_{20}$ electrodes. The effects of the Co layer thickness in the Co/Pd bilayers, the annealing temperature, the Co thickness at the MgO barrier interface, and the number of Co/Pd bilayers on the TMR effect are investigated. Magnetic measurements of the Co/Pd multilayers are performed to characterize the electrodes of the tunnel junctions with respect to the Co layer thickness in the Co/Pd bilayers and to the annealing temperature.

2. Preparation

The samples are prepared in a magnetron sputter system with a base pressure of 1×10^{-7} mbar. The layer stacks are sputtered on top of a thermally oxidized (500 nm) silicon (0 0 1) wafer. The layer stack of the samples is Si wafer/SiO_2/Ta/(Pd 1.8/Co t_{Co})$_X$/interface layer/MgO 2.1/interface layer/(Co u_{Co}/Pd 1.8)$_Y$/protection layers (all numbers in nm). The aim is to tailor different switching fields of the electrodes and a maximal TMR ratio. Therefore, the Co thickness t_{Co} in the lower multilayer, the number of multilayers of the lower electrode X, the Co thickness in the upper multilayers u_{Co}, and the number of multilayers of the upper electrode Y is changed. Additionally, the barrier interface is dusted with Co or $Co_{40}Fe_{40}B_{20}$. The samples are annealed after sputtering at different temperatures for 60 min in a magnetic field of 6500 Oe perpendicular to the film plane to enhance the perpendicular magnetic anisotropy of the Co/Pd multilayers and to crystallize the MgO barrier. The stack is patterned by laser lithography and ion beam etching. The resulting patterns are squares of $7.5 \times 7.5\,\mu m^2$ and $15.5 \times 15.5\,\mu m^2$. These structures are capped with gold contact pads.

* Corresponding author. Tel.: +49 521 106 5427; fax: +49 521 106 6046.
E-mail address: zkugler@physik.uni-bielefeld.de (Z. Kugler).
URL: http://www.spinelectronics.de (Z. Kugler).

0304-8853/$ - see front matter © 2010 Elsevier B.V. All rights reserved.
doi:10.1016/j.jmmm.2010.08.038

The transport measurements are done by a conventional two-probe technique with a 10 mV bias voltage in a perpendicular magnetic field. The low-temperature measurements are done in a closed-cycle helium cryostat (*Oxford* Cryodrive 1.5) with a temperature range of 13–330 K.

3. Results and discussion

First, the magnetic behavior of the SiO_2/Ta/(Pd 1.8/Co t_{Co})$_X$/MgO 2.1 electrodes with $X=9$ is investigated. The Co layer thickness t_{Co} and the annealing temperature T_a are changed. The measurements are done with an alternating gradient magnetometer (*Micro Mag* 2900, *Princeton Measurements Corporation*). The magnetic field is applied perpendicular to the film plane. Fig. 1(a)–(c) shows the saturation magnetization (M_s), remanent magnetization (M_r), and coercivity (H_c) in dependence of t_{Co} and of T_a. Here, t_{Co} is changed from 0.3 to 0.55 nm in steps of 0.05 nm. The annealing temperature is changed for every fixed t_{Co} from room temperature (as-prepared state) to 450 °C. M_s increases with increasing Co layer thickness, as shown in Fig. 1(a). The annealing temperature dependence of M_s shows that M_s first increases with increasing T_a. The maximum M_s is reached for annealing temperatures between 200 and 350 °C, dependent on the Co layer thickness. After reaching this maximum the M_s decreases. The lowest value of M_s is about 108 kA/m for 0.3 nm Co in the as-prepared state, whereas the highest value of M_s is 349 kA/m at 0.55 nm Co and 300 °C annealing temperature.

The t_{Co} and T_a dependence of M_s and M_r as well as their absolute values are very similar, as one can see by comparing Fig. 1(a) and (b), which show M_s and M_r, respectively. Thus, the squareness (M_r/M_s) is nearly one for all of the investigated samples. This shows the very strong PMA and good quality of the Co-based superlattices.

The coercivity, shown in Fig. 1(c), increases with the annealing temperature. After being roughly constant for Co thicknesses between 0.3 and 0.4 nm, dependent on the annealing temperature, the coercivity decreases with increasing t_{Co}. The lowest value is about 157 Oe for 0.55 nm Co in the as-prepared state, whereas the highest value of H_c is 5520 Oe at 0.4 nm Co and 450 °C annealing temperature. This coercivity values are in a typical range for Co/Pd multilayers [21]. It is reasonable that the H_c of the Co/Pd multilayers decreases with increasing Co thickness. For nine bilayers of Co/Pd, as used here, the critical Co layer thickness at which the perpendicular anisotropy turns into in-plane anisotropy is 1.15 nm (not shown).

These magnetic measurements demonstrate, that it is possible to tune the switching field of the multilayers by changing the Co layer thickness in the Co/Pd multilayers. This is an important factor for the use of such multilayers as electrodes in pMTJs to achieve two well-defined switching fields and to stabilize the anti-parallel state. Consequently, the multilayers are integrated as electrodes in magnetic tunnel junctions. The resulting sample stack is SiO_2/Ta/(Pd 1.8/Co t_{Co})$_X$/interface layer/MgO 2.1/interface layer/(Co u_{Co}/Pd 1.8)$_Y$/ protection layers. The Co layer thickness t_{Co} of the lower electrode is changed from 0.25 to 0.5 nm to improve the TMR effect and the switching behavior of the pMTJs. For every sample with one fixed t_{Co}, the Co layer thickness u_{Co} of the upper electrode is varied. The lower electrode is always used as the hard magnetic electrode and the upper electrode as the soft one. This means, that u_{Co} is always larger than t_{Co}. For all samples, the numbers of bilayers X and Y in the electrodes is kept constant at $X=Y=9$, as already used for the AGM measurements. A 1 nm layer of Co–Fe–B is used as an interface layer to improve the growth of the MgO barrier on top of the Pd/Co electrode [22,23]. All samples are annealed after sputtering at 150 °C. Fig. 1(d) shows the TMR effect as a function of the Co layer thickness of the lower electrode (t_{Co}) and as a function of the Co layer thickness of the upper electrode (u_{Co}). A maximum TMR effect of about 9% is observed for $t_{Co}=0.35$ nm and $u_{Co}=0.45$ nm. This maximum is in the middle of the investigated Co thicknesses: for smaller and larger t_{Co} and u_{Co}, the TMR ratio decreases to about 3.3%. The area-resistance products of the samples are in the range of 2–6 MΩ μm^2.

Next, the annealing temperature T_a is optimized. Fig. 2(a) shows the T_a dependence of the TMR effect for the best sample from Fig. 1(d), with $t_{Co}=0.35$ nm, and $u_{Co}=0.45$ nm, $X=Y=9$ and 1 nm Co–Fe–B as the interface layer. The TMR increases from about 7% in the as-prepared state to about 9% at an annealing temperature of 150 °C. For T_a larger than 150 °C, the TMR decreases to 0.6% at 300 °C. This strong decrease of the TMR for higher annealing temperatures is due to Pd diffusion to the MgO

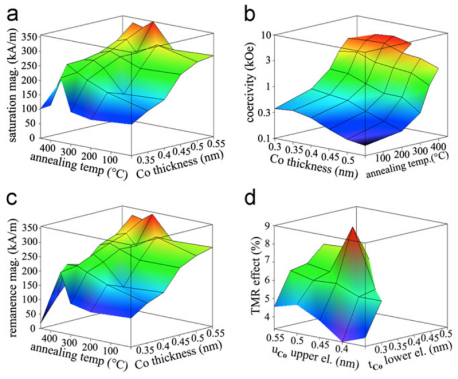

Fig. 1. (a)–(c) Magnetic behavior of samples . . . /(Pd 1.8/Co t_{Co})$_9$/ MgO 2.1 (all numbers in nm) in dependence of the Co layer thickness t_{Co} and annealing temperature T_a. (d) Room temperature TMR of samples . . . /(Pd 1.8/Co t_{Co})$_9$/ Co-Fe-B 1/ MgO 2.1/Co–Fe–B 1/(Co u_{Co}/Pd 1.8)$_9$/. . . as a function of the Co layer thickness t_{Co} in the lower electrode and u_{Co} in the upper electrode.

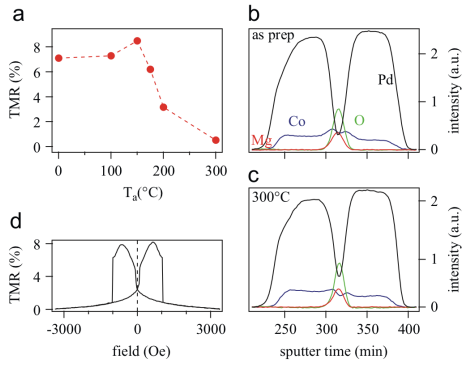

Fig. 2. (a) TMR as a function of annealing temperature for the sample stack . . . /(Pd 1.8/Co 0.35)$_9$/Co–Fe–B 1/MgO 2.1/Co–Fe–B 1/(Co 0.45/Pd 1.8)$_9$/. . . (all numbers in nm). Composition depth profiles of Pd, Co, O, and Mg in the sample (b) before and (c) after annealing at 300 °C for 1 h. (d) Major loop of the sample annealed at 150 °C.

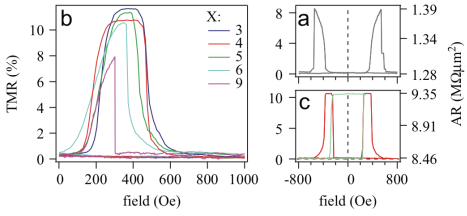

Fig. 3. (a) Major loop of sample …/ (Pd 1.8/Co 0.35)$_9$/ Co 0.7/ MgO 2.1/ Co 0.7/ (Co 0.45/ Pd 1.8)$_9$/…. (all numbers in nm) (b) TMR loops of samples …/ (Co 0.6/ Pd 1.8)$_X$/ Co 0.7/ Mg 0.5/ MgO 2.1/ Co 0.7/ (Co 0.7/ Pd 1.8)$_2$/ … with different numbers X of Co/Pd bilayers in the lower electrode. (c) Major and minor loop of the sample with $X=4$.

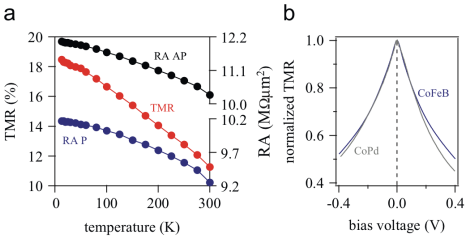

Fig. 4. (a) Temperature dependent transport measurement of the sample …/ (Co 0.6/ Pd 1.8)$_4$/ Co 0.7/ Mg 0.5/ MgO 2.1/ Co 0.7/ (Co 0.7/ Pd 1.8)$_2$/… (all numbers in nm). (b) Normalized TMR as a function of the bias voltage for the pMTJ and for a reference sample …/ Mn–Ir 12/ Co–Fe–B 4/ Al 1.2+Oxidation/ Co–Fe–B 4/ Ni–Fe 3/ … with in-plane anisotropy measured at 13 K.

barrier. In Fig. 2(b) and (c), the composition depth profiles of Pd, Co, O, and Mg are shown for the sample in the as-prepared state and after annealing at 300 °C for 1 h. The profiles are measured by auger electron spectroscopy (AES) depth profiling. The Pd intensity in the region of the MgO is higher in the measurement of the annealed sample, whereas a comparison of the Co intensities in the MgO region shows less Co after annealing. This indicates a diffusion of Pd to the MgO interface, where the Pd replaces the Co at high T_a, thereby reducing the TMR effect. Fig. 2(d) shows the major loop of the sample annealed at the optimum temperature of 150 °C for 1 h. The increase of the TMR before reaching zero field is caused by an additional in-plane component which is most likely produced by the Co–Fe–B layers. To prove this assumption, Co–Fe–B was replaced by a Co interface layer with different thicknesses v. Fig. 3(a) shows the major loop of the sample with $v=0.7$ nm. This sample shows the highest TMR ratio of about 9%, similar to the TMR ratio of the sample with 1 nm of Co–Fe–B at the MgO interface, but no in-plane component can be concluded from the TMR measurement. The hard electrode has a sharp switching field, whereas the magnetization of the soft electrode turns slowly. This is likely due to the strong magneto-static interaction between the soft and hard magnetic layers in the patterned pMTJs. The stray field of one of the perpendicular electrodes on the other electrode always assists the parallel alignment of the magnetization.

The number X of Co/Pd bilayers in the lower electrode is changed from 9 to 3 to control the magneto-static interaction and to ensure the anti-parallel alignment of the magnetization in the electrodes over a certain field range. Fig. 3(b) shows the major loops in the positive field range for 0.7 nm of Co. The upper electrode is kept constant at $Y=2$ with $u_{Co}=0.7$ nm and t_{Co} as 0.6 nm. A thin Mg layer was inserted under the MgO to enable better growing of the barrier. The samples show a TMR effect of about 11% at room temperature and an area resistance product of about 8.5 MΩ μm^2. The switching field of the hard electrode increases from 300 Oe for $X=9$ to about 640 Oe for $X=3$. Whereas the magnetization of the soft electrode turns slowly and has no sharp switching field for $X=9$, a hard switching is reached for $X<5$. The sample with $X=4$ shows two well-defined switching fields, and the minor loop has two separated magnetic states at zero field as shown in Fig. 3(c).

Finally, transport measurements for the optimized sample annealed at 150 °C were performed at different temperatures. Fig. 4(a) shows the temperature dependence of the TMR and the area resistance products in the parallel state P and in the anti-parallel state AP. The area resistance product in the P state changes from 9.2 to 10.2 MΩ μm^2 with the temperature. This is a change of 9.8%, which is in the typical range for the P state for MTJs [24,25]. The area resistance product in the AP state changes by 14.5%, which changes the TMR overall by a factor of 1.7–18.5% at 13 K. This is the highest value reported for pMTJs with Co/Pd multilayers as perpendicular magnetized electrodes [22,26]. In Fig. 4(b), the bias voltage dependence of the TMR effect is shown and compared to an reference sample with Co–Fe–B electrodes and in-plane anisotropy. The MgO barrier of the pMTJs is not considered to be textured, as the TMR-effects are not close to that in the coherence tunneling scheme in epitaxially MgO-bcc systems. Furthermore, X-ray diffraction measurements show fcc (1 1 1) orientation of the Co/Pd electrodes (not shown). Even for MgO barriers with (1 1 1) texture coherent tunneling cannot be expected [27]. Thus, a MTJ with an amorphous Alumina-based barrier is chosen as the reference sample. The reference sample is annealed at 275 °C and shows a TMR effect of 110% at 10 mV and 13 K. The bias voltage dependence of the TMR for the pMTJ with Co/Pd electrodes shows no significant change compared to the in-plane reference sample. A peak-like maximum is observed for zero bias, and the TMR decreases to the half-value for bias voltages of about 400 mV.

4. Summary

In summary, temperature- and bias voltage-dependent transport measurements of pMTJs with Co/Pd electrodes were shown. The temperature- and bias voltage-dependent behaviors of pMTJs show no significant changes compared to MTJs with Co–Fe–B electrodes and in-plane anisotropy. Magnetic measurements of the Co/Pd multilayers were performed to characterize the electrodes of the tunnel junctions. The Co/Pd multilayer films show strong PMA, even in the as-prepared state. The effects of the Co layer thickness in the multilayer electrodes, the annealing temperature, the Co thickness at the MgO barrier interface, and the number of Co/Pd bilayers on the TMR effects were investigated. A TMR effect of about 11% at room temperature and 18.5% at 13 K was measured for an optimum annealing temperature of 150 °C.

References

[1] S.S.P. Parkin, K.P. Roche, M.G. Samant, P.M. Rice, R.B. Beyers, R.E. Scheuerlein, E.J. O'Sullivan, S.L. Brown, J. Bucchigano, D.W. Abraham, Y. Lu, M. Rooks, P.L. Trouilloud, R.A. Wanner, W.J. Gallagher, Am. Inst. Phys., 1999, pp. 5828–5833 ⟨http://link.aip.org/link/?JAP/85/5828/1⟩.
[2] W.H. Butler, X.-G. Zhang, T.C. Schulthess, J.M. MacLaren, Physical Review B 63 (January) (2001) 054416.
[3] J. Mathon, A. Umerski, Physical Review B 63 (May) (2001) 220403.
[4] X.-G. Zhang, W.H. Butler, Physical Review B 70 (November) (2004) 172407.

JOURNAL OF APPLIED PHYSICS **111**, 07C703 (2012)

Co/Pt multilayer-based magnetic tunnel junctions with perpendicular magnetic anisotropy

Zoë Kugler,[a] Jan-Philipp Grote, Volker Drewello, Oliver Schebaum, Günter Reiss, and Andy Thomas
Bielefeld University, Department of Physics, Universitätsstr. 25, 33615 Bielefeld, Germany

(Presented 3 November 2011; received 9 September 2011; accepted 14 October 2011; published online 9 February 2012)

Temperature-dependent transport measurements of magnetic tunnel junctions with perpendicularly magnetized Co/Pt electrodes are presented. Magnetization measurements of the Co/Pt multilayers are performed to characterize the electrodes. The interface magnetization of the Co layers at the Pt interface is estimated in dependence of the annealing temperature. The effect of the annealing temperature on the tunneling magnetoresistance effect of the magnetic tunnel junctions (MTJs) is investigated. Tunneling magnetoresistance ratios of about 19% at room temperature are attained and two well-defined switching fields are observed. The tunneling magnetoresistance of Co/Pt based tunnel junctions changes by a factor of 1.9 if cooled to 13 K. The results are compared to measurements of MTJs with Co-Fe-B electrodes and in-plane anisotropy. © *2012 American Institute of Physics*. [doi:10.1063/1.3670972]

INTRODUCTION

The tunneling magnetoresistance (TMR) effect in magnetic tunnel junctions (MTJs) is of interest for applications such as high-density read heads and nonvolatile memory devices.[1] Large TMR-ratios were theoretically predicted in 2001 for MTJs with an epitaxial MgO barrier[2,3] and experimentally realized in 2004.[4,5] However, for further miniaturization of the devices, the increase of thermal stability and overcoming the shape limitations are remaining challenges. MTJs based on magnetic layers with perpendicular magnetic anisotropy (PMA), so-called perpendicular MTJs (pMTJs), are predicted to have a larger thermal stability as a result of a higher magnetic anisotropy. PMTJs are also predicted to have a lower switching current density for spin transfer torque switching.[6,7] Not only the size limitations, but also the shape limitations of MTJ elements are eliminated, because pMTJs have no limit on the cell aspect ratio of patterned elements.[8,9] A promising class of materials with perpendicular magnetic anisotropy are Co based multilayers, such as Co/Pd or Co/Pt.[10] Recent research concentrates on integrating these materials into MTJs.[11–18] In this study, temperature-dependent transport measurements of MgO-based pMTJs with Co/Pt multilayers as electrodes are presented. The findings are compared to measurements of MTJs with $Co_{40}Fe_{40}B_{20}$ electrodes. The effect of the annealing temperature on the TMR effect is investigated. Magnetic measurements of the Co/Pt multilayers are performed to characterize the electrodes of the tunnel junctions with respect to the Co layer thickness in the Co/Pt bilayers and to the annealing temperature. The interface magnetization of the Co layers at the Pt interface is estimated from the magnetization measurements in dependence of the annealing temperature.

The samples in this study are prepared in a magnetron sputter system with a base pressure of 1×10^{-7} mbar. The layer stacks are sputtered on top of a thermally oxidized (500 nm) silicon (001) wafer. The layer stack of the samples is Si wafer/SiO_2/Ta/(Pt 1.8/Co 0.6)$_4$/Co 0.7/Mg 0.5/MgO 2.1/(Co 0.7/Pt 1.8)$_2$/protection layers (all numbers in nm). The samples are annealed after sputtering at different temperatures for 60 mins in a magnetic field of 6500 Oe perpendicular to the film plane. The stack is patterned by laser lithography and ion beam etching. The resulting patterns are squares of $7.5 \times 7.5\ \mu m^2$. These structures are capped with gold contact pads. The transport measurements are done by a conventional two-probe technique with a 10 mV bias voltage in a perpendicular magnetic field. The low-temperature measurements are done in a closed-cycle helium cryostat (OXFORD Cryodrive 1.5). The magnetic measurements are done with an alternating gradient magnetometer (Micro Mag 2900, Princeton Measurements Corporation).

First, the magnetic behavior of the Co/Pt multilayer electrodes is investigated. The sample structure is Si wafer/SiO/Ta 5/(Co t_{Co}/Pt 1.8) multilayer/MgO 2.1. The Co layer thickness t_{Co} and the annealing temperature T_a are varied. Figures 1(a)–1(d) show the saturation magnetization (M_s), remanent magnetization (M_r), squareness ($S = M_r/M_s$), and coercivity (H_c) in dependence of t_{Co} for the different T_a. Here, t_{Co} is varied in the range from 0.35 to 0.95 nm in steps of 0.05 nm. Due to the use of magnetron sputtering, this is an effective layer thickness, which quantifies the amount of material that is deposited. The annealing temperature is changed for every fixed t_{Co} from room temperature (as-prepared state) to 400 °C in steps of 100 °C. The M_s increases with increasing Co layer thickness, as shown in Fig. 1(a). The M_s increases faster for small t_{Co}, and adapts the Cobalt bulk magnetization of about 1334 ± 194 kA/m for larger t_{Co}. The error results from the inaccuracy of the magnetic volume determination and the measurement procedure. The bulk

[a]Electronic mail: zkugler@physik.uni-bielefeld.de. www.spinelectronics.de.

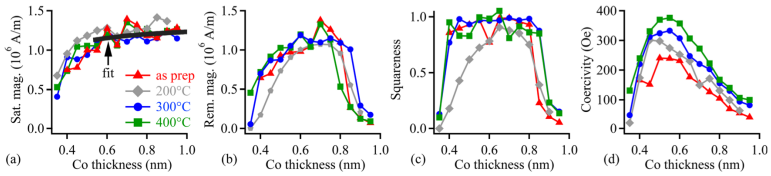

FIG. 1. (Color online) Magnetic properties of Co/Pt multilayers in dependence of the Co layer thickness t_{Co} for different annealing temperatures T_a. The black curve in (a) shows the fit of the saturation magnetization with the interface magnetization as fit parameter for the as prepared state.

magnetization was measured on the sample Si wafer/SiO/Ta 5/Pt 1.8/Co 30/Pt 1.8/MgO 2.1. The M_s stays roughly constant with the annealing temperature for all investigated t_{Co}. The lowest value is about 412 kA/m for 0.35 nm Co and 300 °C annealing temperature, whereas the highest value is about 1365 kA/m for 0.90 nm Co and 200 °C. Figure 1(b) shows the remanent magnetization in dependence of the Co thickness for the different T_a. The M_r increases for small t_{Co}. After reaching a maximum at about 0.7 nm the M_r decreases. The annealing temperature dependence of M_r shows that it is roughly constant, too. The lowest value is about 0.3 kA/m for 0.35 nm Co and 200 °C annealing temperature, whereas the highest value is about 1387 kA/m for 0.7 nm Co in the as prepared state. The t_{Co} and T_a dependence of M_s and M_r as well as their absolute values are very similar for $0.4\,\text{nm} \le t_{Co} \le 0.7\,\text{nm}$, as one can see by comparing Figs. 1(a) and 1(b). Thus, the squareness $S = M_r/M_s$, shown in Fig. 1(c), is about one for the samples with t_{Co} in between 0.4 and 0.7 nm. This shows the very strong PMA and good quality of the Co-based superlattices in this t_{Co}-range. For t_{Co} smaller than 0.4 nm and larger than 0.7 nm S decreases. Also S stays roughly constant with T_a since M_r and M_s are independent of T_a. The coercivity, shown in Fig. 1(d), increases with the annealing temperature. The coercivity first increases with increasing t_{Co}. For $t_{Co} > 0.55\,\text{nm}$ H_c decreases. The lowest value is about 27 Oe for 0.35 nm Co and 200 °C, whereas the highest value of H_c is 351 Oe at 0.55 nm Co and 400 °C.

The cobalt magnetization at the interface to the Pt layer is determined from the saturation magnetization measurements of the multilayers for all annealing temperatures. A sketch of the assumed model is shown in Fig. 2(a). Here, the first Co monolayer at the Pt interface has a thickness t_{ML} and a magnetization M_{inter}. The magnetization of the rest of the Co layer with thickness $t_{Co} - 2 \cdot t_{ML}$ is called M_{bulk}. For $t_{Co} > 2 \cdot t_{ML}$, the total magnetization M_{tot} can be described by an interface term and a bulk term as

$$M_{tot} = \frac{2 \cdot t_{ML}}{t_{Co}} \cdot M_{inter} + \frac{t_{Co} - 2 \cdot t_{ML}}{t_{Co}} \cdot M_{bulk}.$$

The bulk magnetization M_{bulk} was measured on the sample Si wafer/SiO/Ta 5/Pt 1.8/Co 30/Pt 1.8/MgO 2.1 to be 1335 kA/m and t_{ML} is assumed to be 2.6 Å.[19] The annealing temperature dependent interface magnetization M_{inter} was determined by fitting the saturation magnetization M_s from Fig. 1(a) with the equation for M_{tot} for $t_{Co} > 2 \cdot t_{ML}$. The fit was done for every fixed T_a. The black curve in Fig. 1(a) shows the fit for the as prepared state. The results of the fits are summarized in Fig. 2(b). Within the errors of the fit and measurement parameters M_{inter} stays constant with the annealing temperature. The average is about 1141.1 kA/m. This is about 85.5% of the bulk value.

The magnetic measurements demonstrate that it is possible to tune the switching field of the multilayers by changing the Co layer thickness in the Co/Pt multilayers. This is an important factor for the use of such multilayers as electrodes in pMTJs to achieve two well-defined switching fields and to stabilize the antiparallel state. Consequently, the multilayers are integrated as electrodes in magnetic tunnel junctions. The resulting sample stack is SiO_2/Ta/(Pt 1.8/Co 0.7)$_4$/Mg 0.5/MgO 2.1/Co 0.7/(Co 0.6/Pt 1.8)$_2$/protection layers.

The annealing temperature T_a of the tunnel junctions is optimized. Figure 3(a) shows the room temperature TMR loops in the positive field range for the different T_a. In Fig. 3(b), the corresponding TMR-values in dependence of the annealing temperature are listed. The TMR at room temperature increases from about 16% in the as-prepared state to about 18.6% at an annealing temperature of 250 °C. For T_a

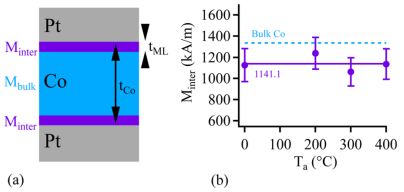

FIG. 2. (Color online) (a) Schematic picture of Co layer with thickness t_{Co} in between two Pt layers. The first monolayer of Co at the Pt interface has a thickness of t_{ML} and a magnetization of M_{inter}. The cobalt bulk magnetization is M_{bulk}. (b) M_{inter} in dependence of the annealing temperature T_a.

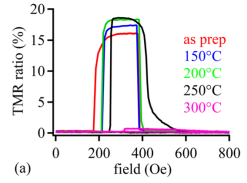

Ta (°C)	TMR (%)
0	16.1
150	17.5
200	18.4
250	18.6
300	0.7

FIG. 3. (Color online) (a) TMR loops of sample…/(Co 0.6/Pt 1.8)$_4$/Co 0.7/Mg 0.5/MgO 2.1/(Co 0.7/Pt 1.8)$_2$/… and (b) TMR values for the different annealing temperatures.

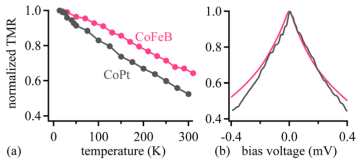

FIG. 4. (Color online) (a) Temperature dependence of the TMR for the pMTJ…/(Co 0.6/Pt 1.8)$_4$/Co 0.7/Mg 0.5/MgO 2.1/(Co 0.7/Pt 1.8)$_2$/… and of a reference sample…/Mn-Ir 12/Co-Fe-B 4/Al 1.2 + Oxidation/Co-Fe-B 4/Ni-Fe 3/… (all numbers in nm) with in-plane anisotropy. (b) Normalized TMR as a function of the bias voltage for the pMTJ and for the reference sample measured at 13 K.

larger than 250 °C, the TMR decreases to 0.7%. The area-resistance product in the parallel state of the samples is about 60 MΩ μm^2. The switching field of the soft electrode increases with increasing T_a, whereas the switching field of the hard electrode is very sharp and firstly remains unchanged. That means that the field range of the antiparallel alignment of the magnetization becomes smaller. For $T_a \geq 250$ °C, the behavior of the hard electrode changes and the magnetization turns slowly. We propose that the abrupt, strong decrease of the TMR for higher annealing temperatures is due to a change of the magnetic behavior of the perpendicularly magnetized electrodes. It behaves very different from the decrease in TMR due to diffusion which we reported for Co/Pd based pMTJs.[20] For Co/Pt based pMTJs, the antiparallel alignment of the electrodes over a certain field range vanishes for $T_a > 250$ °C. We propose the electrodes switch simultaneously. But, this cannot be finally clarified with transport measurements. The magnetization switching of a structured MTJ element must be investigated. As this magnetization is a very small quantity, special samples with arrays of MTJs will be prepared to do this.

Finally, transport measurements for the sample Si wafer/SiO$_2$/Ta/(Pt 1.8/Co 0.6)$_4$/Co 0.7/Mg 0.5/MgO 2.1/(Co 0.7/Pt 1.8)$_2$/protection layers annealed at 200 °C were performed at different temperatures and compared to measurements of a reference sample with CoFeB electrodes and in-plane anisotropy. The MgO barrier of the pMTJs is not considered to be textured, as the TMR-effects are not close to that in the coherence tunneling scheme in epitaxially MgO-bcc systems. Thus, a MTJ with an amorphous alumina-based barrier is chosen as the reference sample. The reference sample is annealed at 275 °C and shows a TMR effect of 112% at 10 mV and 13 K. Figure 4(a) shows the temperature dependence of the TMR for the pMTJ and the reference sample. The TMR of the PMTJ changes by a factor of 1.9 if cooled to 13 K, whereas the reference sample changes by a factor of 1.6. It can be suspected that the temperature dependent magnetic switching behavior of the pMTJ gives an additional component to the overall temperature dependence of the TMR ratio. This behavior is known for tunnel junctions based on materials with perpendicularly magnetized electrodes and can have a large influence on the TMR ratio.[21] In Fig. 4(b), the bias voltage dependence of the TMR effect is shown and compared to the reference sample. The bias voltage dependence of the TMR for the pMTJ with Co/Pt electrodes shows no fundamental change compared to the in-plane reference sample. A peak-like maximum is observed for zero bias, and the TMR decreases to the half-value for bias voltages of about 350 mV.

In summary, magnetic measurements of the Co/Pt multilayers were performed to characterize the electrodes. The interface magnetization of the Co layers at the Pt interface was estimated in dependence of the annealing temperature. The effect of the annealing temperature on the TMR effect of the MTJs was investigated. TMR ratios of about 19% at room temperature and two well-defined switching fields were observed for an optimum annealing temperature of 200 °C. Temperature- and bias voltage-dependent transport measurements of pMTJs with Co/Pt electrodes were shown. The TMR increased by a factor of 1.9 if cooled to 13 K. The results are compared to measurements of an alumina based magnetic tunnel junction with CoFeB electrodes and in-plane anisotropy.

Z.K. and G.R. acknowledge funding from the DFG grant Re 1052/22-1. A.T. and V.D. acknowledge the MIWF of the NRW state government for financial support.

[1]G. A. Prinz, Science **282**, 1660 (1998).
[2]W. H. Butler, X.-G. Zhang, T. C. Schulthess, and J. M. MacLaren, Phys. Rev. B **63**, 054416 (2001).
[3]J. Mathon and A. Umerski, Phys. Rev. B **63**, 220403 (2001).
[4]S. S. P. Parkin, C. Kaiser, A. Panchula, P. M. Rice, B. Hughes, M. Saman, and S.-H. Yang, Nat. Mater. **3**, 862 (2004).
[5]S. Yuasa, T. Nagahama, A. Fukushima, Y. Suzuki, and K. Ando, Nat. Mater. **3**, 868 (2004).
[6]S. Mangin, D. Ravelosona, J. A. Katine, M. J. Carey, B. D. Terris, and E. E. Fullerton, Nat. Mater. **5**, 210 (2006).
[7]H. Meng and J.-P. Wang, Appl. Phys. Lett. **88**, 172506 (2006).
[8]I. Yoo, D.-k. Kim, and Y. K. Kim, J. Appl. Phys. **97**, 10C919 (2005).
[9]N. Nishimura, T. Hirai, A. Koganei, T. Ikeda, K. Okano, Y. Sekiguchi, and Y. Osada, J. Appl. Phys. **91**, 5246 (2002).
[10]P. F. Carcia, A. D. Meinhaldt, and A. Suna, Appl. Phys. Lett. **47**, 178 (1985).
[11]Z. R. Tadisina, A. Natarajarathinam, B. D. Clark, A. L. Highsmith, T. Mewes, S. Gupta, E. Chen, and S. Wang, J. Appl. Phys. **107**, 09C703 (2010).
[12]L.-X. Ye, C.-M. Lee, J.-W. Syu, Y.-R. Wang, K.-W. Lin, Y.-H. Chang, and T. H. Wu, IEEE Trans. Mag. **44**, 3601 (2008).
[13]J.-H. Park, C. Park, T. Jeong, M. T. Moneck, N. T. Nufer, and J.-G. Zhu, J. Appl. Phys. **103**, 07A917 (2008).
[14]R. Law, R. Sbiaa, T. Liew, and T. C. Chong, Appl. Phys. Lett. **91**, 242504 (2007).
[15]G. Kim, Y. Sakuraba, M. Oogane, Y. Ando, and T. Miyazaki, Appl. Phys. Lett. **92**, 172502 (2008).
[16]Y. Wang, W. X. Wang, H. X. Wei, B. S. Zhang, W. S. Zhan, and X. F. Han, J. Appl. Phys. **107**, 09C711 (2010).
[17]K. Mizunuma, M. Yamanouchi, S. Ikeda, H. Sato, H. Yamamoto, H.-D. Gan, K. Miura, J. Hayakawa, F. Matsukura, and H. Ohno, Appl. Phys. Exp. **4**, 023002 (2011).
[18]M. T. Rahman, A. Lyle, G. Hu, W. J. Gallagher, and J. P. Wang, J. Appl. Phys. **109**, 07C709 (2011).
[19]T. Devolder, S. Pizzini, J. Vogel, H. Bernas, C. Chappert, V. Mathet, and M. Borowski, Z. Phys. B: Condens. Matter **22**, 193 (1975).
[20]Z. Kugler, V. Drewello, M. Schäfers, J. Schmalhorst, G. Reiss, and A. Thomas, J. Mag. Mag. Mat. **323**, 198 (2011).
[21]G. Feng, H. C. Wu, J. F. Feng, and J. M. D. Coey Appl. Phys. Lett., **99**, 042502 (2011).